SAPIENZA
UNIVERSITÀ DI ROMA

# Nonlinear Effects in Finite Elements Analysis of Colorectal Surgical Clamping

Scuola di Dottorato

**Dottorato di Ricerca in Automatica, Bioingegneria e Ricerca Operativa (ABRO)**

Indirizzo

**Dottorato di Ricerca in Bioingegneria**

Con il contributo della

**Secretaría Nacional de Educación Superior, Ciencia, Tecnología e Innovación (SENESCYT - ECUADOR)**

**XXXI Ciclo**

**Robinson Gabriel Guachi Guachi**

**Matricola n° 1700342**

Ph.D. Thesis

Academic Year: 2017/2018

**Advisors:**

**Prof. Febo Cincotti**

**Firma_____**

**Prof. Franco Marinozzi**

**Firma_____**

**Co-Advisors:**

**Prof.ssa Francesca Campana**

**Firma_____**

**Prof.ssa Lorena de los Angeles Guachi**

**Firma_____**

*Dedicated to.*

*This thesis is dedicated to my dearest Ronny J. Guachi R. for teaching me that it is not necessary being an adult to be brave.*

***Acknowledgements***

First of all I am really thankful to the Ecuador's Secretary of Higher Education, Science, Technology and Innovation (SENESCYT) scholarship scheme and Sapienza University as well for making it possible for me to study here.

This thesis would not have been possible without the help of my advisor Prof. Franco Marinozzi, and thank to him for being my contact to start my application at Sapienza University. I would like to give my sincere thanks to my advisor Prof. Francesca Campana who encouraged and directed me during my Ph.D. studies. Prof. Francesca has been there for me in every trouble situations and progress in my PhD experience. I thank her for her patience and for introducing me to the wonderful world of FEA.

This thesis is a result of discussions and collaborations with many people, in particular I wish to acknowledge to Ph.D. Michele Bici who has directly helped me with my research. I cordially thanks to all who in diverse way contributed in the completion of this dissertation, Marcelo Calispa, Jean Pierre Cazorla, Ilaria Conforti, Arun, Saber, Dwi, Sooraj, Juan Arcos and Israel Granda.

Thank you very much to my beloved family, my parents (Cesar and Vilma), my brother Cesar and my sisters (Emerita, Fatima, Lorena and Yasmina). My sincere acknowledge to Lorena for her collaboration and support in these years.

Finally I thank to my darling Cristina Robalino for all her love, patience, support, and mainly for believing in me. I am highly grateful for her courage to stay with me during my challenges in the pursuit of my goals.

¡Thank you very much!, ¡Grazie mille!, ¡Muchas gracias!.

Robinson Gabriel Guachi Guachi

2018, Rome, Italy

# Abstract

Minimal Invasive Surgery (MIS) is a procedure that has increased its applications in past few years in different types of surgeries. As number of application fields are increasing day by day, new issues have been arising. In particular, instruments must be inserted through a trocar to access the abdominal cavity without capability of direct manipulation of tissues, so a loss of sensitivity occurs. Generally speaking, the student of medicine or junior surgeons need a lot of practice hours before starting any surgical procedure, since they have to difficulty in acquiring specific skills (hand–eye coordination among others) for this type of surgery. Here is what the surgical simulator present a promising training method using an approach based on Finite Element Method (FEM).

The use of continuum mechanics, especially Finite Element Analysis (FEA) has gained an extensive application in medical field in order to simulate soft tissues. In particular, colorectal simulations can be used to understand the interaction between colon and the surrounding tissues and also between colon and instruments. Although several works have been introduced considering small displacements, FEA applied to colorectal surgical procedures with large displacements is a topic that asks for more investigations. This work aims to investigate how FEA can describe non-linear effects induced by material properties and different approximating geometries, focusing as test-case application colorectal surgery. More in detail, it shows a comparison between simulations that are performed using both linear and hyperelastic models. These different mechanical behaviours are applied on different geometrical models (planar, cylindrical, 3D-SS and a real model from digital acquisitions 3D-S) with the aim of evaluating the effects of geometric non-linearity. Final aim of the research is to provide a preliminary contribution to the simulation of the interaction between surgical instrument and colon tissues with multi-purpose FEA in order to help the preliminary set-up of different bioengineering tasks like force-contact evaluation or approximated modelling for virtual reality (surgical simulations).

In particular, the contribution of this work is focused on the sensitivity analysis of the nonlinearities by FEA in the tissue-tool interaction through an explicit FEA solver.

By doing in this way, we aim to demonstrate that the set-up of FEA computational surgical tools may be simplified in order to provide assistance to non-expert FEA engineers or medicians in more precise way of using FEA tools.

# Contents

# Chapter 1 - Introduction

The surgical simulators and the preoperative planning are the tools that help surgeons in different medical applications such as improving dexterity, or to try to understand the possible issues present in a complicate surgery.

For example in India, the ancient practitioners have used leaves to represent three dimensional (3D) flexible tissues and plan the surgical operation [1]. Nevertheless the problem to elaborate a particular pre-operative planning was an impossible task before the advent of medical imaging, so a century ago the only way to see inside the patient was directly in the operation process or by a dissection in cadavers. Due to these limitations, in the 17th century specific reconstructions were made by a Sicilian doctor, Giuseppe Salerno [2]. In the 19$^{th}$ century a French physician, Louis Thomas Jérôme Auzoux improved and popularized anatomical papier- mâché models [3]. Until today the medical student uses the plastic anatomical models to study and identify the human parts, its popularity is due to the low cost and the realistic representation of the human parts, which can be assembled. Nevertheless these plastic models cannot supply the use of cadavers or animal to train to new doctors. Currently, in addition to surgical simulator based on virtual reality, it is possible to obtain personalized mock-ups in relatively short time by Additive Manufacturing technology. Particularly, Ninjaflex filament can be useful to obtain models more compliant to reality.

Nowadays, due to the increase in number of MIS and its complexity, the demands on surgical education is exponentially increased. Otherwise, it is necessary to speed up the learning process so that the surgical simulator plays an important role for the capability of repeating tasks, doing the surgical simulator a safe and ethical method for surgical training and pre-operative planning.

Surgical simulators based on virtual reality represent the actual evolution of medical and surgical mock-up [4], [5]. They are based on multidisciplinary expertise that ranges from computer engineering, automation and sensors, physics, mechanical engineering and, of course, medical knowledge. The surgical simulator generally uses virtual patients. In this way the surgical simulator can reproduce realistic human anatomy including some pathology, so that students can practice on a

wide range of specific cases with different level of specificity. Hence, when the student is in learning stage the patient safety is not compromised even in some cases the surgical simulators provide haptic feedback to the user. In addition, surgical simulation systems can be used to train health care professional, becoming as a useful tool for pre- and intra-operative planning of medical interventional procedures.

Simulation of the physical behaviour of the anatomical district under investigation, of the related parameters of the patients, and of the effects of the manipulation during surgery is extremely important to reach reliable simulators useful not only for dexterity mentoring, but also to achieve pre-operative plan. The use of simulation system is highly significant when complicated surgical procedures require a customized pre-operative plan prior to perform an operation as it brings the particular anatomical details as well as consider the real geometry of the soft tissues that interact with the surgical device and its properties. These capabilities of surgical simulator may help clinicians to increase accuracy of the surgical procedure and to minimize the patient trauma.

A fundamental research question that has not been answered yet is that how much fidelity is necessary in a surgical simulator in order to provide an appropriate skill for real procedures and it is obvious that the fidelity strictly depends on simulation set-up: geometrical model, mechanical behaviour of the soft tissues and boundary conditions in terms of loads and constraints, and type of approach adopted for the numerical solver. On the other hand, for surgical pre-operative planning, accuracy is much more important than in surgical simulator for dexterity, so that different levels of fidelity can be determined by the clinical application. For example, procedures like stapled colorectal end-to-end or when it is necessary to clarify the mechanics of tissue stapling and associated phenomenon [6] or in procedure like biopsies where we have to understand and predict the trajectory of the needle while penetrating the tissues in order to reach the tumour.

The numerical approach for finding the solution is a topic related to the requirement of real-time solution. It is necessary for the fidelity of the reaction chain medician-tool-anathomical district. The complexity of the physics behind the simulation may ask for different numerical approaches (e.g. linearization of the equations, FEA solvers with different levels of simplifications), with different level of accuracy and thus final fidelity. On the other hand, in any case the, haptic feedback can contribute to the

high fidelity [7] at the moment to reproduce the interaction between the soft tissues and a surgical device.

Figure 1.1 explains such concepts through a general workflow diagram starting from the data acquisition and reaching at the force feedback to user through haptic systems (Figure 1.1). In order to ensure the real-time sensation in the simulation process, the system should guarantee the information flow to the proper speed to obtain a correct haptic and visual feedback.

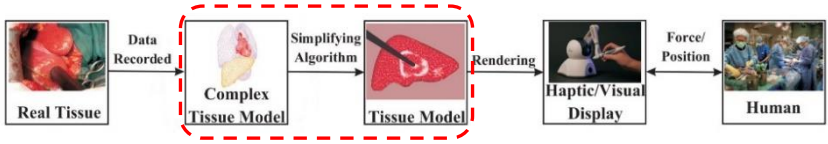


*Figure 1.1. General workflow to simulator development and application. The highlighted area represents the area of interest of this thesis (Reproduced from* [8]*)* .

Each one of these stages can be defined as a filter [8], in which information about force-motion relationship is lost or transformed. Even these "filters" can be understood as product of the equipment or instruments sensitivity. For example: a) when it is necessary to acquire the medical images, or b) in the laboratory tests that collect experimental data with the aim to determine the characteristic constants that describe the soft tissues behaviour. This filter can simply be a simplification of the tissue model to perform a real-time simulation in terms of visual and haptic rendering. In fact, the haptic system has its own dynamics that is affected by control issues in order to transform the virtual force toward the real environment and it is clear that each haptic system has particular resolution.

As shown in the highlighted part of Figure 1.1, the area of interest of this thesis may follow in the field of tissue modelling and simulation. The main goal is to investigate how Finite Element solvers may support medical simulators and their fidelity. In particular we are going to determine the importance of parameter that can influence in the development of complex virtual environment. It is focused on analysis of the effects produced by: a) geometrical model approximations, b) different mechanical behaviour of soft tissues, c) thickness variation and its influence toward force feedback. All of these parameters are analysed when an interaction between the surgical clamp and the soft tissue is

produced. Particularly, this interaction is found in different surgical processes as: colorectal, bariatric, thoracic surgeries, etc. These preliminary results will help to researchers to understand the influence/importance of these parameters in the final results. Indeed these evaluations can be helpful to justify the simplification of complex geometrical models or mechanical behaviour giving the possibility to understand inaccuracy generated by these approximations.

## *1.1. Motivation*

The increase of MIS implies an increased demand in number of professionals with skills such as hand-eye coordination and dexterity, because in MIS the doctor does not have direct access to tissue manipulation. Most important skills are usually acquired through a repetitive process of surgical procedures that are risky if they are performed on patients. Many medical students practice by using corpses or animals but these procedures are subject to ethical problems. At this point, it is important to note that not only ethical issues are present but also anatomical problems arise while using animals. Although certain animals' organs have some similarity with human beings, their anatomy is completely different. Another problem presents while using human corpses is the physiology because they react differently to those of a living patient. Moreover, in all of these problems it must be added the difficult to repeat the process several times in order to obtain the desired skill, since practice on real organs may be done only one time and of course all of these factors provide obstacles in learning.

In recent years with the advance of technology, it is possible to think about recreation of virtual environments that are capable of producing phenomenon similar to those being faced by a surgeon during surgery. However to obtain a simulation that is close to reality, it is thus necessary to consider: a) the effects induced by the soft tissues, b) accuracy of geometrical model obtained through images segmentation, and c) the theory of large displacements, among others. In particular, the simulations using Finite Element Analysis (FEA) that consider the large displacement theory have not extensively documented yet. With this research we aim to understand the phenomena involved in a surgical simulation by evaluating the errors that can lead the parameters approximations induced by the FEA set-up, and thus, contribute to the development of more accurate virtual simulators which are capable of

reproducing the phenomena that are introduced in surgical operations. The use of virtual environment leads a great advantage for surgical students who can repeat the simulation processes as many times as necessary. At the same time, the use of virtual simulators to carry out preoperative plan helps the doctor to understand the possible difficulties that he have to face during a surgical process. Finally, as a third positive relapse, they can even be used for the design of new instruments for highly complex surgical processes.

## *1.2. Scope of the dissertation (dissertation contributions)*

The scope of this work includes the following:

- ✓ Analysing how a linear or a nonlinear description of the mechanical behaviour of the soft tissue affect the mechanical response of colorectal surgical simulation.

  The virtual simulators for preoperative planning or surgical simulators for specific procedures, often assume an approximation for mechanical behaviour where typically a linear elastic behaviour is assigned as mechanical behaviour of the soft tissues. Those considerations are mainly assumed due to large number of computational resources necessary to execute a real time simulation on non-linear behaviour. Having in mind that soft tissue has a non-linear viscoelastic properties. In, this research we quantitatively compare non-linear and linear elastic mechanical behaviours to understand inaccuracy produced while using a linear approximation. In this way, it can be seen that the importance of proper selection of mechanical behaviour for different applications, also considering where it is necessary to provide a force feedback. Aspects related to this point are explained in Chapter 5 and some results are published in [9].

- ✓ Evaluating the effect related to the accuracy of the organ's geometrical reproduction in a surgery simulation.

  In this work, we can investigate colon-rectal surgical simulation with geometrical models of different levels of accuracy, starting from a plane surface and continuing with a cylindrical surface, a

3D-SS surface which was obtained from MRI images (approximation of real model without colon folds) so to arrive towards a real geometrical model which considers the colon folds. Doing so we aim to understand the influence of the organ's geometrical details and related inaccuracies that they produced in terms of stress and strain.
For the two most complex models, to obtain the 3D model, image segmentation and reverse engineering post-processing were also carried out. In particular, we provide two techniques for image segmentation and model refinement. The first one is a semi-automatic technique using the software 3D-slicer and the second one is an automatic technique based on convolutional neural network (Chapter 3). Finally, HyperWorks software has also been used in order to generate the mesh in geometrical models obtained from the process of segmentation. This work is presented in Chapter 5 have also been published in [9]–[11].

- ✓ Effects of FEA model set-up on force contact evaluation.

After the understanding of the role of the material model and the geometric accuracy of the organ, on the stress-strain behaviour, results are discussed in terms of force contact. It is done to better understanding how a specific type of FEA solver, the explicit one, may help in a better description of the non-linearity present in the phenomenon without increasing dramatically the simulation length.
In a clamping of the colorectal tissues, the quantitative evaluation of the force feedback is based on variation of the mechanical behaviour, thickness, and geometrical model. Therefore, in this thesis we investigate the interaction of surgical clamp with soft tissues, evaluating the evolution of the force feedback when the process of clamping is produced by providing a series of translational and rotational inputs to reach the fixing of the tissues. Also the cinematic chain of the surgical clamp is analysed when the surgeon apply a force to fix the tissues. It is important to note that the tissues generate a reaction in response of action on the surgical clamp and this reaction also is transmitted through the same cinematic chain. More importantly this force is appreciated in the handle where the surgeon holds the surgical instrument.

## *1.3. Dissertation Overview*

The dissertation is organized as follows.

Chapter 2 provides an introduction to MIS and surgical simulation in combination with the essential theory of the continuum mechanics and FEA, followed by: a description of the applications already done in this area; a brief explanation of the challenges related to virtual surgery simulations.

Chapter 3 describes the kinematic chain of a generic surgical clamp and it presents the work made on the CT model reconstruction used for the geometrical accuracy investigation. More in details, it introduces an image segmentation process based on convolutional neural network with the aim of obtaining a more accurate geometrical model.

Chapter 4 clarifies the environment, the FEA set-up and related inputs are discussed in combination with the boundary condition for colorectal surgery application, based in preliminary topics necessary to carry out the work.

Chapter 5 presents the results of the sensitivity analysis of four factors important for modelling tool and tissues interaction:

- ✓ Mesh length;
- ✓ The comparison between different soft tissue's mechanical behaviour models for surgical simulation;
- ✓ The importance of geometrical model of the organ;
- ✓ The effects of varying the thickness of soft tissues;

Finally, chapter 6 synthesizes several key points and issues presented in the previously described sections. After it, conclusions and directions for future research in the area of realistic modelling of tool-tissue interactions are introduced.

At the end of each chapter, a brief summary of the related topics is presented according to the overall aim of the work.

# Chapter 2 - State of the Art: Virtual Surgery Simulations, and Finite Element Analysis

Through time people have always intended to understand the human body, for that reason many ways to represent and model the structure of the human body have appeared and evolved over time. These techniques have intended to comprehend and reproduce the functions of observed phenomenon. The motivation to reproduce a complex study case plays an important role into pre-operative planning to try to determinate the most efficient procedure and to anticipate possible complexities present in the surgery process. The medicine as other sciences evolves with the time, in particular the way to carry out a surgical process has changed from an open surgery to MIS.

This chapter aims to provide an overview of the state of the art concerning with this aspects and with the methodologies that will be applied in the next of this work. For these reason, Section 2.1 shows an overview about MIS and surgical simulators, Section 2.2 presents the most popular theories of linear and nonlinear elasticity applied in soft tissues. Section 2.3 provides an overview about Finite Element Analysis. Sections 2.4 presents the FEA apply to soft tissues. Section 2.5 summarises the commercial surgical simulators. Finally the Section 2.6, describes some important guidelines for research in the area of realistic modelling of tool-tissue interactions.

## *2.1. Minimal invasive surgery and surgical simulators*

MIS stands for Minimal Invasive Surgery. It is a procedure that allows surgeons to use endoscopic techniques to address a variety of issues, technically MIS refers to any surgical procedure that is performed through tiny incisions instead of a large opening. During MIS, the surgeon makes several small incisions in the skin, which typically are few millimeters long. As it can be seen (Figure 2.1), trocars are located in the incisions. Through them it is possible insert the necessary surgical instruments to the surgery. One of these incisions is used to insert a laparoscope, which has a tiny, and high-resolution fiber-optic camera on its end. The images from laparoscope are sent to monitors, then the

surgeon can view clearly the area needing surgery. These visual feedback is also used as a guide to see into the surgical area and direct the tools being used, as it is shown in Figure 2.2.

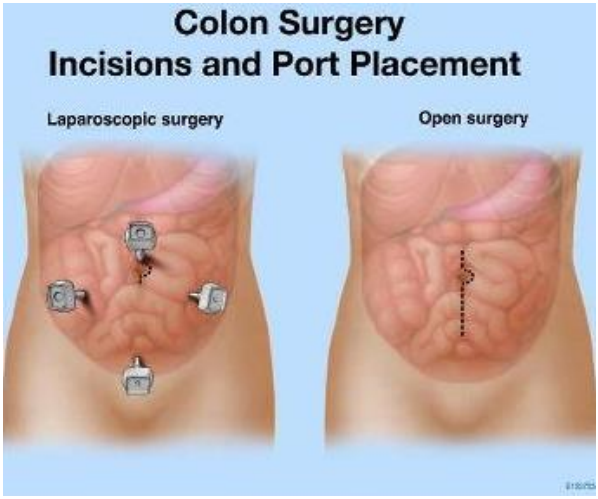


*Figure 2.1. Colon surgery: Laparoscopic surgery vs open surgery (Reproduced from* [12]*)*

Currently it is possible to speak of two different types of MIS, as laparoscopic surgery and Robotic surgery. Laparoscopic surgery has benefits that have been well documented [13]–[19], among them the most relevant are:

- ✓ Less hospital time
- ✓ Faster bowel function return
- ✓ Less trauma to organs
- ✓ A few small cuts versus a large incision
- ✓ Fewer wound related complications (Less trauma to the muscles, nerves and tissues)
- ✓ Less bleeding
- ✓ Less scarring
- ✓ The postoperative short-term effects and morbidity are less.
- ✓ Less pain and reduced use of narcotics
- ✓ Less effect on the immune system
- ✓ Faster Recovery

In some cases, it is also possible say that the MIS offer a Higher Accuracy Rate, because of MIS procedures use video-assisted equipment,

and by the use of a camera is possible to magnify the internal organs in the screen to obtain a better visualization (Figure 2.2).

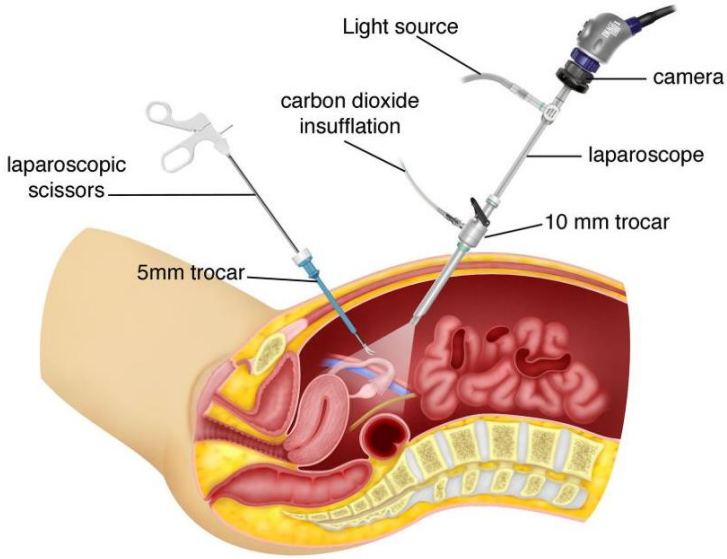


*Figure 2.2. Overview about laparoscopic surgery (Reproduced from* [20]*)*

Nevertheless some MIS procedures and surgeries may not be suitable for every patient, and there are some disadvantages of MIS as following:

- ✓ Minimally invasive surgery requires specialized high-end medical equipment
- ✓ Surgeons need specialized training
- ✓ The equipment used with MIS is more expensive
- ✓ There are various procedures, especially the most recent surgeries that may take longer

In view of the great advantages presented by MIS, in the last years has increased its application in different medical fields. Generally the student of medicine, or the new surgeons need a lot hours of practice before to do a real surgery process. More in details, it is important to mention that the MIS implies that surgeons practice a series of tasks to improve their dexterity skills before to practice in the real patient, like 3D-orientation, instrument handling and one of most important skill is the hand-eye coordination.

Surgical education has traditionally depended on the apprentice-mentor relationship, and it is the basis of residency training programs. However, the utmost problem for the surgeons to reach a high level of technical skills is the difficulty to practice in the same conditions that are presented in a real surgery. Typically the practice process of learning particular surgical operations involves animals, cadavers, physical patient models, and real patients, but all of these present disadvantages. For example:

a) When animals are used, its anatomy is so different despite of having certain similarity in some organs or in the form that these work.

b) In the case of cadavers once the blood flow has stopped, the physiology drastically changes, so not only the different biological and anatomical are present, indeed to obtain cadavers or animals to practice a certain number of times to achieve the skill desired represent a very big trouble and obviously adding the ethical and moral problems.

c) By other hand the physical patient models like the pelvi-trainer presents a lack of realistic anatomical features, and it is so difficult to practice directly in a real patient. All of these difficulties commonly decrease the speed of learning in the new surgeons.

Some approaches have been introduced in recent years which exploited the advancement in computer hardware and software that can help to resolve several mentioned problems by means of Virtual Reality (VR) applied in medicine. Important applications of virtual Reality are cited as follows:

- ✓ Computer Aided Surgery
- ✓ Diagnosis
- ✓ Pre-operative planning
- ✓ Training
- ✓ Tele-surgery
- ✓ Rehabilitation

Applications in surgical training system use the knowledge of VR in combination with simulation techniques for tissue deformation to build virtual environments for surgical simulators that presents a more cost-effective and efficient alternatives to traditional training methods by avoiding ethical problems and providing the facility to repeat the

procedure for desired number of times. Additionally, the surgical process based on VR has become a technology that can teach new techniques to surgeons, to improve their current skills and even determine their level of competence before they operate patients [21].

Thanks to capability of the computers to solve a lot of differential equations in shorter period of time and the development in the computer graphics in order to obtain high-fidelity graphics have made it possible to create simulations of medical procedures. In addition, the main purpose for making surgical simulators is to create a virtual environment that is able to produce the phenomenon present in surgical process. In this case the emphasis is given to the user-environment interaction that means real-time interaction among medicians, surgical tools and simulation of the involved physical process through VR.

In virtual environment there are different methods to create physical modelling of the organs to analyse the deformation of the internal tissues. The most used are:

- ✓ Mass-spring damping method
- ✓ Finite element method (FEM)
- ✓ Long element Model (LEM) method

Each of them has a different level of accuracy in predicting the physical behaviour, so that they are useful only for a limited subset of VR applications. Generally speaking pre-operative planning is one of the most difficult to be set-up according to the fact that it asks for real-time rendering of complex and multiple aspects (from local anatomy, to soft tissue behaviour, to stress-strain and pressure registration, and so on).

In 1991 was presented the “Karlsruhe Endoscopic Surgery Trainer” [22]. Figure 2.3 shows one of the first virtual simulator for endoscopic surgical process, which allows real-time visualization of the surgical procedure along.

The commercial surgical simulators typically make some simplifications to reduce the computational cost so to achieve the real-time simulation [21]. Commonly these simplifications are based on two methods:

a) Methods that apply linear elastic mechanical behaviour instead of hyperelastic mechanical behaviour, and

b) Methods that solve the deformations fields from full non-linear to linear analysis.

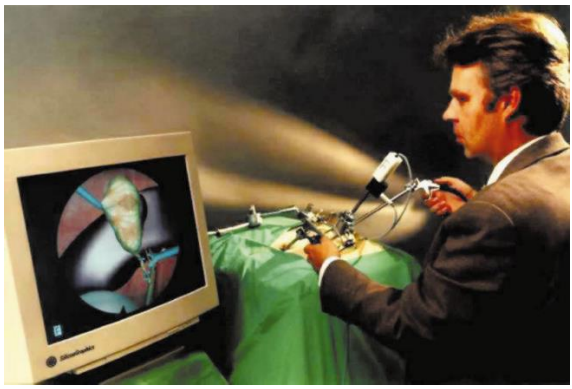

*Figure 2.3. The MIS training system for VR-based simulation of the cholecystectomy (Reproduced from* [22]*)*

Indeed some of these surgical simulator are used to train new surgeons through virtual reality and are focused on dexterity for haptic devices that mimic the surgical tool where these assumptions are applicable. Nevertheless the linear solution method as described in [21], [23], solves only (locally) linear deformations, so its assumptions can be seen as a drawback that should be noted.

Nowadays, the approaches of the surgical simulators based in VR are not only useful for applications above mentioned. They also are suitable to optimize the design of surgical tools to create "smart" instruments capable of assessing pathology, or force-limiting novice surgeons, as well as to understand tissue injury mechanisms and its damage thresholds [8]. In these cases are necessary the development of realistic surgical simulation systems, taking into account the accurate modelling of organs, real soft tissues mechanical behaviour and the correct solver able to calculate in accurate way the deformations produced by interaction between surgical instruments and organs. Therefore, the use of hyperelastic models [24]–[27] are required, because of a major accuracy is requested in the stress-strain evaluation, like in preoperative planning of surgeries phases as tissue detachment and implant analysis.

Finite Element Analysis (FEA) is currently one of the most accurate ways to simulate the interaction among non-rigid components. Thus its adoption in medical application can be relevant for a better understanding

of the phenomena. Otherwise, it has major drawbacks in computation times, so it is not suitable to be extensively applied in VR. Nevertheless it can be adopted as a preliminary set-up tool.

The realistic modelling and simulation of tissue mechanics is an active research area, due to difficulty in finding a mathematical formulation that describes the behaviour of tissues in different ranges of strain in an accurate way and the difficulty to elaborate experimental tests to determine tissue parameters.

To obtain a virtual environment where the surgeons can practice by means of fully immersed realistic environment which implies that the surgical simulator must be able to show in an accurate and realistic manner for anatomical details, deformation of the organs and also deliver an authentic feedback for tool-tissue interaction to the user.

## *2.2. Continuum Mechanics of soft tissues*

The mechanics of the continuous medium is a branch of mechanics that starts from the mechanics of particle system. The mechanics of the continuous medium gives us the possibility of study the deformation or motion of a continuous material under the action of forces [8], [28]. The present section provides a brief introduction to the mechanics of soft tissues using the theories of linear and nonlinear elasticity.

The human organs and the majority of the soft tissues are inhomogeneous, anisotropic, and viscoelastic, for this reason it is necessary to establish complex experimental protocols to obtain in accurate form their mechanical behaviour.

The mechanical properties of tissue can be measured either “in vivo” or “ex vivo”. Nevertheless, to determine an accurate soft tissue model, it is necessary to measure the tissue properties in vivo due to the physiology change that effect drastically in an ex vivo specimen as a result of the variation in temperature and blood circulation, becoming as a characteristic that hardly can be consider in an ex vivo test. In literature, the effects of different testing conditions [29] has been studied, which demonstrated that the mission of choosing or determine an appropriate soft tissues constitutive law capable to describe the stress-strain response when the tissues is subjected a different load conditions is not straightforward.

In field biomechanics, many laboratory tests [30]–[33] have been performed to determine the mechanical properties of soft tissues in both people and animals. Considering that colon and surrounding tissues [33] have a mechanical behaviour that is nonlinear viscoelastic but due to difficulties in performing laboratory tests different work [33], [34] has introduced for mechanical behaviour approximations as linear elastic and hyperelastic material models.

Linear Elastic

Simplified material models such as linear elastic model has been used in bioengineering simulations that does not involve high accuracy in the stress-strain evaluations like training of new surgeons through virtual simulators based in virtual reality. In fact in this case, the focus is on dexterity of using haptic devices that mimic the surgical tool [8].

Materials exhibiting linear elasticity obeys the generalized Hooke's Law, which relates the stress σ, and infinitesimal strains ε, by the fourth-order tensor of elastic moduli, $\tilde{C}$, as:

$$\sigma = \tilde{C} : \varepsilon \tag{2.1}$$

where: σ represent the Cauchy stress tensor, $\tilde{C}$ is a fourth-order tensor usually called the stiffness tensor or elasticity tensor and ε is the strain tensor.

Colorectal tissue studies based on destructive test [27] have determined that, from the statistical point of view, the colorectal tissue can be assumed to be an isotropic tissue. Also in this case, in order to reduce the complexity of the problem, some authors [27], [30], [35] have considered the simplified Linear Elastic (LE) mechanical behaviour of the tissue. It provides a linear approximation of the stress-strain behaviour through the Hook law, Figure 2.4 When the material is isotropic, the tensors are reduced and the material properties can be described by using young modulus (E) and Poisson ratio (ν).

In the continuum mechanics the law of elasticity of materials is one of the crucial consideration to take in account at the moment to select the type of analysis.

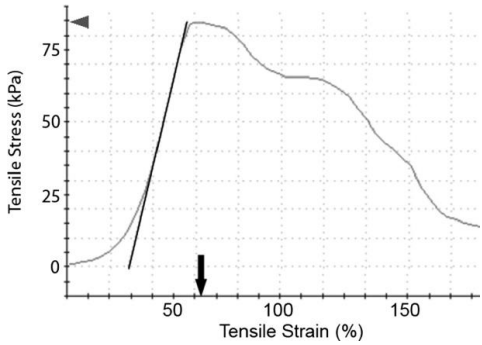


*Figure 2.4. Linear approximation of nonlinear mechanical behaviour (Reproduced from* [36]*).*

Hyperelastic

When the materials are undergoing deformation with large strain typically higher than 1%-2% to obtain a better fitting of their mechanical behaviour, it is thus, necessary to describe them by nonlinear elasticity theory. On the contrary, the hyperelastic models [25]–[27], [37] are demanded when the stress-strain evaluation requires a major accuracy such as preoperative planning of surgical phases which includes tissue detachment and implant analysis. Hyperelastic models may replace a nonlinear visco-elastic if the simulation does not requires load cycling as it happens in relaxation phenomenon [38].

Concerning hyperelastic models for bioengineering tissues, many formulations have developed that have been applied and compared in literature. All of them are based on the strain energy density function (*W)*, that can be described in different ways as a function of the first ($I_1$) and second invariant($I_2$), or according the deviatoric principal stretches ($\lambda_i$). As a consequence of this, each of them requires the evaluation of numerous empirical parameters that in some cases may be numerous. This causes a more difficult calibration set-up and generally a more difficult application. Nevertheless, some complex cases require the use of this kind of method. For example, in [39] dynamic response of artery segments in different states (healthy or with pathologies) are resolved through dedicated numerical simulations in Matlab. In that research, Mooney-Rivlin model is applied as a good trade-off between accuracy and easiness of implementation and parameterization, thanks to a reduced number of parameters to be calibrated through experimental characterization of the materials.

Also the simulations made in Abaqus with the Neo-Hookean model are described in [40] for simulating the tendon of diaphragmatic hernia. In this case, approximations have been made according to the specific knowledge of the problem such as isotropic behaviour of the central tendon.

Among more sophisticated models, the Holzapfel–Gasser–Ogden model (HGO) results is able to accomplish many phenomena present in biological tissues according to the field of strains that occurs [41]. Its description is based on the strain energy function formulated through different terms which are activated according to the strain field achieved (linear isotropic behaviour at small strains; anisotropy and visco-elastic behaviour in the range of large strains). It is applied in cardio-vascular applications as reported in [42], where pathologies involve a wide range of strain.

The most popular used models to describe rubber or soft tissues hyperelastic behaviour are described as follow:

*Mooney-Rivlin model*

The hyperelastic Mooney-Rivlin model is described using the strain energy density function $W$ in terms of the first($\bar{I}_1$) and second($\bar{I}_2$) invariant. This phenomenological model uses the constants characteristics of the material $C_{10}$ and $C_{01}$, that work well for moderately large stains generally up to 100% in uniaxial elongation and shear deformation [35], [43], [44]. It is important note that this particular model cannot capture the upturn (S-curvature) of the force-extension relation in uniaxial test and the force-shear displacement relation in shear test [45].

For a compressible material, the model has a form as follows:

$$W = C_{10}(\bar{I}_1 - 3) + C_{01}(\bar{I}_2 - 3) + \frac{1}{D_1}(J_{el} - 1)^2 \qquad (2.2)$$

*Neo-Hookean model*

Neo-Hookean model is so similar to Hooke's law although it corresponds to a hyperelastic model. Commonly it is simple to use and can make good approximation at relatively small strains and it typically up to 20% [46]. Sometime this model can be seen as a special case of Mooney-Rivlin form with $C_{01}$= 0, and it can be used when material's data is insufficient. [45].

But, it neither can capture the upturn of stress strain curve. This model is given as:

$$W = C_{10}(\bar{I}_1 - 3) + \frac{1}{D_1}(J_{el} - 1)^2 \quad (2.3)$$

*Full polynomial model*

This particular model depends on the first ($\bar{I}_1$) and second ($\bar{I}_2$) invariant of the left Cauchy-Green deformation tensor.

The polynomial model is given as:

$$W = \sum_{i,j=0}^{N} C_{ij}\ (\bar{I}_1 - 3)^i(\bar{I}_2 - 3)^j + \sum_{i=1}^{N} \frac{1}{D_i}(J_{el} - 1)^{2i} \quad (2.4)$$

where:

$C_{ij}$ = material constants that control the shear behaviour and can be determined from uniaxial, biaxial and planar tests.
$D_i$ = material constant that control bulk compressibility and is set to zero for fully incompressible rubber. It can be estimated from volumetric test.
$J_{el}$ = Elastic volume ratio
N = Number of terms in strain energy function.

*Yeoh model*

The main characteristics of this phenomenological model consist on: i) it can capture upturn of stress-strain curve, ii) it has good fit over a large strain range, and iii) it can simulate various modes of deformation with limited data [45]. This model is described by using the strain energy density function (*W)* in terms of the first ($\bar{I}_1$) invariant. The Yeoh model is also known as the reduced polynomial model because it corresponds the form of third-order polynomial.

For compressible rubber, this model can be given as:

$$W = \sum_{i=1}^{3} C_{i0}\ (\bar{I}_1 - 3)^i + \sum_{i=1}^{3} \frac{1}{D_i}(J_{el} - 1)^{2i} \quad (2.5)$$

Where $J_{el}$ stands for the Elastic volume ratio; $C_{10}$*, is the* constant characteristics of the material and $D_1$ is a material constant that controls bulk compressibility.

*Ogden model*

The Ogden model also corresponds to phenomenological model with the particularity that is based on principal stretches $\lambda_1$, $\lambda_2$, and $\lambda_3$ instead of invariants. The model is able to capture upturn (stiffening) of stress-strain curve and modelling rubber accurately for large ranges of deformation for extensions up to 700% [45].

$$W = \sum_{i=1}^{N} \frac{2\mu_i}{\alpha_i^2}\left(\overline{\lambda_1^{\alpha_i}} + \overline{\lambda_2^{\alpha_i}} + \overline{\lambda_3^{\alpha_i}} - 3\right) + \sum_{i=1}^{N} \frac{1}{D_i}(J_{el} - 1)^{2i} \qquad (2.6)$$

where $\overline{\lambda_i}$ is the deviatoric principal stretch. $\mu_i$, and $\alpha_i$ are temperature dependent material properties.

*Arruda-Boyce model*

Arruda-Boyce model is a hyperelastic and viscoplastic constitutive model [47] based on molecular chain network. In contrast to the constitutive models that are used for metals, the Arruda-Boyce model can not define the transition point between elastic and inelastic response clearly.

It has two parameter shear model based only on $I_1$ and works well with limited test data [45]. It is given as:

$$W = \mu \sum_{i=1}^{5} \frac{C_i}{\lambda_m^{2i-2}}\left(\overline{I_1} - 3^i\right) + \frac{1}{D}\left(\frac{J_{el}^2 - 1}{2} - ln(J_{el})\right) \qquad (2.7)$$

where:

$C_i$= characteristic constant of the material
$D$ = material constant that control bulk compressibility
$J_{el}$ = Elastic volume ratio
$\lambda_m$ = stretch

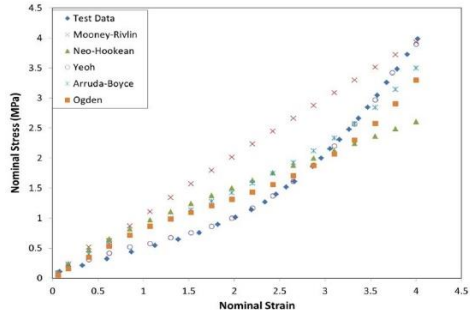


*Figure 2.5. Fitting of different hyperelastic models with uniaxial data (Reproduced from* [45]*)*

Viscoelasticity

The soft tissues often have inherently viscoelastic mechanical behaviour due that they are comprised of substantial amounts of interstitial fluid. Therefore, this mechanical behaviour involves a response that changes with the time as a product of tissue relaxation which implies different properties from a traditional solid materials that typically are described with a linear elastic or hyperelastic behaviour.

The viscoelastic behaviour shows:

- ✓ A reduction in stress with respect to the time when a strain is applied and is held constant over time. See Figure 2.6(a)
- ✓ A continue strain over time when a stress is applied and is held constant over time. See Figure 2.6(b)
- ✓ The stress values are dependent on the rate at which strain is applied. Figure load-unload

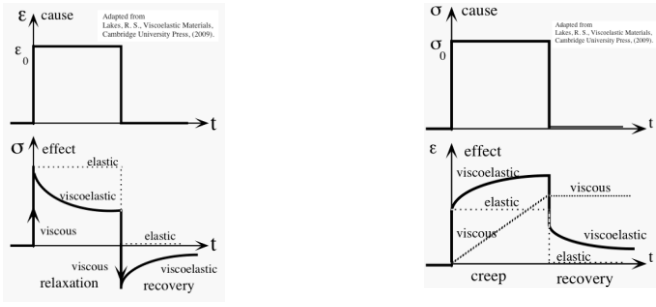


(a) (b)

*Figure 2.6. (a) Scheme of uniaxial strain applied and maintained to a long slender member associated with time-dependent stress and strain response. The time-dependent reduction in stress follows a fixed increase in strain that represents a typical stress relaxation response; (b). Scheme of a tensile stress applied and maintained to a uniaxial member associated with time-dependent stress and strain response. The time-dependent reduction increases in strain following the application of a constant stress which represents a typical creep response (Reproduced from*[48] *).*

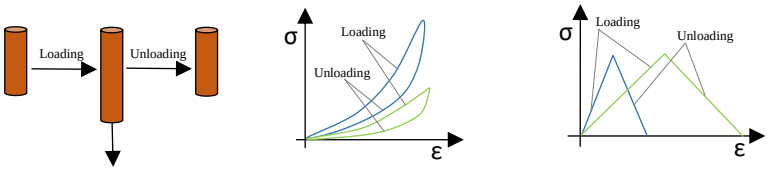


(a) (b)

*Figure 2.7. Relationship stress-strain analysed in load and unload process*

Figure 2.7 represents loading and unloading curves for a typical (viscoelastic) soft tissue. Where we can see the non-linear nature of the loading and unloading curves as well as the difference between the loading curve and the unloading curve. The stress response also depends on the rate at which strain is applied (b). Time course of strain for the material responses shown in (a). Note that the faster strain rate (red) results in higher stress.

All the above mentioned characteristics together with a nonlinear stress-strain relationship is difficult to do the characterization of biological tissues in a similar way to linear materials (e.g., most metals). Due to these difficulties in performing laboratory tests to characterize the soft tissues some researches [32], [33] have introduced mechanical behaviour approximations as linear elastic and hyperelastic material models but it is necessary to have in mind that the hyperelastic models may replace a nonlinear visco-elastic only if the simulation does not require load cycling like as it happens in relaxation phenomenon [38]. It has recently been confirmed in bioengineering simulations [49], where visco-elastic properties are invoked in the relaxation step in analysis of breast tissues by considering time that tend towards infinity.

## *2.3. Finite element Analysis (FEA)*

The Finite Element Method (FEM) is a numerical technique that has been developed by using concepts based on energy principles for example the virtual work principle or the minimum total potential energy principle in order to find a solution for engineering problems. It is difficult to solve a real life problem with the continuous material approach so the basis of all numerical methods is to simplify the problem by discretizing it. The FEA method was originated from the structure analysis problems in both civil engineering and aeronautical engineering. By searching approximate solutions to complex mechanical problems especially in elasticity and vibration analysis [50]. FEM solves partial differential equations on a defined domain which allows the description of the present phenomenon in a discrete model.

FEM yields approximate values of the unknowns at discrete number of points over the domain. As it can be seen in Figure 2.8, the continuum is divided into finite number of regions called elements which are connected by nodes that can be triad, quad, tetrahedrons, brics, etc. [23],

[51]. Also interpolation functions are used to approximate the behaviour of the field variables.

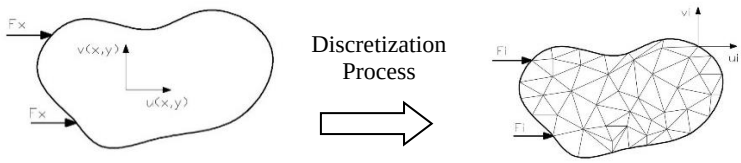


Continuous system Discrete model

*Figure 2.8. Discretization of continuum*

So far between the numerical methods, the FEM has a very good performance to solve partial differential equations over complex domains that can vary with time.

The characteristic partial differential equation that can describe the elements behaviour by the motion of material points of a continuum can be expressed as a discrete system of differential equations:

$$M\ddot{u} + C\dot{u} + Ku = F - R \tag{2.8}$$

where:

M= mass matrices

C= damping matrices

K= stiffness matrices,

u=is the vector of nodal displacements,

F and R are the external and internal node force vectors respectively.

Each and every one of the elements are defined in terms of the element's material and geometric properties also by distribution of loading at the nodes of the element. It is important to note that all these matrices and vectors may be time dependent.

Typically there are two types of analysis: a) linear and b) non-linear depending on the characteristic of problems and its condition and thereafter it is possible to select a solver implicit or explicit.

Linear analysis

In industry, typically it is easy to find some problems where certain type of assumptions are possible. Many of these problems are presented in structural analysis and due to the linear assumption it can be solved

with a linear finite element solver. The nature of the problem can greatly be simplified if higher order terms are dropped from the deformations and the material behaviour is assumed to be linear.

There are some parameters to consider when the problem can be analysed as linear, which are as follow:

- ✓ Small deflections
  Small deflections occur when obtained or predicted deflections are smaller than the size of the structure. Therefore, for thin structures a deflection that is less than the thickness would be considered a small deflection.
- ✓ Small rotation
  In the FEA codes with linear solver, all rotations are assumed to be small. It means that any angle measured in radians should be small enough that the tangent is approximately equal to the angle. Then the typical range to consider the rotations within a linear analysis should be less than 10 -15 degrees.
- ✓ Material properties
  In a linear analysis all materials are assumed with a linear elastic behaviour. Despite of the fact that some materials have an inherent nonlinear elastic behaviour and although they do not necessarily yield, their nonlinear behaviour enforce the use of nonlinear codes for solution. On the other hand, it is also important to consider the case when a structure is going to be loaded beyond its yield point even in this case the nonlinear analysis would also be required.
- ✓ Constant boundary conditions
  To consider a linear analysis into a FEA, the boundary conditions must not be dependent on the load application. Therefore, to consider a linear analysis the boundary conditions should be constant.

If all the above mentioned conditions are fulfilled, it is possible to select the linear solver approach for Eq. (2.8). Usually in the mechanical applications, the system is in equilibrium under an action of balanced forces and torques that can be defined as a static state where the constant $\dot{u}$ and $\ddot{u}$ are equal to 0. So the system remains at rest and considers a static load. In some cases where the load changes slowly the structure's response may be determined with static analysis by considering the quasi-static particular case.

A static problem that uses finite element solvers will solve the following equation:

$$Ku = f \tag{2.9}$$

where:

$K$: It is the global stiffness matrix (an assembly of individual element stiffness matrices).

$u$: It is the displacement vector response to be determined.

$f$: It represents the external forces vector applied to the structure.

The above equation is the equilibrium of external and internal forces and can be solved either by a direct or an iterative solver.

The acquired equilibrium equation for an element can be applied to each and every one of the elements into which the continuous system has been divided. Therefore, the equilibrium of each and every one of them is individually guaranteed. If the equilibrium equations of all nodes that join all the elements are presented, a set of equations is obtained that represents the equilibrium of the whole structure. These equations are obtained by assembling the equilibrium equations of the different finite elements that make up the structure. In every simulation iteration, a large number of element-stiffness and element-force vectors are assembled in a global system which leads to a system of algebraic equations.

When the nodal displacements of the elements are calculated the next step is to calculate the stress by using the constitutive relations of the material. In the linear static analysis where the deformations are in the elastic range, the stresses (σ) are assumed to be linear functions of the strains (ε). So, Hooke's law can be used to calculate the stresses.

Non-linear analysis

The nonlinear analysis refers to large displacement and rotations which are typically more that 5%. In a FEA there are three basic source of nonlinearity as follows:

- ✓ Geometric Nonlinearity
  In analyses involving geometric nonlinearity considers the change of the geometrical cross section as a result of large deformations. This nonlinearity can be related to large rotation

and large displacement. All of these geometrical changes such as structure deformations are considered in formulating the constitutive and equilibrium equations. In industry it is possible to find engineering applications based on geometric nonlinearity which involves the use of both large deformation analysis or small deformation analysis. Additionally, the effect of the geometry changes may implies a change in the load applied directions [50].

- ✓ Material Nonlinearity

  In the real industry, almost all engineering materials are inherently nonlinear but due to the difficulty to elaborate a single constitutive law for the entire range of environmental conditions such as loading, temperature and rate of deformation. Thus, some approximations are performed to simplify the mechanical behaviour in order to consider the most representative effects for the analysed case. So in this field, the linear elastic mechanical behaviour is the simplest assumption of all which is often called Hook-law.

  The material nonlinearity involves a nonlinear response in the stress-strain relationship which can occur when the stress exceeds the yield stress or force-displacement law is not linear. A brief classification of nonlinear mechanical behaviour can be given as follows:

  1. Nonlinear elastic
  2. Hyperelastic
  3. Elastic-perfectly plastic
  4. Elastic-time independent plastic
  5. Time dependent plastic (Creep)
  6. Strain rate dependent elasticity – plasticity
  7. Temperature dependent elasticity and plasticity
  8. Linear elastic-perfectly plastic
  9. Linear elastic-plastic
  10. Nonlinear elastic model which characterize materials with no fixed definition of yield point such as plastic but the strain is still limited up to 20 %.

  The hyperelastic models used to characterize the soft tissues have been presented in section 2.2

- ✓ Constraint and Contact Nonlinearity
  This type of nonlinearity often occurs due to the nature of simulated phenomenon. Many times the boundary conditions can be changed through its addition or remotion as the analysis progress. So the nonlinearity involves contact sets in the model which can get engaged or disengaged as a response of applied loads. Since this is a dependent nonlinear behaviour load, a linear solver will not handle properly this type of problem.

In the dynamic case that uses a nonlinear analysis, the Eq. (2.8) can be solved by considering the parameters $\ddot{u}$ and $\dot{u}$. Figure 2.9 summarizes the application.

To solve a problem using FEA, there are two integration schemes and its application depends directly on the condition of the problem.

- ✓ In an explicit FEM analysis, the state at a given instant is a function of the previous states. The explicit method does the incremental procedure and at the end of each increment it updates the stiffness matrix based on geometry changes (if applicable) and material changes (if applicable). Then a new stiffness matrix is built and the next increment of load (or displacement) is applied to the system. An explicit scheme can easily be implemented by avoiding the matrix inversion process but it potentially requires increments that are small enough to provide a suitable accurate and stable solution.

- ✓ In an Implicit FEM analysis, the state at a certain instant cannot be explicitly expressed as a function of the state at the previous time step because after each increment the analysis do Newton-Raphson iterations in order to enforce equilibrium of the internal forces with the externally applied loads. The equilibrium is usually enforced to some user specified tolerance. This scheme presents the particularity that it is necessary the inversion of the stiffness matrix at each time step, which is often a computationally expensive process.

The Implicit scheme is often known as unconditionally stable scheme whereas the explicit scheme is a conditionally stable scheme. The Figure 2.9 shows the common fields of application of these schemes [52].

For all characteristics and advantages described about FEA to obtain a discrete approximation in complicated geometrical model (free form geometrical models) and the capability of the computers to solve a lot of differential equations in shorter time with good results, the FEM has been extended to medical fields to simulate soft tissue deformation [25]–[27], [53]–[55] to create simulations of medical procedures.

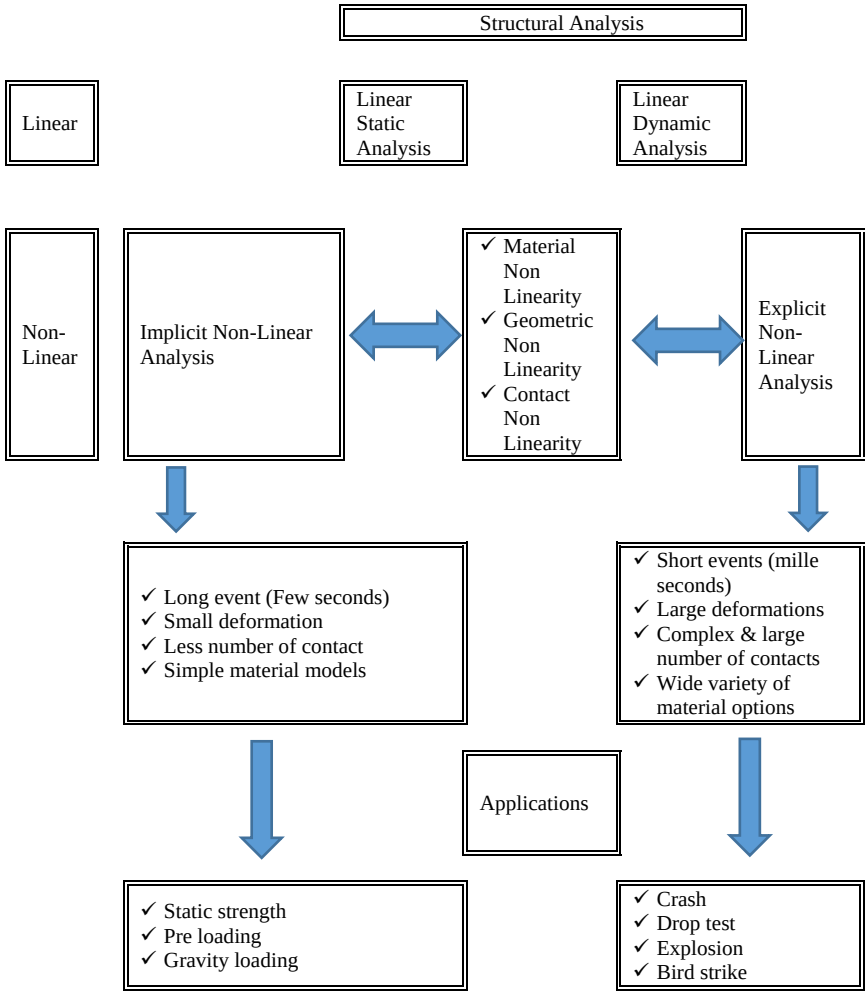


*Figure 2.9. Applications of implicit and explicit analysis* [52]

Commercial FEA codes for hyper elasticity

Nowadays, there are lot of commercial softwares available to FEA as for example Abacus [56], Ansys [57], HyperWorks [52], Comsol [58], Nastran [59], MCS/Marc [60] among others. (Table 2.1)

In Table 2.1, a summary of the most applied material model formulations is given together with basic references and commercial FEA codes that have already been implemented.

| Hyperelastic Material Model | Formula | Model description by: | Software that implement it |
|---|---|---|---|
| Ogden [45] | $W = \sum_{i=1}^{N} \frac{2\mu_i}{\alpha_i^2}\left(\overline{\lambda_1^{\alpha_i}} + \overline{\lambda_2^{\alpha_i}} + \overline{\lambda_3^{\alpha_i}} - 3\right) + \sum_{i=1}^{N} \frac{1}{D_i}(J_{el} - 1)^{2i}$ | First, second and third stretches | Abacus/ Ansys/ MSC-Marc/ HyperWork/ Comsol |
| Yeoh [45] | $W = \sum_{i=1}^{3} C_{i0}\ (\overline{I_1} - 3)^i + \sum_{i=1}^{3} \frac{1}{D_i}(J_{el} - 1)^{2i}$ | First invariant | Abacus/ Ansys/ MSC-Marc/ HyperWork/ Comsol |
| Mooney-Rivlin [39], [45] | $W = C_{10}(\overline{I_1} - 3) + C_{01}(\overline{I_2} - 3) + \frac{1}{D_1}(J_{el} - 1)^2$ | First and second invariant | Abacus/ Ansys/ MSC-Marc/ HyperWork/ Comsol |
| Neo-Hookean [40], [45] | $W = C_{10}(\overline{I_1} - 3) + \frac{1}{D_1}(J_{el} - 1)^2$ | First invariant | Abacus/ Ansys/ MSC-Marc/ HyperWork/ Comsol |
| Arruda-Boyce [45] | $W = \mu \sum_{i=1}^{5} \frac{C_i}{\lambda_m^{2i-2}}\left(\overline{I_1^i} - 3^i\right) + \frac{1}{D}\left(\frac{J_{el}^2 - 1}{2} - ln(J_{el})\right)$ | First invariant | Abacus/ Ansys/ MSC-Marc/ HyperWork/ Comsol |

To better understanding of continuum mechanics is necessary to review the concepts of tensors and operations with them, as well as the differential equations among others concepts. An overview of tensor analysis is beyond the scope of this chapter, but [61]–[63] it can provide a good introduction to this subject and its application to continuum mechanics.

## *2.4. FEA in soft tissues.*

In recent years, FEA has increased its applications in medical field particularly for making preoperative plans to simulate the response of tissues and organs, design of prosthesis, orthosis and to analyse implants and simulations of surgery [53]. Soft tissue simulations such as colorectal simulations (Figure 2.10) may be adopted to understand the interaction between colon tissues and surrounding tissues as well as the effect of instruments used in this kind of surgical procedures. In this way, FEA may improve the surgical procedure by optimizing or designing new instruments for robot-assisted laparoscopic or other minimally invasive surgeries [64]. Moreover, FEA may be useful to set up a virtual prototyping tool for the preoperative plan according to the particular characteristics of the patient involved in the surgery [27].

The literature presented in this section is refer to tasks that do not involve tissues rupture, it mean that is do no insert a surgical tools in soft tissues. The interaction simulations using FE method is presented in relation to mechanical behaviour as linear elastic and nonlinear elastic (hyperelastic)

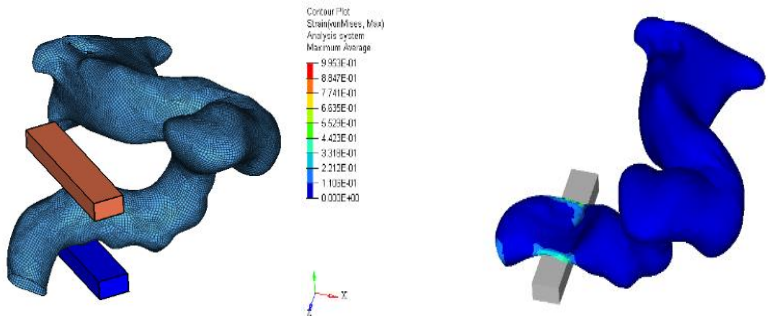


*Figure 2.10. FEA in soft tissues application*

Linear elastic finite element models

The linear elastic mechanical behaviour is probably the most popular assumption to simulate the tissues deformation into virtual surgery simulators. Linear elastic mechanical behaviour based on Hooke`s law presents some advantages for example: it needs only two constants to determine its behaviour (in isotropic and homogenous materials) it presents a simple way of implementation that has lower computational cost. These advantages enables real-time haptic rendering.

FEA commercial software (Table 2.1) often cannot simulate a phenomenon in real time because these software involved some steps to set-up the problem before to run FE calculation. Therefore researchers have introduced several approaches focused on optimizing FE based computational techniques to be applicable to surgical simulators where the real time can be a mandatory factor.

Some researchers have presented non-real-time surgical simulation system using linear FE modelling. In [65], is used a traditional form to solve a problem using the linear FE model, this approach is applied to simulate soft tissue deformations in a craniofacial surgery. [54] Presents a FEA to analyse the feminine pelvic mobility to understand the stresses experienced by women's pelvic system when simply standing or participating in physical activities and during different physiological functions. While in [27] is analysing the influence of Geometry and Mechanical Properties in simulation of woman pelvic floor with the aim to understand the mechanism that produce abnormal mobility.

In [66] the authors present a condensation method to an FE model for real-time surgical simulations, this method suggest to render part of all the nodes only which mean that only nodes undergo displacement and the near nodes need to be rendered. A comparison between the proposed method and the conventional linear FE analysis present similar results in terms of nodal displacement. Another research [67] present a real time simulation, thanks to a pre-processing of elementary deformations derived from a finite element method wherein the bulk of the computations were performed during the pre-processing stage of the FE calculation, this method was tested in a real-time hepatic (liver) surgery simulations.

In surgical simulation, it is possible to find FEA that considers the fluid-structure interaction, [68] presents a fast technique for simulating

fluid-filled elastic objects so this research can be useful to simulate organs filled with fluid. This approach was compared with experimental deformation data taken from a fluid-filled phantom.

Hyperelastic finite element model

Generally a nonlinear analysis involves large displacement and a hyperelastic mechanical behaviour as is the case of soft tissues undergo large deformations during surgical procedures. Even in this case the FEA continue to be a useful and accurate tool. Concerning the hyperelastic models it is necessary to select the correct model to describe the mechanical behaviour of the soft tissues, the Section 2.2 present some models based in the strain energy function.

In [27] the author present a comparison between Yeo, Neo-Hookean and linear elastic, applied to the soft tissues that make up the women pelvic floor to analyse the displacement when a pressure as product of the cough is applied, while in [25] the Yeo model to the rectum, bladder and vagina, is applied with the aim to analyse the pelvic organ prolapse (POP) that is present in women. It allows the surgeon to estimate the functional impact before implementation.

With the aim to obtain a realistic behaviour of deformable object in simulation for surgical training, in [69] is implemented the hyperelastic Mooney-Rivlin model. This work includes a propose scheme for mesh adaptation based on an extension of the progressive mesh concept to enable real-time computation of deformation.

Nowadays, it is possible to find software focused on the interactive computational medical simulation as SOFA (Simulation Open Framework Architecture), which facilitates collaboration between specialists from various domains, the most important feature of SOFA is that the simulator is organised in independent components in a scene graph data structure. Then, in each component it is possible to encapsulate a particular aspect regarding the simulation such as the degrees of freedom (DOF), the forces and constraints, the differential equations, the main loop algorithms, the linear solvers, the collision detection algorithms or the interaction devices. In [70] SOFA present an application to simulate the virtual ablation of a cardiac arrhythmia which is caused by an abnormal electrical activity in the myocardium. For this simulation was consider the phenomenological model from Mitchell Schaeffer [71]; which is able to reproduce the human electrophysiology using

physiological parameters. Even SOFA can be used for applications based on augmented reality [72]; this type of simulation allows us to estimate in real-time, the position of the liver internal structures by considering liver deformations.

## *2.5. Commercial surgical simulation.*

The surgical simulator system based on virtual reality proves to be a good option to train new surgeons, to practice new process, to elaborate preoperative planning that can help to understand tissue injury mechanisms even to evaluate the mechanical behaviour parameter that influence in the response of tissues and damage thresholds.

Figure 2.11 shows an example of virtual surgical simulator that focus on the hysteroscopy training.

*Figure 2.11. Hysteroscopy training simulation environment coupled with haptic device (Reproduced from* [73]*).*

Many applications of virtual simulations can be focused on the real phenomena that presents when there is an interaction between organs, surrounding tissues and surgical tools instead to obtain a real-time effect on the simulation. As in the case of pre-operative planning, where there are certain parameters that can influence an achieved accuracy of the simulation in terms of stress-strain distribution and force feedback.

Nowadays, it is possible to find several commercial virtual simulators focused on surgical simulations. However, the method used by the companies to simulate the soft tissues deformation is not easily available. Most of the commercial surgical simulators have an extensive emphasis on producing models that are visually appealing. Further, tissue material parameters are tweaked that are based on qualitative evaluation performed by few surgeons rather than actual material testing [8].

With the aim to obtain a realistic simulation and a complete immersive experience some surgical simulators provide a force feedback to the user by the use of haptic systems. For example Reachin Technologies AB [74] presents a cholecystectomy simulator (laparoscopic surgery process).

Depending to the surgical process in which the surgeons desire to get trained, it is possible to find different surgical simulator for each particular case for example Simbionix USA Corp. [75] sells GI Mentor IITM, URO MentorTM, PERC MentorTM, LAP MentorTM and ANGIO MentorTM. The Immersion Medical [76] provides different surgical simulator for vascular access and phlebotomy, bronchoscopy and gastro-intestinal procedures, percutaneous transluminal angioplasty and stenting procedures, myomectomy and basic hysteroscopy skills and laparoscopic abdominal procedures. Another companies that provide surgical simulator are; Surgical Science Ltd. [77], Haptica Inc. [78], Mimic Technologies Inc. [79], and Mentice AB [80],

Among the surgical simulators there are some that don't provide a force feedback but instead they focuses on training basic surgical skills or to provide superior visualization capabilities. Some companies that provide these type of simulators are: Medical Educational Technologies Inc. [81], and VRmagic GmbH [82].

For the use of this type of tools as a method for training or pre-operative planning it is, necessary to carry out a validation process in order to promote and motivate their use at hospitals or universities but it is so far for the validation techniques to be subjective [83].

## *2.6. Summary*

This chapter present an overview of MIS, its benefits and disadvantages as well as an introduction on continuum mechanics focused on soft tissues modelling with the goal to model surgical tool and

tissue interactions for the aim of increasing the assessment of structural simulation of soft tissue for the purpose of a better development of multipurpose surgical simulators.

We reviewed different mechanical model that are capable to describe the behaviour of the soft tissue when it undergoes to external forces. These mechanical models are described by characteristic constants acquired via experimental tests.

The theory and the simulations that are described here it is focused on the field of modelling methods that employed principles of continuum mechanics and used FE methods for simulation. These topics were divided that based on linear elasticity and nonlinear elasticity. Even in Section 2.5 is described some of the commercially surgical simulators available.

The literature presents many researches using FEA applied to tissues deformations and tool-tissue interactions using linear elasticity. However, it is limited the number of studies that have been conducted using the more realistic hyperelastic models (nonlinear elasticity). On the other hand, some researches and commercial softwares use a different approach principally employed to enable simulations to run in real time but in most of these simulations, the accurate physics behind tissue deformation is not considered a priority.

# Chapter 3 – Problem definition for colorectal surgery

With the aim to speed up the surgical simulations it is necessary to elaborate a sensitivity analysis of the nonlinearities by FEA.

## *3.1. Problem pipeline*

The following pipeline (Figure 3.1) summarizes the main stages involved in a surgical simulation process.

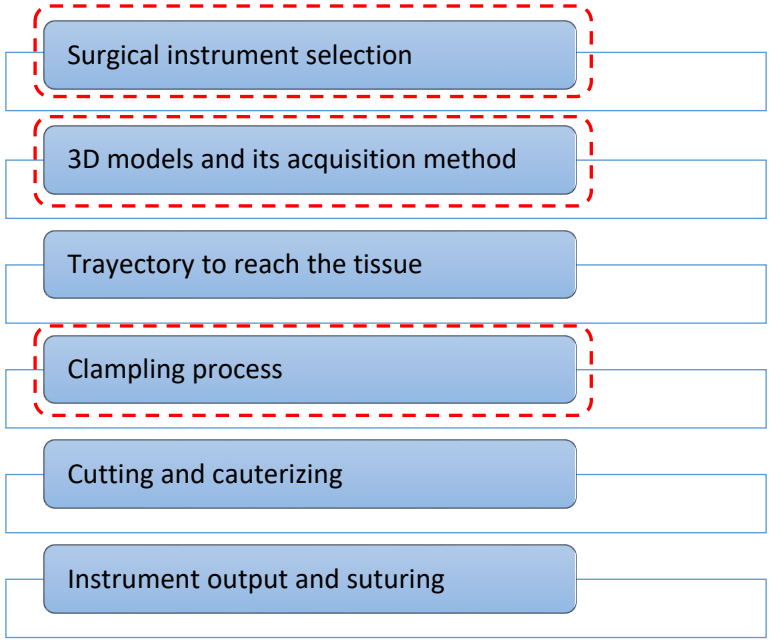


*Figure 3.1. Pipeline to elaborate a surgical process (The highlighted area is the main focus of this chapter).*

Each one of these stages is to represent a task in virtual environment. The area of interest of this thesis corresponds to the highlighted part of Figure 3.1. In particular, this chapter presents a description of selected surgical instrument and its kinematic chain analysis that in many cases is important to configure the haptic systems (Section 3.2) as well the 3D

models and its acquisition methods (Section 3.3). While the analysis of tissues clamping is explained in Chapter 4.

## *3.2. Surgical Tool: clamp*

In a laparoscopic surgical process, tools are always necessary to perform manipulation task as surgical clamp, needle drivers, etc.

As it was explained in Section 2.1, the MIS has become a popular technique due to lot of advantages either by using surgical assistant robot or following traditional (manual) way [84]. Nevertheless, due to increase in application fields, new issues also arise. In particular, instruments must be inserted through a trocar to access the abdominal cavity without capability of direct manipulation of tissues so that a loss of sensitivity occurs. This is caused by the absence of a direct force-feedback resulting from the interaction between surgical instruments and soft tissues in conjunction with an indirect field of view which makes the surgeons to undergo a series of training to acquire proper hand-eye coordination and the correct use of the tools before to do a surgery on real patient. Although the manoeuvring of most surgical tools are rather simple, the way in which MIS is carried out, makes the use of mechanisms involved in tool and is really challenging because of using this surgical tool to manipulate the tissues causes a reduction in the sense of touch.

While performing surgeries of a high level of complexity through robots or trocar-guided instruments, lack of force-feedback represents a great challenge and for this reason it is important to analyse the concerned kinematic chain. More in detail, the lack of force-feedback represents a problem in several areas that are strongly linked to engineering simulations. For instance:

- ✓ PREOPERATIVE PLANNING: The insertion of instruments during surgery causes deformations not only on target and surrounding tissues but also on instruments involved. The knowledge of force-feedback can help during preoperative phase in order to let the instrument be able to reach the specific target areas by planning its line of action and displacements. In addition, it is possible to protect instruments and organs from damage by optimizing lines of action.
- ✓ SURGICAL SIMULATORS AND TELEOPERATION: The complexity and wider diffusion of MIS require skilled and

trained operators. For this reason surgical simulators have been developed in order to accelerate the learning curve. Currently, these surgical simulators report feedback principally in terms of visual output with lack of haptic information about forces. This is also due to the fact that a simulation of the real behaviour of soft tissues may request high computational resources. The analysis of contact forces through simulation can avoid damage to tissues by improving skills. Analogous issues arise with teleoperation systems.

- ✓ SURGICAL ROBOT ASSISTANT: Mainly a robot can allow the use of instruments with reduced dimensions by giving the possibility to reduce the number of access points. This is one of the fundamental aspects of MIS [84] that allows faster recovery for the patient. In addition, the natural vibrations of the operator's hand can be avoided by using robot. Last but not least, a robot assistant can make a surgery safer through the use of virtual fixtures in order to avoid possible haphazard that are accidentally made by the surgeon. Currently, the usage of virtual fixtures involves significant physical constraints on the instrument. The increase of force-feedback accuracy can lead to an optimized use of the virtual fixtures (improving safety, accuracy and speed of the robotized tools) [24].

As explained, FEA tools may increase the understanding of those phenomena that is present in surgery when they use to elaborate preoperative plans and to improve surgical procedures. It is necessary to emphasize that the kinematic analysis of a particular instrument involved in a surgical process and principally in a laparoscopic surgery does not represent an isolated analysis. Therefore, FEA may play an important role to understand the distribution of stress-strain in the clamps and to evaluate contact force on instrument-tissue. Hence, with the kinematic chain analysis and by correct haptic system, it is possible to transmit the contact force to the surgeons by providing a force-feedback.

Clamp's cinematic chain.

This section provides models (Figure 3.2) and relationships which can be used to understand the force propagation in designing advanced grasper, clamps needle drivers and force-reflecting systems.

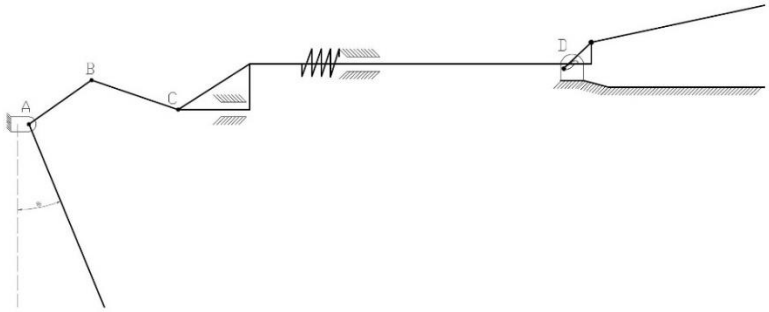


(a)

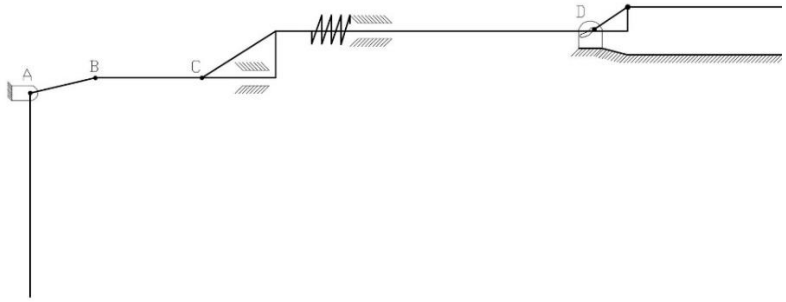


(b)

*Figure 3.2. Scheme of a generic surgical clamp (a) surgical clamp in maximum open position (initial position), (b) surgical clamp in maximum close position (final position).*

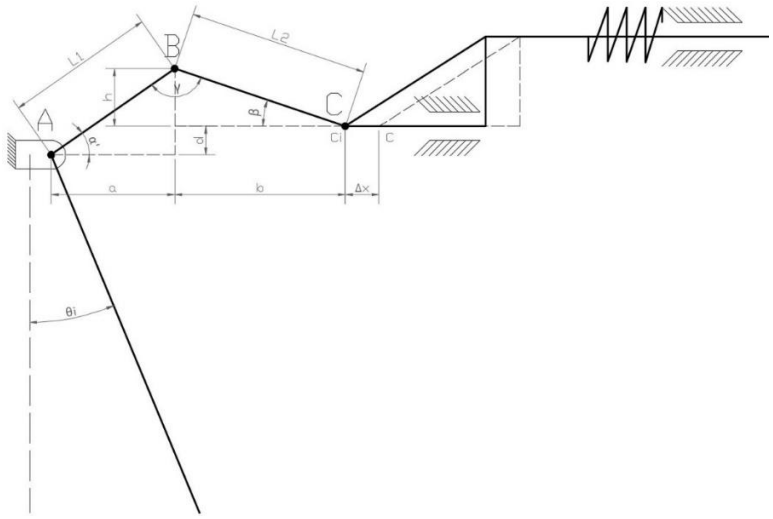


*Figure 3.3. Surgical clamp scheme (initial position).*

Relationship between links that makes the kinematic chain can be understand from Figure 3.3

$$\sin(\alpha) = \frac{d}{L_1} \tag{3.1}$$

$$\cos(\alpha) = \frac{a}{L_1} \tag{3.2}$$

$$\alpha' = \alpha + \theta \tag{3.3}$$

$$\sin\alpha' = \frac{h+d}{L_1}$$

$$h = (\sin\alpha')L_1 - d \tag{3.4}$$

$$\sin\beta = \frac{h}{L_2}$$

$$\sin\beta = \frac{(\sin\alpha')L_1 - d}{L_2}$$

$$\sin\beta = \frac{sin(\alpha+\theta)L_1 - d}{L_2}$$

$$\sin\beta = \frac{(\sin\alpha * \cos\theta + \sin\theta * \cos\alpha)L_1 - d}{L_2}$$

$$\sin\beta = \frac{\left(\frac{d}{L_1} * \cos\theta + \sin\theta * \frac{a}{L_1}\right)L_1 - d}{L_2}$$

$$\sin\beta = \frac{(d\cos\theta + \sin\theta\, a) - d}{L_2}$$

$$\sin\beta = \frac{\left(d\cos\theta + \sin\theta\sqrt{L_1^2 - d^2}\right) - d}{L_2} \tag{3.5}$$

Horizontal displacement of point "*C*"

$$\Delta x = C - C_i \tag{3.6}$$

where:

C= current position of point "C" in function of $\theta$

$C_i$= initial position of point "C" in function of initial value of $\theta$ . For this purpose it is called as $\theta_i$

The current position reached for point "C"

$$C = [\cos \propto' * L_1] + \sqrt{L_2^2 - h^2}$$

$$C = [\cos(\alpha + \theta) * L_1] + \sqrt{L_2^2 - [\sin \alpha' * L_1 - d]^2}$$

$$C = [(\cos \alpha \cos \theta - \sin \alpha \sin \theta) * L_1] + \sqrt{L_2^2 - [\sin (\alpha + \theta) * L_1 - d]^2}$$

$$C = \left[\left(\frac{a}{L_1}\cos \theta - \frac{d}{L_1}\sin \theta\right) * L_1\right] + \sqrt{L_2^2 - [(\sin \alpha \cos \theta + \sin \theta \cos \alpha) L_1 - d]^2}$$

$$C = [(a * \cos \theta - d * \sin \theta)] + \sqrt{L_2^2 - \left[\left(\frac{d}{L_1}\cos \theta + \sin \theta \frac{a}{L_1}\right) L_1 - d\right]^2}$$

$$C = \left[\left(\sqrt{L_1^2 - d^2} * \cos \theta - d * \sin \theta\right)\right] + \sqrt{L_2^2 - [(\mathrm{d} \cos \theta + \sin \theta * a) - d]^2}$$

$$C = \left[\left(\sqrt{L_1^2 - d^2} * \cos \theta - d * \sin \theta\right)\right] + \sqrt{L_2^2 - \left[\left(\mathrm{d} \cos \theta + \sin \theta * \sqrt{L_1^2 - d^2}\right) - d\right]^2} \quad (3.7)$$

The initial position of point "C" depends of the initial angle of $\theta_i$

$$C_i = \left[\left(\sqrt{L_1^2 - d^2} * \cos \theta_i - d * \sin \theta_i\right)\right] + \sqrt{L_2^2 - \left[\left(\mathrm{d} \cos \theta_i + \sin \theta_i * \sqrt{L_1^2 - d^2}\right) - d\right]^2} \quad (3.8)$$

The maximum displacement of point "C" corresponds to the maximum position of clamp closure and so;

$$\text{in C; } \varphi = \frac{\theta_i}{2} \quad (3.9)$$

$$in\ C'; \ \varphi = \frac{\theta}{2} = 0 \quad (3.10)$$

The condition that is above mentioned is strongly linked to the design of cam (Figure 3.4) by means of which the superior clamp is moved to reach the closed position.

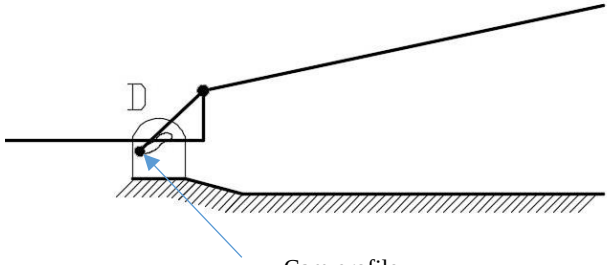


*Figure 3.4. Cam profile to reach the close or opened position.*

To understand the force propagation through surgical clamp it is necessary to analyse its mechanism (Figure 3.5).

$$M_a = F_i * L_3 \tag{3.11}$$

$$F_b = \frac{M_a}{L_1} \tag{3.12}$$

$$F_b = \frac{F_i * L_3}{L_1}$$

$$F_b' = F_b * \cos\varphi$$

$$F_t = F_b' * \cos\beta$$

$$F_t = F_b * \cos\varphi * \cos\beta$$

$$F_t = \frac{F_i * L_3}{L_1} * \cos\varphi * \cos\beta$$

$$F_t' = \frac{F_i * L_3}{L_1} * \cos\varphi * \cos\beta - k(\Delta x) \tag{3.13}$$

$$M_0 = F_t' * m$$

$$F_g = \frac{M_0}{n}$$

$$F_g = \frac{F_t' * m}{n} \tag{3.14}$$

It is important to note that the force feedback reached to the surgeons depends on the dimension of mechanism and the constant of spring used.

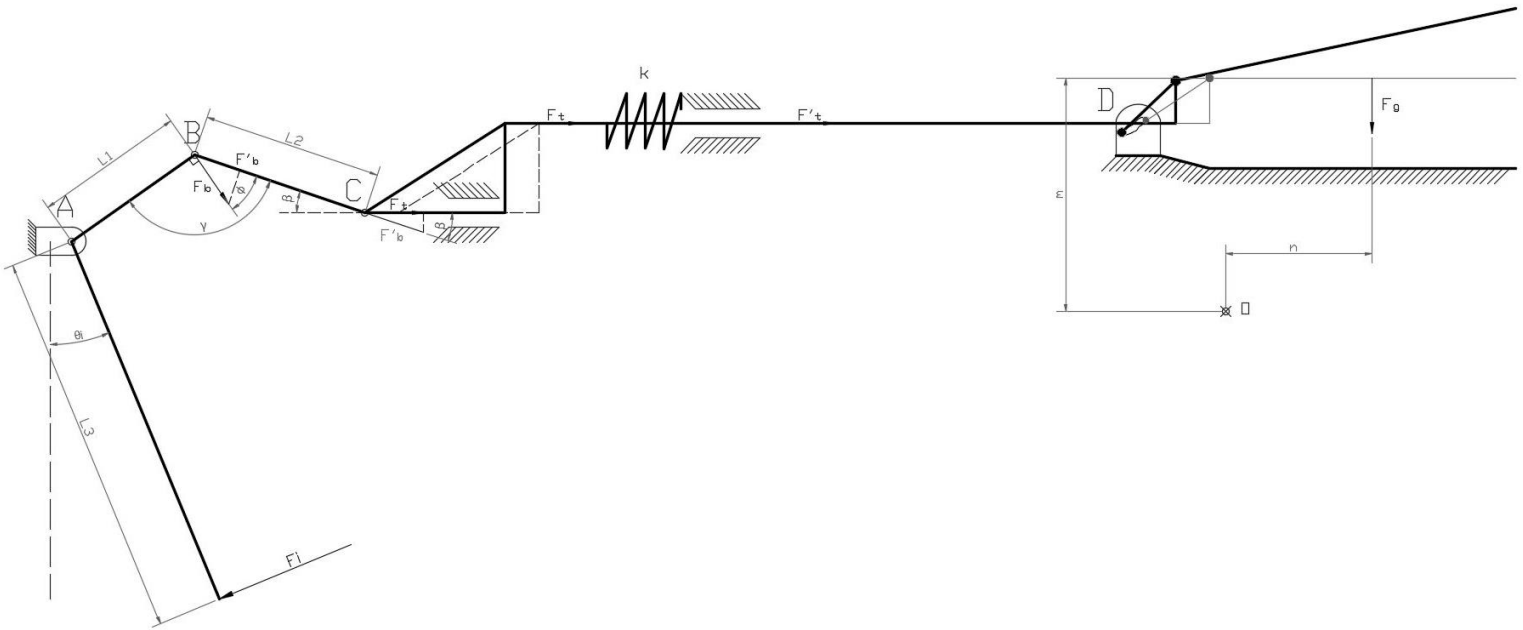


*Figure 3.5. Scheme of force propagation through surgical clamp mechanism*

Clamp's FEA

For our analysis and simulations, we work with the measured geometry from generic clamps (Figure 3.6).

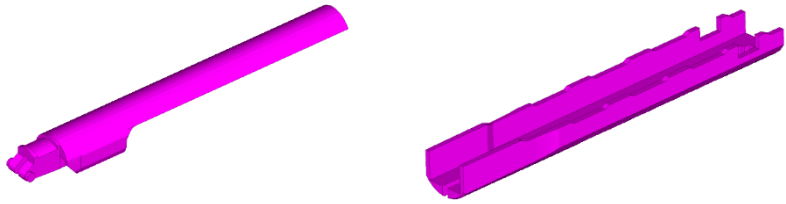

(a) (b)

*Figure 3.6. Geometrical model of surgical clamp (a) upper surgical clamp, (b) lower surgical clamp.*

The analysis is carried out on two geometries: surface models as shows in Figure 3.6 and FEA meshes as depicts in Figure 3.7. Both geometries are modelled with hexahedron and tetrahedron elements.

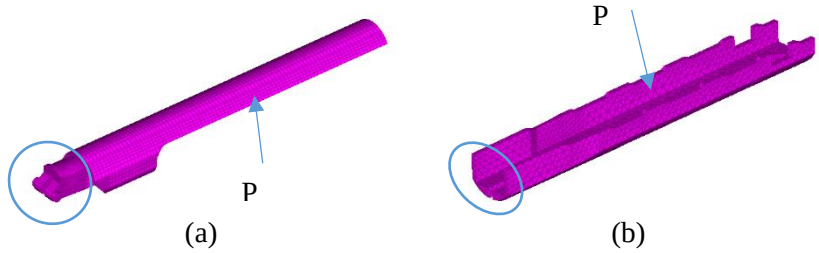


(a) (b)

*Figure 3.7. Geometrical model of surgical clamp (a) upper surgical clamp mesh (b) lower surgical clamp mesh.*

The material used for surgical instrument is often the AISI 301 which has an elastic modulus E=200GPa, density of 7850Kg/m$^3$, Poisson ratio of 0.28 and yield strength of 205MPa.

The load on the clamp during its closing is consistent with the recommended pressure measured for completely closing the section of the colon, 8 gr/mm$^2$ [85]. In our simulations, the half of pressure value is directly applied on the upper and the lower mesh of surgical clamp as shown in Figure 3.7. In Particular, the “P” value (4 gr/mm$^2$) represents

the pressure (in green, Figure 3.8) exerted on the surgical clamp to guarantee the grasping of tissues between the two sides of the clamp.

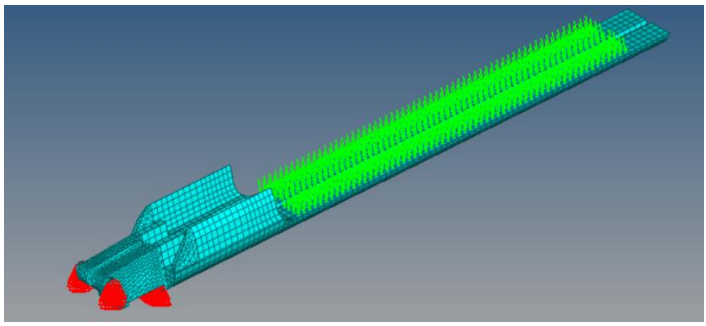

*Figure 3.8. Geometrical model of upper surgical clamp is shown in light blue; related applied load is shown in green and the boundary constraint in red.*

Concerning boundary conditions and constraints they are defined similar to real behaviour. In our case, the boundary condition zone of blue circles (Figure 3.7) have been performed by fixing rotations and displacements in all axes (Figure 3.8).

FEA simulation corresponds to implicit static analysis is carried out in HyperWorks by using the OptiStruct solver. Results are discussed according to the achieved stress distributions.

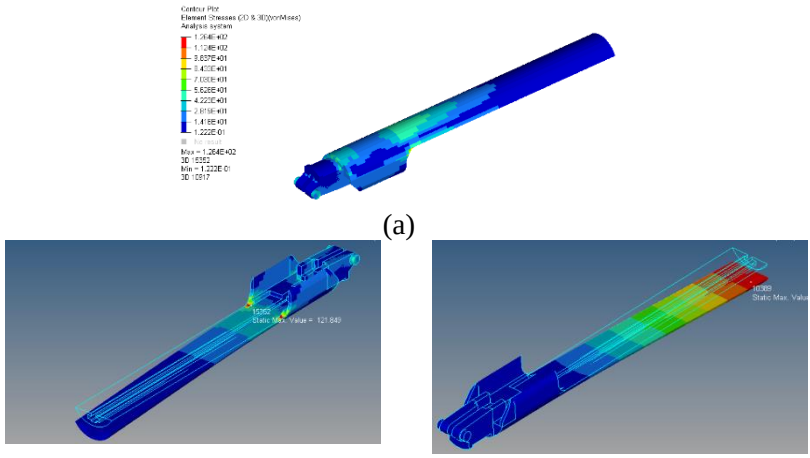

(a)

(b) (c)

*Figure 3.9. Contour-Maps with the value of maximum clamp tightening: (a) Maximum stress in the upper clamp and (b) Maximum displacement obtained in the upper clamp*

Figure 3.9(a), and Figure 3.9(b) shows the maximum equivalent stress distribution of the upper clamp by assuming a pressure value of 4 gr/mm$^2$. The upper clamp has stress concentration around 122 MPa while the maximum displacement corresponds to 0.4 mm (Figure 3.9(c)).

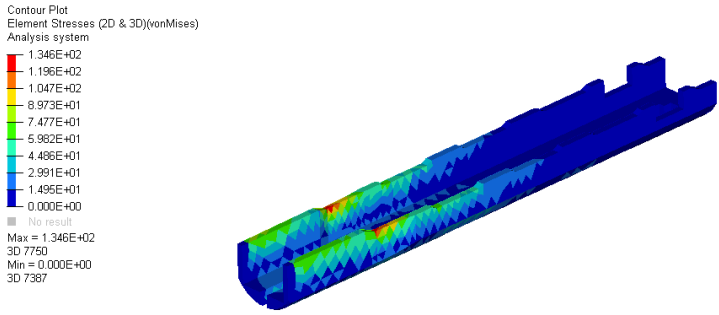


*Figure 3.10. Stress Contour-Map of lower clamp with the value of maximum clamp tightening*

Figure 3.10 shows the maximum equivalent stress distribution of the lower clamp by assuming a pressure value of 4 gr/mm$^2$. The upper clamp has stress concentration around 135 MPa.

The two evaluated clamps helps us to understand the security range in which these works. So with the obtained maximum stress result, the upper clamp presents a security factor of 1.77 while the lower clamp presents a security factor of 1.52.

The above security factor value suggests that the clamps resist the conditions present in surgical procedures. Once it is obvious that the clamps will not fail when a surgical environment is being developed, particularly, when soft tissue deformation is under observation so the surgical clamp can be considered as a rigid body.

## *3.3. 3D model of the organ*

From images to 3D: the segmentation process

Segmentation techniques are relevant in many application fields from artificial vision systems to medical applications and mechanical engineering. In particular, this field is successfully applied on microstructure analysis of materials [86]–[89] and it has also peculiar applications related to reverse engineering of components where it is

applied for mechanical feature recognition and modelling or measuring [90], [91]. So, the method described in [92] starts from a voxel subdivision of the digitized shape where some image analysis techniques are used to classify the 3D feature from the edges of the part.

Image segmentation is a technique that deals with separating input data into meaningful parts of the images (which represents different objects of interest) with their respective borderlines to perform the geometry digitalization. It is aimed to increase the quality of data and information present in a 2D image by isolating areas of interest (operatively, this process can be seen as a reduction of misclassified pixel on the image) [93].

Medicine is a constantly expanding field that also applies on medical image segmentation in several imaging and acquisition modalities (MRI, Computed Tomography (CT)[94], Positron Emission Tomography (PET), X-RAY, and Ultrasound). Medical image segmentation identifies and isolates areas of interest in input data in order to analyse the geometrical model of a tissue or an organ. It splits up the input data into organs and tissues using features such as colors, texture, motion and edges among others. However, the automatic segmentation is still a challenge due to the presence of added noise, artefacts, limitations and unclear edges [95]. Concerning medical applications, soft tissue segmentation is a fundamental issue for the development of Computer Aided Diagnosis System (CAD) based on Computed Tomography (CT). In the recent years, soft tissues segmentation such as colon segmentation has increased its applications in modern medical fields which use CAD in order to overview the 3D model of the organ and reduce the doctor's dependance for diagnosis to locate the prior tissue lesions timely and effectively [91].

In medical field, the colon segmentation of human abdominal CT scan is the basis for analysis and identification of cancer nidus by providing powerful information on CAD such as early polyp detection which can reduce the incidence of colon cancer [90], [91], [96]. Moreover, the colon segmentation may also be introduced to make preoperative planning and simulations of general surgery [84], [96]. In order to safely differentiate the colon (foreground) and the no colon (background) pixels, an accurate process is required to avoid erroneous classification. In these cases, colon pixels may be wrongly recognised instead of noise, artifacts, limitations, unclear edges [95] and other organs (such as the lung, stomach, and small intestine) or different areas with the same intensity values as the colon.

The segmentation manual process usually demands a lot of time to identify and draw borderlines around tissues present in a single tomographic image. The issue is magnified because of the large number (300–600) of images that are required to span the head-to-foot anatomy of an individual through steps of about 3 mm. For this reason, in the recent past, semi-automatic and automatic segmentation have been extensively subject of research efforts [90], [97].

Some works related to colon segmentation have been introduced in literature, each one has its own model, computational complexity, and overall quality such as region-based statistics analysis [91], [94], [98], [99] which builds local models of the tissue of interest instead of a global model. Therefore, a segmented image consists of homogeneous regions characterized by some statistical properties. In [99] an isotropic volume that is reconstructed from the CT images is used to extract a thick region encompassing the entire colon where the mean curvature, dimensionless ratio sphericity and minimum polyp size are used as parameters to filter anomalies and reduce false positives. Other approaches have adopted probabilistic techniques [100], [101]. The authors in [100] used probabilistic boosting tree for learning discriminative models for the appearance of patterns/objects of interest. Also probabilistic Markov Random Field was introduced in [101], in order to handle the problem of an accurately un-supervised segmentation.

On the other hand, most recent deep learning technique (particularly Convolutional Neural Network, CNN) has found applications for medical image analysis focused on medical pattern recognition [102], abnormal tissue detection [91], [103] and tissues classification [104] to cover a broad range of problems related to ophthalmology, pathology, radiology and disease monitoring for personalised treatment suggestions [99]. Consequently, authors in [103] have used CNN in a set of colorectal tissue samples to classify regions corresponding to pathological tissues.

In literature, some works have demonstrated how CNN provides effective results to analyse colon images, those are based on the segmentation of image regions that contain pathological colorectal tissues [103], [105] and glandular colon structure [106], where particularly the segmentation process is performed on histology images [105], [106] and biopsy images [103]. Hence, the analysis of colon tissues as pre-processing task for applications such as preoperative planning and simulations of tissues on general surgery has been handling with the colon

segmentation technique through the use of a deep and hierarchical learning about colon features on CT images with CNN. As different from state-of-the art based CNN methods, the proposed method is focused on CT image analysis and the network architecture ends with two full connected layers as a reduced input patch size of 28 x 28 to demonstrate that smaller patch size provides enough information to classify the centered pixel and achieve a high effectiveness with an expected reduction of filtering operations.

In order to overcome the problem of misclassifying colon tissue pixels, a new method for automatic colon tissue segmentation was presented which is based on spatial features learnt with use of CNN. The proposed method was tested with a set of input image patches from CT slices.

CNN application for image segmentation of the colon.

In order to predict the probability that a pixel could be part of the colon tissues or background, we propose a colon tissue segmentation method based on binary classification by using LeNet-5 network for handwritten digit classification [107] with the aim of learning colon features in a deep and hierarchical way. CNN is trained with patches dataset built from CT images with hundreds of slices to identify colon tissues for each centered pixel location. Only in the training patches dataset, each patch provides labeled information to show whether a centered pixel value is part of the colon tissue pixels or background. Each training patch passes through a sequence of convolution layers, layers of ReLU (rectified linear unit), activation functions (It is used throughout each layer), pooling layers and full connected layers to give output of the binary classification label. During this phase, lower level features (such as lines, edges, curves) are learned in the first hidden layers which are compounded in higher level in the subsequent hidden layers. The workflow of the proposed method is schematized in Figure 3.11. In the following sub-sections, the main steps are described.

CNN architecture

CNN architecture depicted in Figure 3.11(a) is particularly structured as a sequence of stages composed of repeated types of convolutional layers and pooling layers that are followed by a series of fully connected layers and end with classifying layers in order to perform operations on the input patches for feature learning and classification purposes.

*Convolutional layers*

They convolve the input data with an established number of (k) linear convolution filters with a defined size. This layer slides the filters over the input by computing dot product between the input data and the entries of the filters to detect and learn local conjunctions of features from the previous layer. Eq. (3.15).

$$(f_k)_{ij} = (W_k * x)_{ij} + b_k \tag{3.15}$$

where *k=1,…, K* is the index of the *k-th* feature map, $(i, j)$ is the index of neuron in the *k-th* feature map and $x$ is the input data. $W_k$ and $b_k$ are trainable parameter weights and biases from the visible units to the hidden units and $(f_k)_{ij}$ is the learning *k-th* feature map.

*Pooling layers*

These are non-linear down-sampling layers to progressively reduce the spatial size after obtaining features by using convolutional layers in order to diminish the amount of parameters and computation in the network. Its purpose is to merge semantically similar features into one.

Pooling layers establish the size of the regions $s_p = m \times n$ to pool the convolved features over, then divide convolved features into disjoint $m \times n$ regions and take the mean or maximum feature activation over disjoint regions to obtain pooled convolved features which can then be used for classification.

Summary statistics based on mean "mean pooling" or max "max pooling" value of a particular feature over a region of the input data are likely computed to obtain much lower dimensions with respect to the use of all extracted features which can also control overfitting (the production of an analysis that corresponds too closely or exactly to a particular set of data).

*Fully-connected layers*

These are linear combination layers where each node is connected to all nodes of the previous layer. Eq. (3.16).

$$y_k = \sum_l^{sl} W_{kl}\, x_l + b_k \tag{3.16}$$

where $y_k$ is the *k-th* output neuron and $W_{kl}$ is the *kl-th* weight between $x_l$ and $y_k$.

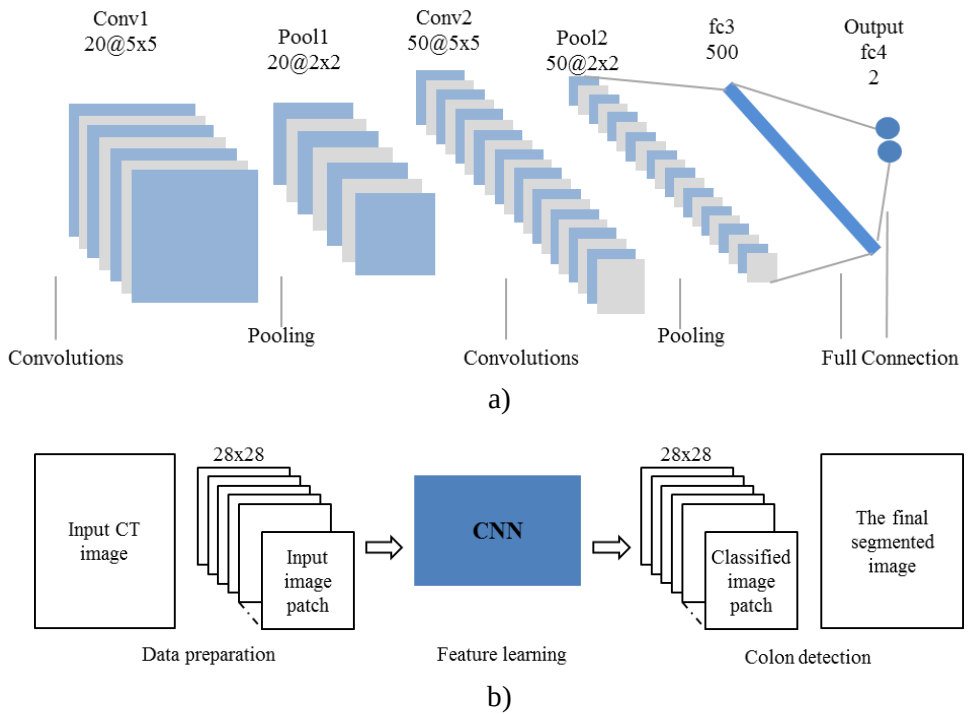


*Figure 3.11. Workflow of the colon segmentation method: a) CNN architecture; b) Overview of the proposed method*

*Activation functions*

They often follow a pooling layer or fully-connected layer and apply a non-linear activation operation to encode complex patterns of the input through transformations of the sum of weights of input that goes into the artificial neurons. There are some activation functions such as sigmoid, hyperbolic tangent and rectified linear unit (ReLU). However, ReLU activation function is used in practice for deep neural networks which is different from other functions due to it is not continuously differentiable and does not vanish for high activations. ReLU is given by Eq. (3.17).

$$f(z) = \max(0, x) \tag{3.17}$$

*Output layer*

It is the last layer in the network and holds the name of the loss function used for training the network for multiclass classification, the size of the output (number of output units) and the class labels.

✓ Classifier layer
It computes a class label probability of the input data. Softmax classification layer is the most extensively used in CNNs. Its purpose is to transform all the net activations in the final output layer to a series of values which can be interpreted as probability vector values between 0 and 1 (which has to be positive, smaller than 1 and sum up to 1). Softmax classification layer applies a categorical probability distribution based on exponential function as in Eq. (3.18) which denotes for the k-th class and an input $X$.

$$P(y = j|X; W, b) = e^{X^T W_j} / \sum_{k=1}^{K} e^{X^T W_j} \tag{3.18}$$

✓ Loss layer
It computes the difference between true class labels and its corresponding predicted class labels to determine the goal of learning by matching parameter settings as current network weights to a scalar value that establishes the “badness” of the settings. Thus, the learning purpose is to find a weights setting that minimizes the loss (called also error, cost or objective)

function. The most widely loss layer for CNNs is the cross-entropy loss given by Eq. (3.19).

$$E = -\sum_n (t_n \ln(y_n) + (1 - t_n) \ln(1 - y_n)) \quad (3.19)$$

where $t_n = t(x)$ and $y_n = p(T_c|x_n)$ is the probability that the indexed sample $x_n$ belongs to a given class.

Data Preparation

Prior to colon tissue segmentation, 75% of the gray scale slices of CT colon images [108] (each CT image has approximately 1600 slices) are preprocessing to generate a patch dataset that reads the CNN.

Based on the sample size expected by the network [107], the size of each training patch is 28 x 28 centered on each pixel for the colon pixel identification. Data set generation uses ground truth images manually labeled by human in order to assign the corresponding label value to give input as image patches (that is "1" if the center pixel belongs to the colon tissues, otherwise "0").

Deep learning framework; CAFFE allows us to process data that comes from normal image format (.jpg, .png and so on) and LMDB format. Thus, after obtaining the set of patches, LMDB data set file is generated to be used as input for the CNN by considering that LMDB is a compressed format for working with large dataset.

Feature Learning

The feature learning is performed in the CNN training which is done through the entire model from input data to loss layer without disjoining the feature extraction and the classification step. CNN receives raw input data in LMDB format to produce classification output.

CNN training allows us to learn the hidden patterns from the input data by using a training dataset. It starts with the first convolutional layer (conv1), where each input image patch $P(x)$ from the patch LMDB dataset is convolved with 50 learnable filters of size 5 x 5. After that, a down-sampling is performed through the pooling layer (pool1) of size 2x2 with stride of 2 in order to reduce the spatial size of representation to a ¼ of its previous size and thus reduce the amount of parameters and computation in the network (Similar settings have been used for the second convolutional and pooling layers). At the end, the full connected

layers (fc3 and fc4) act as classifier and contain 500 and 2 output units, respectively.

Different from original LeNet5 [107] that uses a layer with sigmoid activation function after each full connected layer as all layers in the proposed method are followed by one layer of ReLU activation function to cause sparsity in the features.

The output from the convolutional and pooling layers represent high-level features of the input image patches (feature extractors). While the purpose of the full connected layers is used for these features for classification of the input image into various classes/labels based on the training dataset. Therefore, fc3 and fc4 layers encode the details of patterns of the input patches. The sum of output probabilities of fc4 is 1. This is ensured by using the softmax as the activation function that takes the output of fc4 as source to provide the central pixel probability distribution over the labels. The softmax function takes a vector of arbitrary real-valued scores and forces it into a vector of values between zero and one that sums up to one.

In the training stage, the deep learning framework CAFFE was used to learn the weights of convolutional and full connected layers, which are being learnt by back-propagation with cross-entropy loss function. Eq. (3.19), which is particularly for the proposed method $y_n = p(T_c|x_n)$ is the probability that the indexed sample $\mathrm{x_n}$ belongs to the colon tissue. The loss function $E$ measures how far is the predicted output of the CNN from the correct output, while back-propagation process propagates the loss function gradient to previous layers. The gradient descent is carried out based on loss function gradient $\triangle E/\triangle w_{i,j}$ to adapt the weights in order to decrease the loss function output by changing the direction that is contrary to the direction of increasing gradient with a learning rate of 0.001.

CNN used a patch training set of 282 x $10^6$ colon image patches where patches were sampled randomly from the available samples of training. The bias was initialized with a value of 0.1. The optimization strategy uses a mini-batch size of 1,000 training sample patches. The training stage was performed in 45 x $10^3$ iterations where we can see a training error of 0.041 and a test error of 0.0485 (based on loss function). Different from previouly mentioned work [109], weights were initialized randomly with a Gaussian distribution in order to preserve local structures in the original

collection of data and perform a stable introduction of the data, throughout an association between the dimension of the features produced by the network that still keep the metric information of the original data and its complexity [99], [110].

Colon Detection

This stage use the trained CNN where achieved probability ($p(T_c|x_n)$) by each output patch allows to classify each center pixel as colon tissue pixel or not colorectal pixel. At the end, it composes all patches in order to obtain each corresponding final segmented image.

Results

As a preliminary result, the proposed colorectal segmentation method has been qualitatively validated on the last 407 slides of CT colonography images [108] (Similarly to training stage, input slide images were divided into input patches of size 28 x 28). Some resulting segmented images obtained in colon detection stage are depicted in Figure 3.12. With respect to the ground truth images, it can be observed that the proposed method identifies a sufficient number of pixels of the colon tissues leading to less misclassified pixels produced by close tissues or organs with similar texture or color which can be erroneously classified as colon tissue.

For purpose of numerical comparison between accuracy metrics reported in [90], several approaches that have been introduced in [90], [98], [101] were also compared to the proposed method. Results summarized in Tab. 1, depicts the average values of the sensitivity (Se), specificity (Sp) and accuracy (Ac) by using Eq. (3.20), Eq. (3.21), and Eq. (3.22) respectively.

$$Se = \frac{TP}{FN + TP} \tag{3.20}$$

$$Sp = \frac{TN}{FP + TN} \tag{3.21}$$

$$Ac = \frac{TP + TN}{FP+FN+TP+TN} \tag{3.22}$$

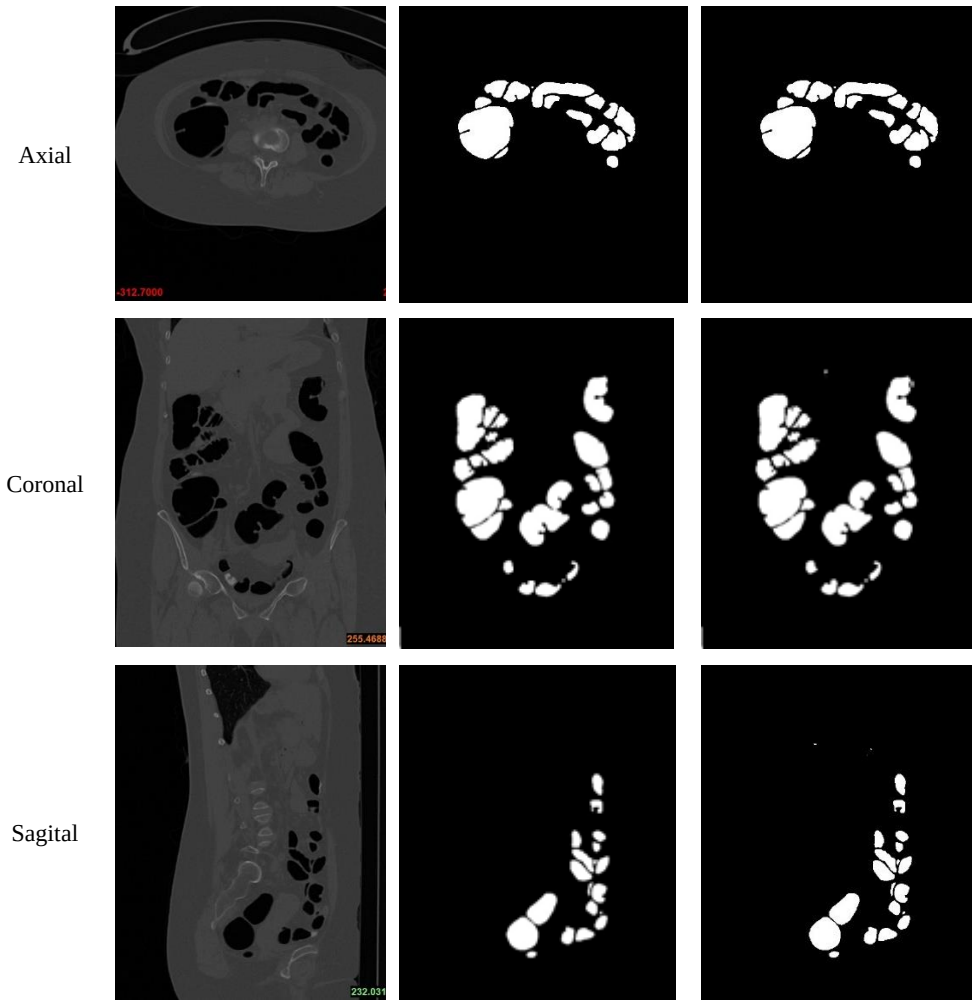


*Figure 3.12. Some qualitative results: a) CT abdominal image; b) Ground truths; c) Segmented Image.*

where TP is the number of pixels correctly detected as colon tissue; TN is the number of pixels correctly detected as background; FP is the number of pixels wrongly detected as colon tissue; FN is the number of pixels wrongly detected as background.

Table 3.1. demonstrates that the proposed method performs better evaluated datasets in terms of sensitivity and specificity with respect to the compared methods, maintaining a very close accuracy value to the

highest one. By taking average of all Se, Sp and Ac metrics, it can be seen that the proposed method reaches the highest overall score. The closets average score (Avg) that is represented by existing method [90] which is based on neural network trained with Bayesian regulation algorithm. The high rates of true positivity shows that was expected as a patch size of 28 x 28 which provides sufficient tissue information to classify the centered pixel as colon tissue or background pixel. The relationship between sensitivity and specificity as depicted in Figure 3.13 shows that proposed approach provides better ability to correctly identify colon tissues pixels and background pixels.

Tab. 3.1: Average sensitivity, specificity, and accurate values.

| *Method* | *Se* | *Sp* | *Ac* | *Avg* |
|---|---|---|---|---|
| [101] | 94.1% | 94.3% | 90.8% | 93.07% |
| [87] | 96.02% | 96.08% | 97.6% | 96.57% |
| [90] | 96.75% | 97% | **98%** | 97.25% |
| Proposed method | **96.9%** | **98.7%** | 97.9% | **97.83%** |

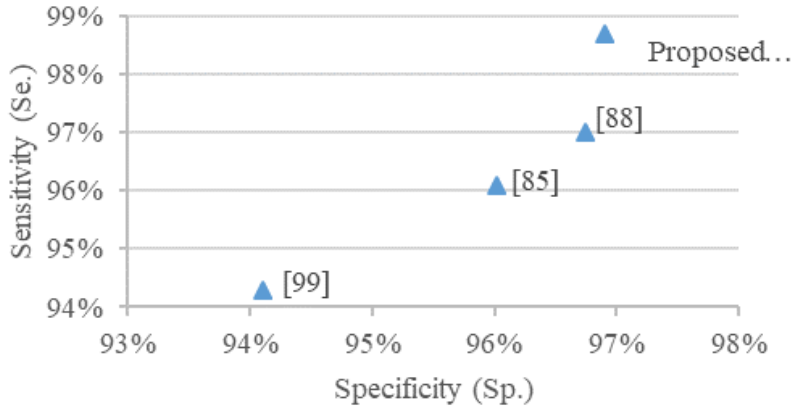


*Figure 3.13. Plot of sensitivity vs. specificity.*

Final 3D model

In order to predict tissue deformations in the preoperative planning which depends on simulation it is mandatory to have: a) the patient organ geometrical model, b) knowledge of the organ anatomy, even in some cases c) knowledge of its surrounding tissues.

For these case studies, a clinical application of the colorectal surgery was considered where colon tissues are being compromised. Figure 3.14 shows the area of interest. In particular, for our analysis and simulations, we assume to work on part of the entire colon that is placed in the zone between the sigmoid area and the rectum area.

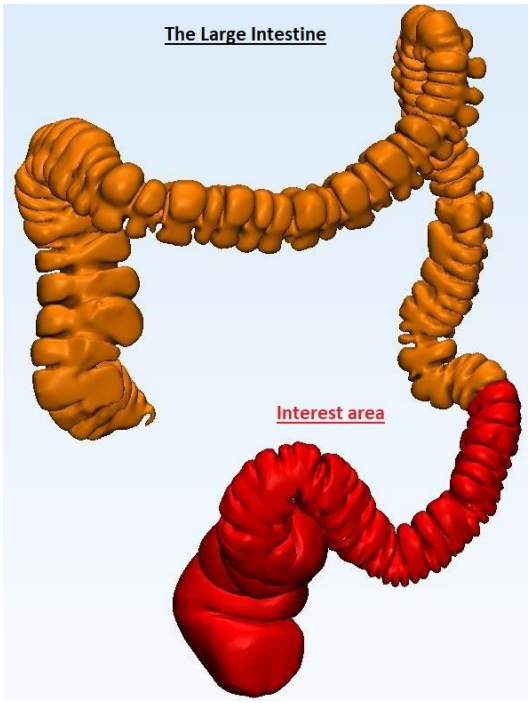


*Figure 3.14. Large intestine (Colon).*

The length of the considered part is about 100 mm (7% of the entire colon). In this colorectal zone, the average outer diameter of the intestine is about 25 mm. It represents the 3D-Surface (3D-S) geometric model adopted in the thesis as the real reference.

## *3.4. Summary*

The Chapter 3 presents the pipeline of the main stages involved in a surgical simulation process. First of all, we analyse the kinematic chain of a generic surgical clamp which can be useful to keep in mind when haptic system calibration is required. Furthermore, with the aim of increasing the speed of the surgical simulations, it was necessary to analyse the mechanical integrity of clamps by FEA. After verifying that the security factor of the clamps will not allow the failure whenever interaction with soft tissue is occurred, the surgical clamps can be considered as rigid body within surgical simulation.

On the other hand, in order to obtain an accurate geometrical model, a new segmentation process has been proposed which predicts the probability that a pixel could be a part of the colon tissues or background. This particular method is based on binary classification by using LeNet-5 network with the aim of learning colon features in deep and hierarchical way. Therefore, CNN is trained by using (patches) dataset built from CT images with hundreds of slices to identify colon tissues for each centered pixel location. (Figure 3.15)

The post process of geometrical model is the same as described to 3D-Surface (Section 4.2). Figure 3.15 shows the 3D-S model after it has been checked and optimized into CATIA.

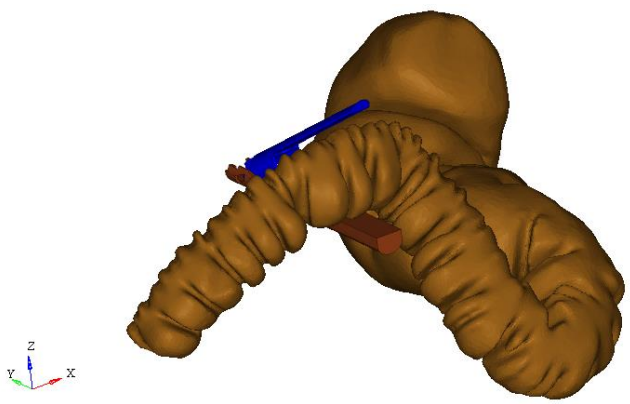


*Figure 3.15. Colon 3D-Surface (3D-S).*

# Chapter 4 - FEA set-up and input for the Sensitivity Analysis

## *4.1. Introduction*

As discussed in Chapter 2 most of the research works has been implemented to improve the simulation environment in order to get a real time sense in terms of realistic organ deformations, haptic feedback or surgical path planning. Nevertheless, any of these studies considers the meticulous application of boundary conditions exerted by surrounding tissues. Some studies works with simple geometry, as in [111], to analyse the prostate deformation by assuming the prostate as an egg-shaped while the rectum was considered as a cylinder. Meanwhile [27] encouraged the use of 'generic'' symmetric geometrical models to avoid difficulties produced from substantial patient to patient variability and asymmetry but these types of assumptions bring difficulty to analyse the relative influence of geometry.

Following this research line in [112] and [27], the authors analysed the effects in terms of mesh displacement when linear and nonlinear mechanical models were used. Most of the studies mentioned above, highlights the importance of the soft tissue's nonlinear mechanical behaviour. However, few works also incorporate anatomical details in their simulations and particularly in the colorectal surgery that effects both material properties and realistic anatomical details (colon folds) have not been quantified to obtain accurate simulations as for example in the tissues clamping.

According to this review, in the chapter, we analyse three different issues concerning FEA accuracy of a clamping process:

a) The influence of considering different colon geometrical model approximations
b) The effect of thickness variation in different geometrical models of colon
c) The influence of the geometrical model in the force feedback.

All the above mentioned case studies also consider the variation of the colon's mechanical behaviour passing from linear elastic to hyperelastic material models.

This chapter is organized as follow: Section 4.2 delivers an explanation about the different geometrical models used for the case studies that goes from a very strong approximation to more accurate model that considers the colon folds present in a true colon. The Section 4.3 presents the values of the constants involved in the description of the different mechanical behaviour as well as the characteristic thickness of colon tissues. While the final Section 4.4 explains the FEA set-up and the solver selection.

## *4.2. Geometrical models*

Generally speaking, in simulations, accuracy of free-form shapes is time consuming. Since we want to reduce computation time, we want to understand how less accurate geometries change the result. In such context, three simplified geometrical models are presented as follows in order to investigate this aspect.

The three simplified geometries always reproduce a surface that may be able to provide an equivalent reaction of a clamping actual case. Where the reference diameter is ∅ 25 mm, the thickness 1.2 mm, length of the organ portion 100 mm.

Planar surface (PS)

The first simplified geometrical model presented is called Plane Surface (PS) (Figure 4.1) and it is the simplest geometrical model that assumes the tissue as a planar surface. Its dimensions are 100 mm for length, $25/2 * \pi \approx 39.3\, mm$ for width and $1.2 * 2 = 2.4\, mm$ for thickness. These values are considered for the colon approximated by a cylinder with an outer diameter of 25 mm that is divided in two semi-cylinders. These semi-cylinders undergo a plane net operation and then stacked. From the loading condition point of view, it is assumed to be completely in contact with the tool that simulates the surgical grasper. It can be noticed that this model wants to simulate the behaviour of the material models when the clamp is completely closed.

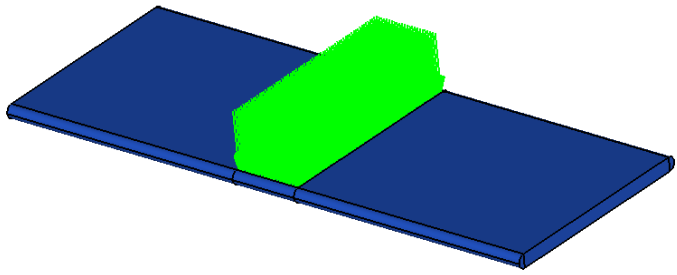

*Figure 4.1. Plane Surface (PS) (blue colour), and related applied load (green colour)*

Circular surface (CS)

The second simplified geometrical model is a Cylindrical Surface (CS) (Figure 4.2). It is an idealization of the colorectal tissue geometry modelled with an outer diameter of 25 mm and a length of 100 mm. This model corresponds to a geometry in a position prior to the interaction with the surgical grasper that in the simulations is assumed as rigid body. (As it was explained in chapter 3)

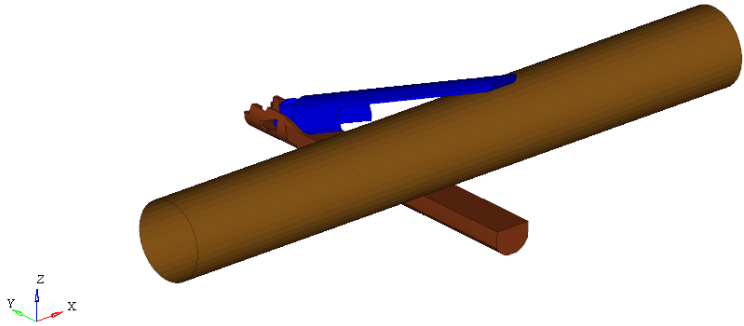


*Figure 4.2. Cylindrical Surface (CS).*

3D-Simplified-Surface (3D-SS)

The third geometrical model represents a simplified 3D model, derived from MRI (3D-SS), (Figure 4.3). MRI was acquired by means of 1.5 T scanner (Sonata Siemens, Erlangen, Germany), with a phased-array body surface coil. The 3D-SS model was obtained by a semi-automatic segmentation by means of Slicer3D (Version 4.5) [113] according to DICOM procedures. Generally, manual operations may increase local accuracy but they are more complex to be checked and replicated on a

large number of slices. Nevertheless, they are a valid option in case of limited parts of organs or small details as in the considered case. After segmentation process, the 3D model has been imported in CATIA to be checked and optimized. Outliers deletion and holes recovery was necessary to model the colorectal surface via NURBS, as shown in Figure 4.3. NURBS modelling [114] has been made in CATIA, starting from the stl tessellation of the 3D model and by adopting reverse engineering techniques for free-form modelling. This geometrical model is definable as a 3D-Simplified-Surface (3D-SS), because the obtained surface approximates the real one without considering the colon folds. The assumption of smoothing the colon folds is due to the goal of reduction of time consumption maintaining a complex surface close to the real 3D-Surface (3D-S).

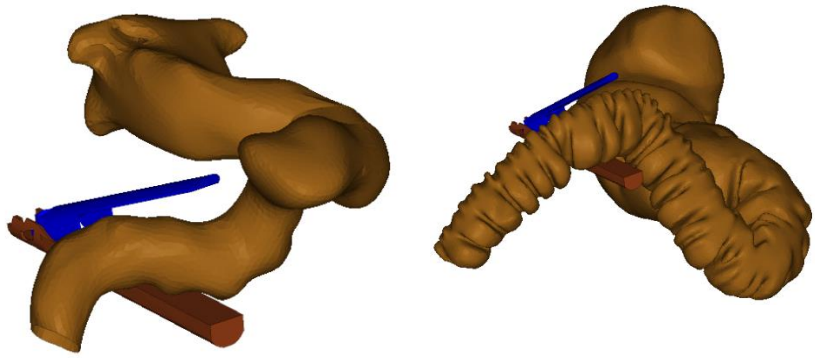

(a) (b)

*Figure 4.3 (a).1 3D-Simplified-Surface (3D-SS); (b) 3D-Surface (3D-S).*

Some authors recommend to study a simplified geometry as uniform and symmetrical as possible in order to understand the physical behaviour in a general way [27]. Then, this understanding can be used to evaluate results of increasing realistic cases so to reach upon the real patient case. In our case, FEA related to CS may help to understand the distribution of stress-strain without considering particular geometrical irregularities that are present in 3D-SS and 3D-S. In particular, as it is shown in Figure 4.3(a) and Figure 4.3(b), 3D-SS has many local diameter changes (colon folds) while 3D-S model does not.

## *4.3. Constitutive models for soft tissue behaviour*

The inherent complexity in the biological tissue's mechanical behaviour and difficulties to acquire the parameters to describe the relationship stress-strain, has given place to an active area of research based on realistic modelling and simulation of tissue deformation that is still a challenge. Until today there is not a standard protocol that is able to reproduce the ex-vivo and in-vivo experimental tests to characterize the mechanical behaviour of soft tissues. It is due to the biological tissues characteristics that are inhomogeneous and anisotropic with nonlinear viscoelastic behaviour [115]. However, most of the works in the biomechanics domain are to understand the fundamental properties of various tissues [115], [116].

From the real-time simulation point of view, owing to limitations in computational resources, simplified models such as linear elastic models are often assumed, with the aim to simulate surgical procedures. So, there is much work in computer graphics that is focused on the modelling of deformable bodies [37] whose aim is to obtain a realistic graphic feedback regardless the physic underlying tissue deformation. Otherwise, the hyperelastic models can describe in a more precise way the relation within stress and strain in the biological tissues for most surgical procedures that involve organs, and in general soft tissues that are subjected also to large strains.

An overview concerning to different mechanical models approach to replicate the soft tissue's mechanical behaviours has been already presented in Chapter 2. Then this section provides a brief description of material models used to obtain the sensitivity analysis. As explained in Section 2.2, hyperelastic formulation may replace visco-elastic models when loads do not involve relaxation or cycling conditions. Instrument's closure during colorectal surgery pertains this case and may also benefit the hypothesis of isotropic behaviour [27]. Among the hyperelastic models, we investigate the Mooney-Rivlin material model (HE-MR) and the Yeoh material model (HE-Y). They are phenomenological material models used for FEA in case of large deformations of materials such as rubber [117] or soft tissues [118]. Recent works [45] on mechanical characterization and FE modelling of a hyperelastic material reported that nonlinearity is captured by describing the stored energy in unit of the reference volume of the material in terms of strain through the invariants

of the Green deformation tensor. More in detail, in the Mooney-Rivlin model, the stored energy density function, *W*, is described through the first and second invariants of the Green deformation tensor ($I_1$, $I_2$) according to [45]:

$$W = C_{10}(\bar{I_1} - 3) + C_{01}(\bar{I_2} - 3) + \frac{1}{D_1}(J_{el} - 1)^2 \qquad (2.2)$$

where $J_{el}$ stands for the Elastic volume ratio; $C_{10}$, $C_{01}$, are constant characteristics of the material and $D_1$ is a material constant that controls bulk compressibility.

By considering the tissue as incompressible, the equation becomes

$$W = C_{10}(\bar{I_1} - 3) + C_{01}(\bar{I_2} - 3) \qquad (4.1)$$

The Yeoh model is described only through the first invariant of the Green deformation tensor [45]:

$$W = \sum_{i=1}^{3} C_{i0}\ (\bar{I_1} - 3)^i + \sum_{i=1}^{3} \frac{1}{D_i}(J_{el} - 1)^{2i} \qquad (2.5)$$

By considering the tissue as incompressible, the equation becomes

$$W = \sum_{i=1}^{3} C_{i0}\ (\bar{I_1} - 3)^i \qquad (4.2)$$

In this case, the constant characteristics of the material are described by $C_{i0}$.

Figure 2.4 (taken from [36]) gives a qualitative overview of how a hyperelastic material works in terms of force-displacement. In this case, nonlinearity is based on the first and second invariants of the Green deformation tensor as it happens in the Mooney-Rivlin model. The characteristic constants ($C_{10}$, $C_{01}$ for Mooney-Rivlin or $C_{i0}$ for Yeoh Model) of the material have to properly fit the shape of the curve according to the actual behaviour of the material.

In [27], the constant values are set to $C_{10}$ = 0.085 MPa and $C_{01}$ = 0.0565 MPa. These values are sufficient to define the hyperelastic Mooney-Rivlin model when the used materials are incompressible. In the same way, the work elaborated by [25] presents the constants $C_{10}$ = 0.088 MPa; $C_{20}$ = 3.092 MPa; and $C_{30}$ = 2.871 MPa, to describe the hyperelastic Yeoh model. As explained in Section 2.2, there are some particular applications where an approximation of the mechanical properties of the soft tissues are required. For this reason, some laboratory tests [33] have

found an experimental approximation to the linear mechanical behaviour corresponding to $E$ = 5.18 MPa.

The Poisson's ratio $(v)$ is the last factor useful to determine the mechanical behaviour of soft tissues (where applicable). In HyperWorks, it is only used for computing the bulk modulus. Since the colon tissues are considered as pure incompressible materials, 0.5 corresponds to poisson's ratio $(v = 0.5)$. This value of Poisson's ratio implies an infinite value for the bulk modulus. Therefore, the recommended Poisson's ratio for incompressible materials into HyperWorks is 0.495 $(v = 0.495)$. Higher values of the Poisson's ratio may lead to a small time step value or divergence in both implicit and explicit simulations [52].

## *4.4. FEA set –up and input conditions*

FEA has been carried out in the HyperWorks environment through OptiStruct and RADIOSS solvers. This choice has been justified by the necessity of evaluating the adoption of material models within a commercial code that does not ask for specific implementations. In addition, RADIOSS have also been evaluated according to its advantages in managing contact algorithms and large displacements since it is an explicit solver oriented to reduce computation time in FEA with high non-linearities [23].

It is important to highlight that simulations performed on geometrical models named CS, 3D-SS and 3D-S, are considered empty. Which is consistent with patient's preoperative plan that asks for emptying digestive system before the surgical operation. Table 4.2 summarizes investigated conditions related to material models, solver and geometrical models.

Mesh

PS model has been discretized in OptiStruct by using 3D elements (hexahedral elements), [23] (Figure 4.4).

CS and 3D-SS models have been carried out in RADIOSS by using 3 or 4-noded Shell elements (named shell3N and shell4N) with 3 integration points along the thickness, [23], [52] (Figure 4.5, Figure 4.6 and Figure 4.7). The mesh elements have been verified to guarantee values suitable for FEA. In particular for each analysis, the parameters as:

max length, the maximum skew angle, the minimum jacobian, equia skew among others have been verified to obtain a good mesh-quality.

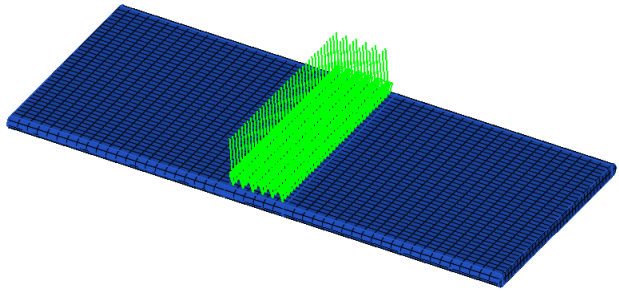

*Figure 4.4. PS geometrical model discretised*

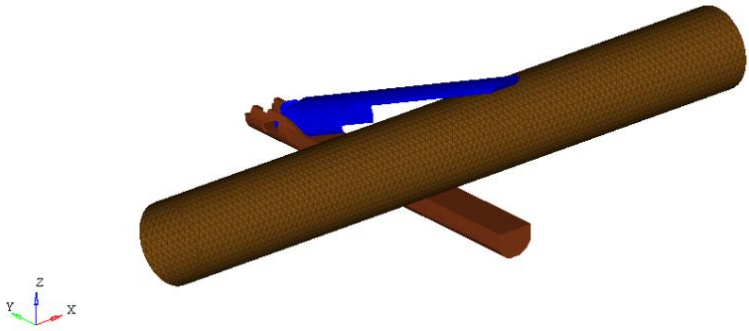


*Figure 4.5. CS geometrical model discretised*

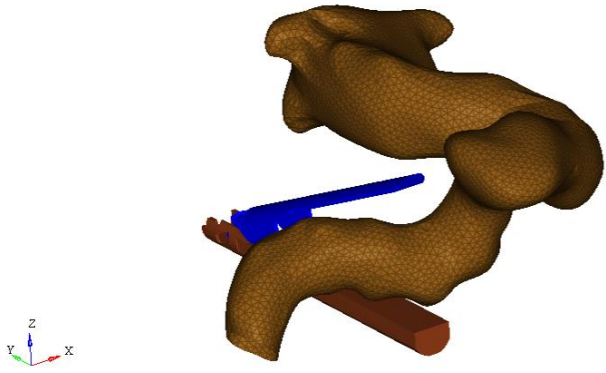


*Figure 4.6. 3D-Simplified-Surface discretised*

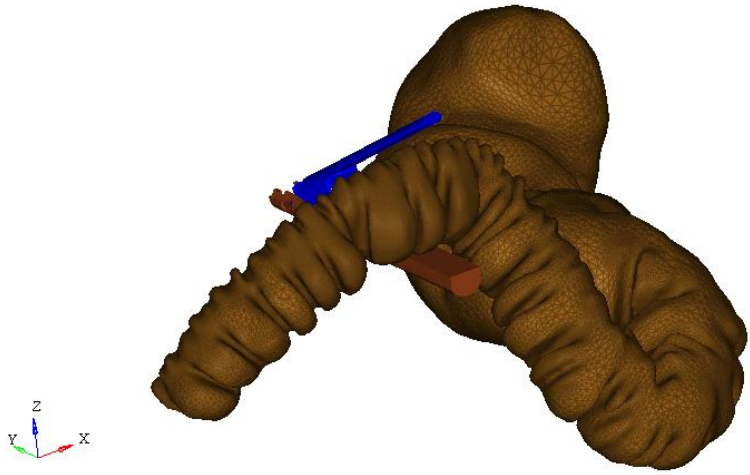


*Figure 4.7. 3D-S discretised*

To conclude the FEA set-up, two numerical considerations must be provided.

The first one concerns with the minimum element length necessary to achieve reliable results. Table 4.1 summarizes the investigated values hence, to assess mesh dependency and sensitivity.

The second numerical consideration pertains to the hourglass checks, necessary for the explicit simulations performed with RADIOSS, Hourglass was managed by QEPH shell formulation, which is recommended for high number of elements.

Table 4.1. Characteristics of the elements used in different geometrical models.

| *Type of Geometry* | *Element length (mm)* | *Element Type* |
|---|---|---|
| PS | 4 ; 2;1; and 0.5 | Hexa8N |
| CS | 4 ; 2;1; and 0.5 | Shell4N |
| 3D-SS | 4 ; 2;1; and 0.5 | Shell3N- Shell4N |
| 3D-S | 4 ; 2;1; and 0.5 | Shell3N- Shell4N |

Load & Boundary conditions

The loads have been applied following two different schemes. The first one is for the PS case with Optistruct, represents a distributed force acting like the grasper tightening (load#1). The values used for load#1 come from experimental data [85] that recommends a value of P=8 $g \cdot mm^{-2}$ (0.078MPa), suitable for manipulating soft tissues without tearing.

The laparoscopic surgery commonly use surgical staplers which are continually being developed. In [119], the integrity factor of the staple line is analysed which depends on adequate tissue compression. This factor is important to create a stable anastomosis. As the thickness of each tissue varies, the staple height also varies depending on the tissue-specific properties and in some cases it is also crucial to regard the tissue pathology. Nowadays, in medical field it is possible to find a classification of stapler and cartridges that depends on the target tissues and these cartridges are identified with colours. For colorectal surgery, a blue staple cartridges often is used which has 1.5 mm closed staple height.

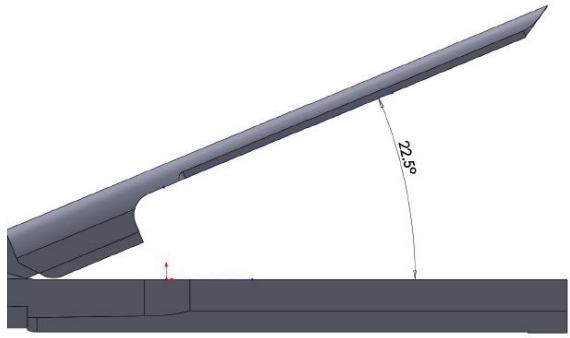


(a)

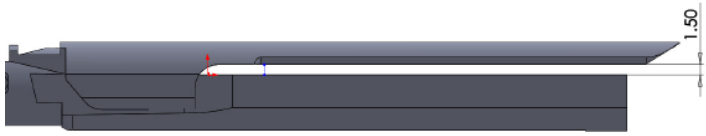


(b)

*Figure 4.8. Surgical clamp, (a) initial angle of surgical clamp, (b) final gap between upper and lower clamp.*

For other geometrical cases, displacement is the second load simulated with RADIOSS and its initial position is depicted in Figure 4.8(a), while the final position is determined by the closed staple height as shown in Figure 4.8(b) (load#2). This displacement is exerted on the tissue with contact of the surgical clamp during its motion.

The organ deformations when interacting with surgical tools is also influenced by boundary constraints as effect of the surrounding tissues (structures) that support the organ. Relating to boundary conditions similar to real behaviour in a colorectal surgery, it is difficult to define because of support structures such as ligaments and fasciae that are not clearly distinguishable in clinical images. Nevertheless, in a colorectal surgery, the surgeon tries to isolate the colon from the surrounding tissues in order to have an enough area to manipulate the colon and to ease the task of inserting the colon into surgical tool clamps.

In order to recreate constraints similar to the conditions present in tissue while performing colorectal surgery, a simplification of the boundary conditions has been performed at the ends of the considered geometries. In particular, we have released rotations in all axes and displacement along colon axial direction at the ends.

The boundary constraints above mentioned are so far from the area where the surgical clamp interacts with the colon tissue which only allows to study the geometry, thickness and material behaviour as factors affecting deformation of colon in order to understand and quantify the significance of each item as well as how these parameters affect the force feedback towards surgical clamps.

Thickness

The inherent soft tissue characteristics complicate the experimental tests to accurately obtain the thickness value which also depends on whether the tissues are healthful or not [119].

In order to consider all assumptions mentioned above, in Section 5.1, colon wall thickness value is set at 1.2 mm, which is considered constant throughout the entire geometry. On the other hand in Section 5.2, the colon wall thickness value is set in range from 0.8 up to 2 mm. All these values are according to data found in literature [30], [31], [120].

Contact

In HyperWorks the contact interfaces are defined by using the penalty method because it is most commonly used in explicit codes and can be found in most of the RADIOSS interfaces as well as it is based on master/slave treatment. Contact can only occur between a set of slave nodes and a set of master segments where the segment corresponds to the element surface.

Due the contact conditions present when the colon portion is fixed into surgical clamp, the "Type 7 interface" has been selected, which is a multi-usage impact interface. In case studies more than one contact “Type 7 interface” were used in order to guarantee the correct evolution of simulation and to define self-contact and the contact between colon tissues and surgical clamp.

Solver

OptiStruct has been used for the PS case study by considering the latest step of the real clamping process. It concerns with the compression of the soft tissue caused by the grasper tightening. On the other hand, RADIOSS has been used to analyse tissue deformation during surgical grasper motion in case of CS, 3D-SS and 3D-S case studies.

Table 4.2. Conditions of material models, solver and geometrical models.

| *Geometrical model* | *LE* | *HE-MR* | *HE-Y* | *Load condition* | *Solver* |
|---|---|---|---|---|---|
| PS | ✓ | ✓ | ✓ | Load#1 | OptiStruct |
| CS | ✓ | ✓ | | Load#2 | RADIOSS |
| 3D-SS | ✓ | ✓ | | Load#2 | RADIOSS |
| 3D-S | ✓ | ✓ | | Load#2 | RADIOSS |

## *4.5. Summary*

The chapter 4 is dedicated to establish all parameters necessary for FEA set-up and related inputs are discussed. In particular, to assess the effects of the geometry in the accuracy of the results, three simplified models have been introduced (planar surface, circular surface, 3D-SS and

3D-S). The simplification switches from smoother and more regular shape towards the actual real segment according to some authors that recommend to study a simplified geometry as uniform and symmetrical as possible in order to understand the physical behaviour in a general way [27]. The geometrical models consider a range of wall thickness from 0.8 up to 2 mm. These results are useful to elaborate a sensitivity analysis of the nonlinearities. Also, hyperelastic mechanical models were presented such as Mooney-Rivlin and Yeoh as well as linear elastic model with its characteristic constants.

All the parameters mentioned above were introduced into HyperWorks, which in combination with the load and boundary condition allowed the simulation of clamping process in order to have an evaluation of the effects induced by the curvature and possible folds on the stress-strain field, and also to evaluate the possible discrepancies among different material models without presence of curvature.

# Chapter 5 - Numerical Results

In this chapter, we are going to analyse and discuss how different FEA set-up and input of chapter 4 may influence the accuracy of the results in terms of stress-strain distribution, global deformation, contact force on the grasp and as a consequence of this, force feedback on handling of the surgical instrument exists.

Results are grouped according to the acronyms given in chapter 4, here some are reported for simplicity:

PS: Plane Surface

CS: cylindrical surface

3D-SS: 3D-simplified surface

3D-S: 3D-Surface

LE: Linear Elastic material model

HE-MR: Hyper-Elastic Mooney-Rivlin formulation

HE-Y: Hyper-Elastic Yeoh formulation

## *5.1. Case study changing the material models in different geometrical models*

3D-SS simulations

According to table 4.2, 3D-S and 3D-SS are investigated according to LE and HE-MR, the thickness of 1.2 mm and averaged element length of 2 mm should be considered. The Figure 5.1 shows contour-plots and describe the stress and strain distribution at the complete closure of the clamp. Particularly, the figures presented here consider average element length of 2mm, thickness equal to 1.2mm and Mooney Rivlin mechanical behaviour.

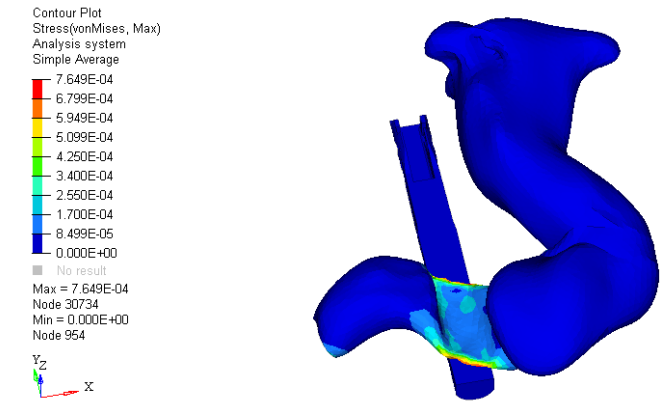


(a)

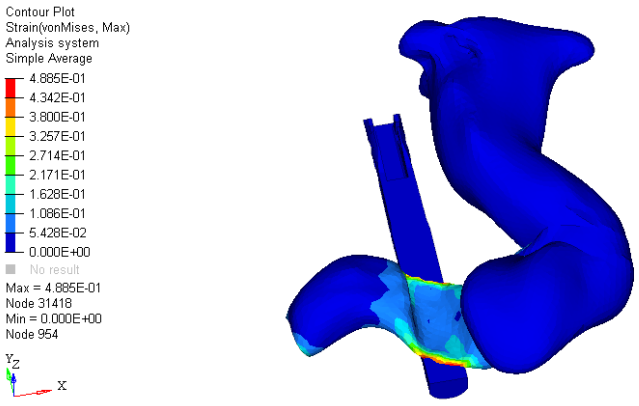


(b)

*Figure 5.1. (a): Stress contour-map in the 3D-SS (GPa), (b): Strain contour-map in the 3D-SS. All cases are presented by using a simple average method.*

Figures 5.2 shows the results related to the 3D-SS in terms of maximum stress and strain by changing material model and mesh length. They are referred to the maximum values of the equivalent von Mises' stress which occur in the areas of stress/strain concentration, as shown in Figure 5.1.

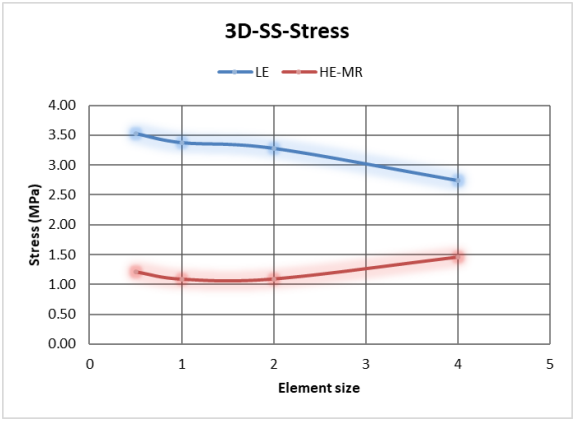


(a)

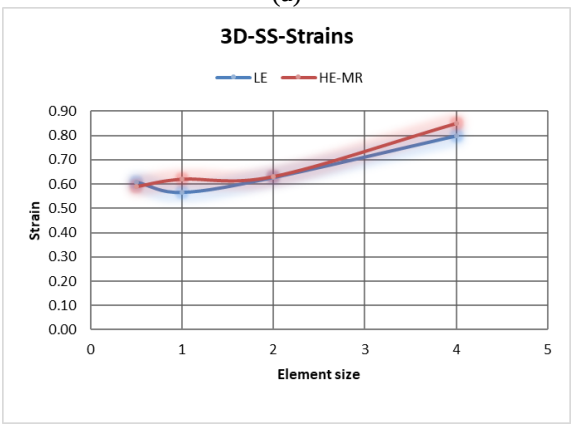


(b)

*Figure 5.2. (a): 3D-SS stress sensibility respect with the length of the element and material model, (b): 3D-SS strain sensibility with respect to the length of the element and material model.*

LE model overestimates the stress values with an average ratio of 3:1 since it has intrinsic stiffer behaviour than HE models. On the contrary, the strain results are similar since the load conditions are related to an imposed displacement condition (see Chapter 4) this is due to the closure of the grasp.

By increasing the mesh size, the stiffness of geometrical model and hence, maximum stress tends to converge. It can be due to a difference in local deformation of HE-MR set-up because of the mesh length. In such a way, the stiffness of mesh compensate the major strain aptitude of the HE-MR. Thus, it can be affirmed that mesh length and material model that switch from LE to HE has interaction effects.

Comparison with CS

The CS case-study represents a simplified model towards the 3D-SS and 3D-S models. Figure 5.3 shows the results concerning the stress and strain contour maps when complete closure of the clamp occurs.

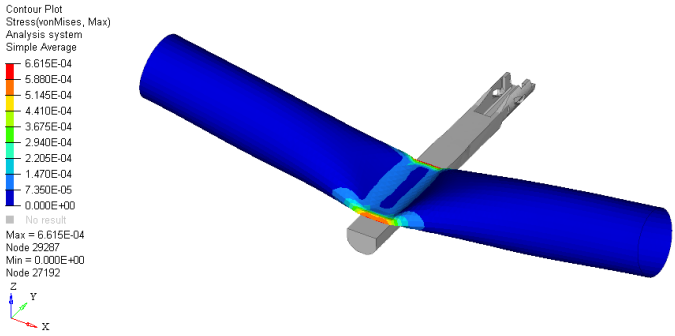


(a)

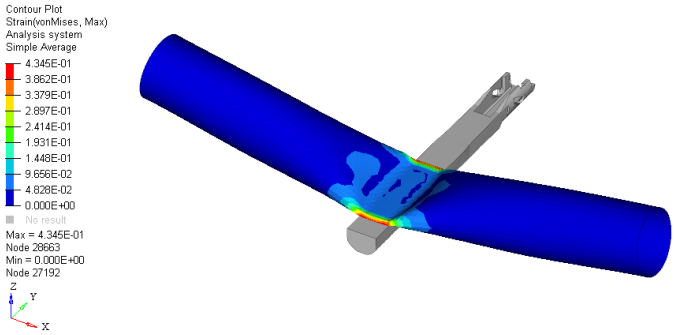


(b)

*Figure 5.3. (a): Stress contour-map in the CS geometrical model (GPa), (b): Strain contour-map in the CS geometrical model,*

Figures 5.3 and 5.4 shows the results concerning simulation on the CS model. Particularly, in Figure 5.4(a) and Figure 5.4(b), the maximum stress and strain achieved according to the two material models are shown together with their sensitivity towards the element length at the time of complete closure of the clamp.

By adopting the LE and HE-MR models, stress maximum values increases when the length of element increases. Regardless the changes in the number of elements that pass from LE to HE-MR model, its variation is about 4.2:1 for the maximum stress.

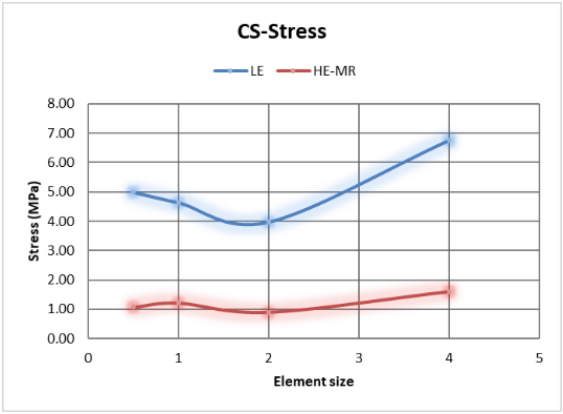


(a)

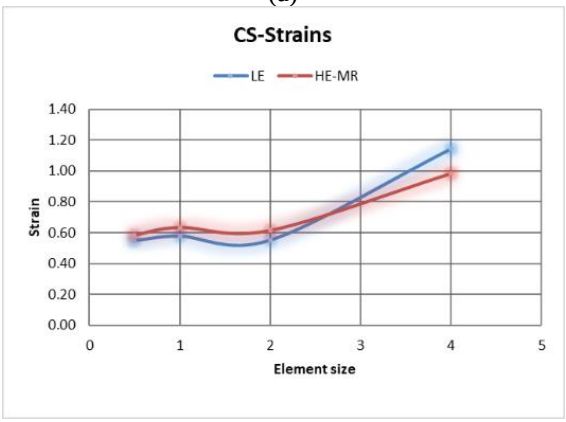


(b)

*Figure 5.4. (a): CS stress sensibility with respect to the length of the element and material model, (b): CS strain sensibility with respect to the length of the element and material model.*

In order to better understand this phenomenon, we have analysed the instant in which the surgical grasper starts to be in contact with the tissue. Figure 5.5(a) shows the deformed shape in an instant that immediately follows the contact by presenting particular characteristics in the central zone. Figure 5.5(b) and 5.5(c) shows the stress contour plot in the same instant as in case of HE-MR and LE respectively. We can observe that the HE-MR stress gradient starts from the lateral zone (free edges) of the CS model and not in the central area where the contact with the grasper starts as it happens in case of LE. This behaviour of the HE-MR model is caused by the nonlinearity of material that results as a major flexibility which involves a local displacement of the tissue in the contact area during grasping process before local stress generation starts.

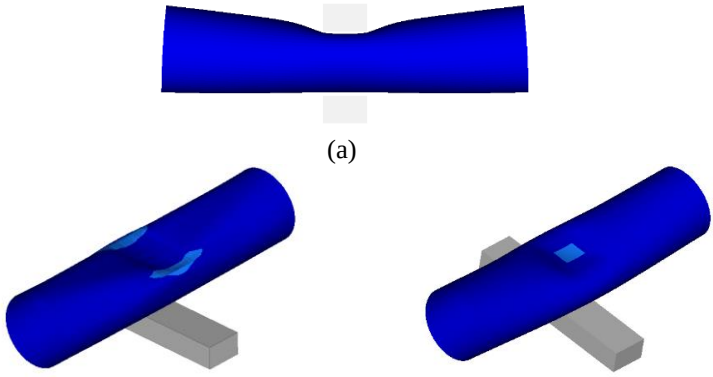

(a)

(b) (c)

*Figure 5.5. CS simulation (a). Particularly the deformed shape at the contact instant, (b):Stress gradient with the HE-MR model (blue zone with stress < 0.006 MPa, cyan zone with stress between 0.006 and 0.01 MPa), (c): Stress gradient with the LE model (blue zone with stress < 0.4 MPa, cyan zone with stress between 0.4 and 0.8 MPa).*

In the LE model for CS case (Figure 5.5(c)), we can observe an opposite effect with respect to the HE-MR model. Due to a more rigid behaviour, local consented displacements of nodes appear before the generation of stress and they are lower than those of the HE-MR model. This produces the appearance of stress gradient in the area where the contact with the surgical grasper starts.

By concerning the sensitivity of the number of elements (changing the length of the element), it seems to have an effect on the LE model and not to the HE-MR in term of stress.

Once the influence of element length in each geometrical model is determined, Figure 5.6 highlights the comparison between strain and stress at the moment of complete closure of the clamp by changing geometrical model and length but the mechanical behaviour either linear elastic or Mooney-Rivlin remains constant. They are referred to the maximum values of the equivalent von Mises' stress which occur in the areas of stress/strain concentration.

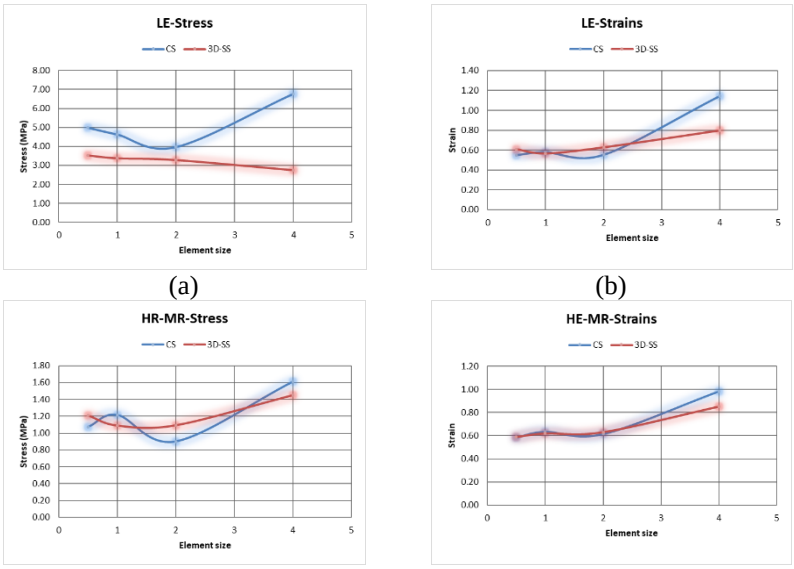


*Figure 5.6. Geometrical influence analysis (a): Stress sensibility with respect to the length of the element and geometrical model using a linear elastic mechanical behaviour, (b): Strain sensibility with respect to the length of the element, and geometrical model using a linear elastic mechanical behaviour, (c): Stress sensibility with respect to the length of the element and geometrical model using a hyperelastic Mooney-Rivlin mechanical behaviour, (d): Strain sensibility with respect to the length of the element and geometrical model using a hyperelastic Mooney-Rivlin mechanical behaviour.*

By concerning changes in element length, both geometrical models show changes although both models have irregular trends. This can be seen as an effect of the local changes in the diametrical sections as also shown in Figure 4.6 and Figure 4.**7**, in the flat area in contact with the upper part of the clamp.

Relating to the stress trend, Figure 5.6(a) shows a different behaviour between CS and 3D-SS. It happens when the LE mechanical behaviour is used. In fact, the CS model presents a greater concentration of stress in comparison with 3D-SS. While Figure 5.6(c) depicts a trend of stress which is quite similar as with use of the HE-MR mechanical behaviour. Concerning the strains, the trend in the both cases (CS and 3D-SS) are similar. It can be understood due to the fact that the thickness is set as constant value and the final position of the surgical clamp considers as a constant gap of 1.5 mm (to avoid excessive tissue compression and local

tearing). Even this condition gives a minimum variation in terms of strain when the mechanical behaviour models change.

PS simulations

To complete the overview of the material model effect and the simplicity of the geometry, simulations on a PS case-study have been added.

In the PS geometry, an applied load of $P = 8\,\mathrm{g}\,mm^{-2}$ (0.078MPa)[85], is used to analyse the behaviour of the three types of material models: LE, HY-MR, HE-Y.

Figure 5.7 shows aggregated results by concerning simulations on the PS model. In particular, it plots the maximum stress (Figure 5.7(a)) and strain (Figure 5.7(b)) that is achieved according to the three material models together with their sensitivity for the mesh density.

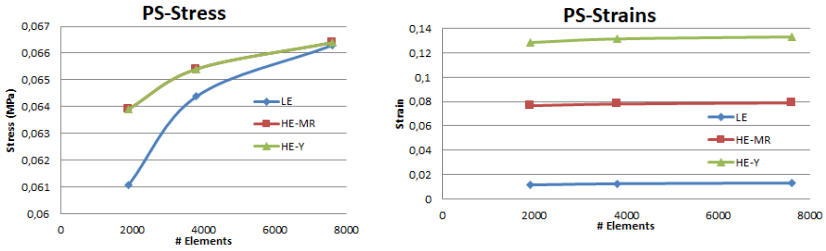


(a) (b)

*Figure 5.7. PS simulations (a): PS stress sensibility with respect to the length of the element and material model, (b): PS strain sensibility with respect to the length of the element and material model.*

Concerning the maximum stress, as in the Figure 5.7(a), a different trend between linear elastic and hyperelastic models is observed although the numerical values are rather similar with an average maximum stress of the tests that is equal to 0.065 ± 0.002 MPa.

With reference to the maximum strain as shown in Figure 5.7(b), the behaviour seems to be quite similar concerning the trend with increasing levels of strain changing from the LE to the HE-MR and then to the HE-Y (0.018 mm/mm, 0.080 mm/mm and 0.130 mm/mm respectively). The highest strain value is achieved with HE-Y while the lowest strain value is obtained with LE. Therefore, this result is consistent with the theory that describes the linear elastic approximation [45] as a stiffer model than the hyperelastic ones.

Difference between the hyperelastic models (as in case discussed here) can be quantified as an increase of the maximum strain with a ratio of 1.6, passing from HE-MR to HE-Y. Concerning the sensitivity to the mesh density, it is not remarkable for the strain. In the case of the maximum stress, the increase in number of elements moves the maximum stress of the LE model toward the values of the HE models (in Figure 5.7(a), a trend of convergence can be seen for number of elements higher than 4000). It can be seen as a consequence of a slight changes in the surface compliance due to the increase of nodes.

Figure 5.8 shows contour-plots that describe the stress distribution in this case. Passing from Figure 5.8(a) to Figure 5.8(b), so that by increasing the number of elements from 2000 to 8000, a change of the local stress distribution on the surface is produced with an increase (about 3 ÷ 8%) of the maximum value. A stress concentration is shown at the free-edges of the model. The distribution is similar for each of the three material models.

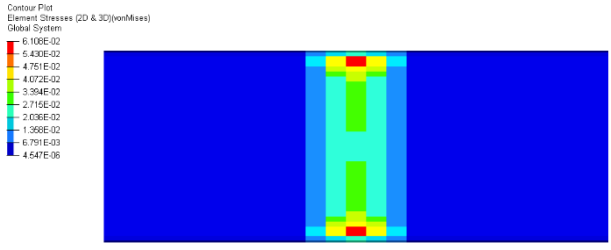


(a)

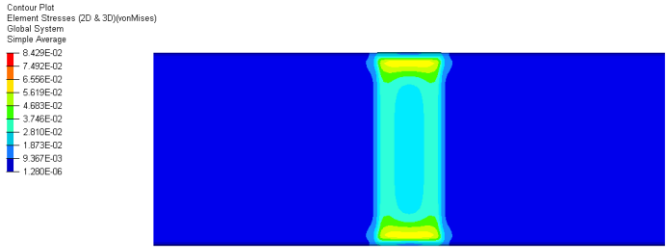


(b)

*Figure 5.8. Colour map using linear mechanical behaviour (a): Colour map of the stress (MPa) distribution in the PS model (2000 elements), (b): Colour map of the stress (MPa) distribution in the PS model (8000 elements).*

## *5.2. Thickness effect on different geometrical models*

Numerous studies performed with various tissue types (gastric [121], colorectal,[122] and pancreatic [123]) provide data that demonstrates the importance of a surgeon's familiarity with tissue thickness and compressibility in order to optimize stapler (surgical clamp)–tissue interaction. In fact, in the literature is possible to find different values of colon thickness, these values change no only by the different laboratory procedures in order to obtain the thickness value, but also by a wall thickening that can occur in pathological situations [119]. Due to all these consideration a sensitive analysis based in the variation of the thickness has been done.

In this section, we analyse the influence of thickness changes on three geometrical models (CS, 3D-SS and 3D-S).

The Figure 5.9 shows contour-plots to describe the stress and strain distribution at the closure of the CS, 3D-SS and 3D-S models. Particularly, the presented figures consider element's average length of 1mm, thickness equal to 2mm and Mooney Rivlin mechanical behaviour.

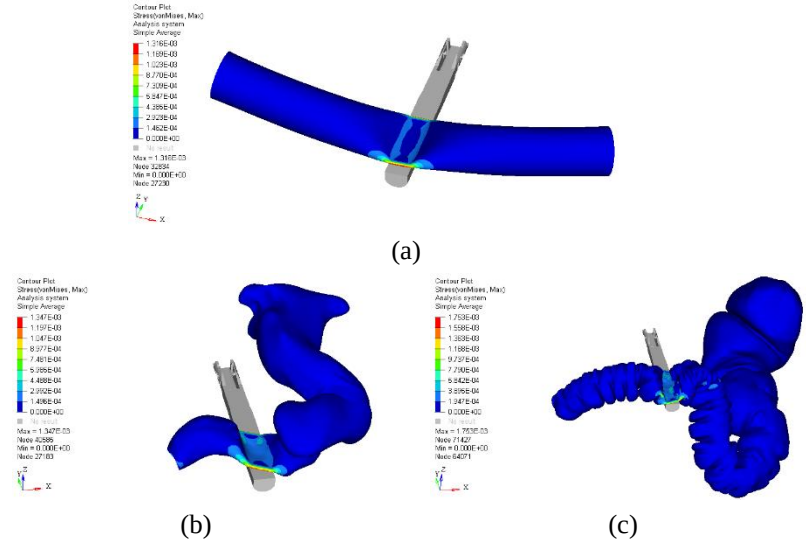


*Figure 5.9. Stress Contour-Maps (GPa) at the moment of maximum clamp tightening: (a) Stress Contour-Map in the CS Geometrical model, (b) Stress Contour-Map in the 3D-SS Geometrical model, and (c) Stress Contour-Map in the Co-S Geometrical model. All represented models consider thickness of 2mm.*

Figures 5.10 shows the results concerning simulation. In Figure 5.10(a), Figure 5.10(c) and Figure 5.10(e), the maximum stress achieved according to the two material models are shown together with their sensitivity to the thickness at the moment of complete closure of the clamp. On the other hand the Figure 5.10(b), Figure 5.10(d) Figure 5.10(f) shows the maximum strain achieved according to the same conditions as stress. By adopting the LE and HE-MR models, both stress and strain maximum value decreases while the thickness decrease. Regardless of the changes in the thickness, passing from LE to HE-MR model, their variation in the maximum stress is about 3.7:1 for CS model, 3.4:1 for 3D-SS model and 5.7:1 for 3D-S model.

The phenomenon of overestimation in terms of stress, when LE mechanical behaviour is used can be understood by its natural behaviour that is more rigid with respect to the HE-MR model. In particular, the HE-MR model presents a major flexibility which involves a local displacement of the tissue in the contact area during the grasping process before the local stress generation while the LE model presents an opposite effect. This phenomenon is present in the three geometrical models, in each value of thickness considered. This overestimation phenomenon is explained in detail in section 5.1.

Figure 5.11 highlights the comparison between strain and stress at the time of complete closure of the clamp by changing geometrical model and initial thickness and the mechanical behaviour remains constant, either linear elastic (Figure 5.11(a) and (b)) or Mooney-Rivlin (Figure 5.11(c) and (d)). They are referred as the maximum values of the equivalent von Mises' stress that certainly occurs in the areas of stress/strain concentration as shown in Figure 5.9.

Concerning change in thickness, all geometrical models show an increase although the 3D-S has irregular trends. This can be seen as an effect of the local change in the diametrical sections of the 3D-S as also shown in Figure 4.7, in the flat area in contact with the upper part of the clamp. Effectively, in 3D-S during clamp motion, the contact between tissues and clamp is not regularly distributed and involves only several portion of surfaces. As a consequence of it, irregular distribution of areas in contact causes an irregular distribution of stress (and thus, strain), as shown in Figure 5.11(b) and Figure 5.11(d).

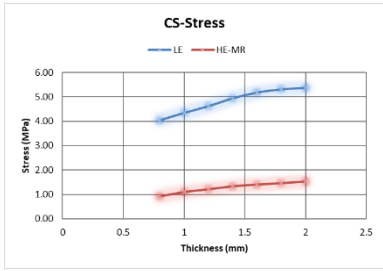


(a)

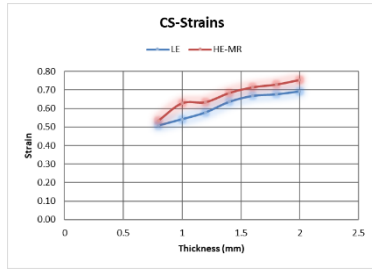


(b)

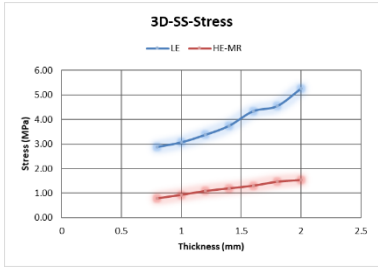


(c)

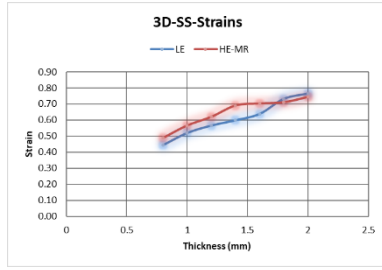


(d)

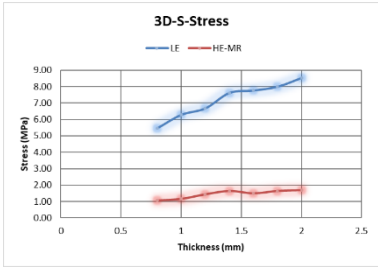


(e)

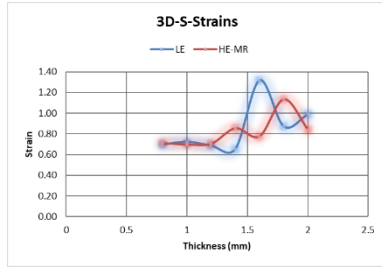


(f)

*Figure 5.10. (a): CS stress sensibility with respect to the thickness and material model, (b): CS strain sensibility with respect to the thickness and material model, (c): 3D-SS stress sensibility with respect to the thickness and material model, (d): 3D-SS strain sensibility with respect to the thickness and material model. (e): 3D-S stress sensibility with respect to the thickness and material model, (f): 3D-S strain sensibility with respect to the thickness and material model.*

By increasing trend as in Figure 5.11 is an obvious consequence of the increase of the initial thickness. In fact, a higher thickness means a higher volume with the possibility of absorbing a higher level of energy that is locally converted into stress and strain. In addition, the increasing trend may also be partially connected to the fact that the FEA condition has an imposed motion on the clamp that is stopped at a specific gap-value (1.5mm) related to clamp tighten. This means a maximum limit for the

distance between clamps but with an increase of the initial thickness, it leads to higher stress in the tissue that is more compressed.

Despite the presence of an irregular trend of stress and strain, the 3D-S increment of the stress and the strain according to the range of the initial thickness is 54% for the stress and 43% for the strain. In 3D-SS that shows higher values about 83% for stress and 73% for strain while CS shows values of 33% for stress and 35% for strain (Figure 5.11(a) and Figure 5.11(b)) all these values are considered as a linear elastic behaviour. On the other hand, when a Mooney Rivlin behaviour is used, the variation increment of the stress and the strain according to the range of the initial thickness are as follows: 3D-S 55% for stress and 18% for strain. In 3D-SS 94% for stress and 50% for strain while CS shows values of 64% for stress and 39% for strain (Figure 5.11(c) and Figure 5.11(d)).

In general way, the three geometrical models with a linear elastic behaviour (Figure 5.11(a)) depicts different stress values between them which generally are higher than those depicts for the geometrical models that use a Mooney-Rivlin behaviour (Figure 5.11(c)). As already explained in [11], it can be correlated to the local irregularities of the 3D-S that involve the large displacement hypotheses more intensively than other models.

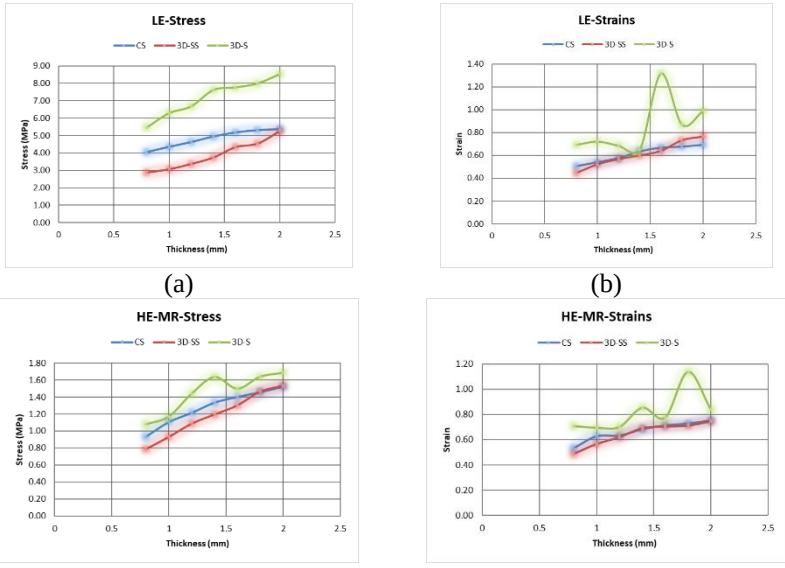


*Figure 5.11. (a): Stress sensibility with respect to the thickness and Geometrical model using a linear elastic mechanical behaviour, (b): Strain sensibility with*

*respect to the thickness and Geometrical model using a linear elastic mechanical behaviour (c): Stress sensibility with respect to the thickness and Geometrical model using a hyperelastic Mooney-Rivlin mechanical behaviour, (d): Strain sensibility with respect to the thickness and Geometrical model using a hyperelastic Mooney-Rivlin mechanical behaviour.*

## *5.3. Sensitive analysis of force contact*

The type of tissue (mechanical behaviour and its characteristic constant) and its geometrical model could significantly affect tissue deformation as well as the magnitude of contact force and contact pressure provided during surgical simulation.

The three FEA cases have the set-up conditions established in Section 4.4. In all cases, an explicit FEA simulation has been made by RADIOSS, by considering contact and dynamics during grasping. Results are discussed according to the achieved force and pressure contact.

Figure 5.12(a) and Figure 5.12(c), shows the results concerning the maximum contact force (between clamp and tissue) achieved according to the two material models together with their sensitivity to the element length. Obviously the contact force is a reaction of the tissue upon the clamp and the correlated pressure at the time of complete closure of the clamp.

By using the LE and HE-MR models, the contact force value decreases when the element length decreases and by concerning the sensitivity to the number of elements (changing the element length), it seems to stabilize from 2mm in CS model and from 1mm in 3D-SS model. Regardless of the changes in element length that passes from LE to HE-MR model, their variation in the maximum contact force is about 6:1 for CS model and 3:1 for 3D-SS model. Therefore, the phenomenon of overestimation caused by linear elastic behaviour is present as in the case of stress and strain evaluation.

On the other hand, the contact pressure behaviour seems to be roughly steady when the Mooney-Rivlin model is used while an irregular contact force trend is depicted when the linear elastic model is applied.

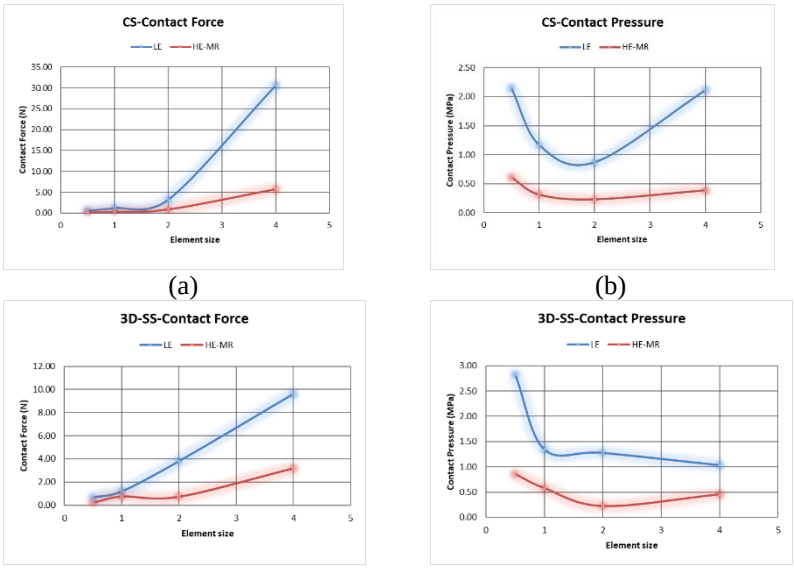


*Figure 5.12. (a): Contact force sensibility in CS geometrical model with respect to the element size and using LE and HE-MR mechanical behaviour, (b): Contact pressure sensibility in CS geometrical model with respect to the element size and using LE and HE-MR mechanical behaviour (c): Contact force sensibility in 3D-SS geometrical model with respect to the element size and using LE and HE-MR mechanical behaviour (d): Contact pressure sensibility in 3D-SS geometrical model with respect to the element size and using LE and HE-MR mechanical behaviour.*

Figure 5.13 shows an interaction analysis between mechanical behaviour and thickness change on contact force between clamp and tissue (it is a reaction force of the tissue upon the clamp). While in the correlated pressure, the values correspond to the maximum contact force that is achieved at the time of complete closure of the clamp.

By concerning change in thickness, all geometrical models show an increase in both force and pressure contact as consequence of the increase of the initial thickness although the complexity of geometrical model seems to affect the trend of force and pressure contact. In Figure 5.13, it is easily identifiable that a more irregular trends in the geometrical model becomes more irregular. This can be seen as an effect of the local change in the diametrical sections of the 3D-SS and 3D-S models as also shown in Figure 4.7. This effect is more evident in 3D-S during clamp motion due to the contact between tissues and clamp is not regularly distributed

and it involves only several portion of surfaces which leads to an increase in terms of pressure.

Like all previous cases of sensitive analysis, the three geometrical models that use a linear elastic behaviour depicts values higher than those that use geometrical models with Mooney-Rivlin behaviour (Figure 5.13).

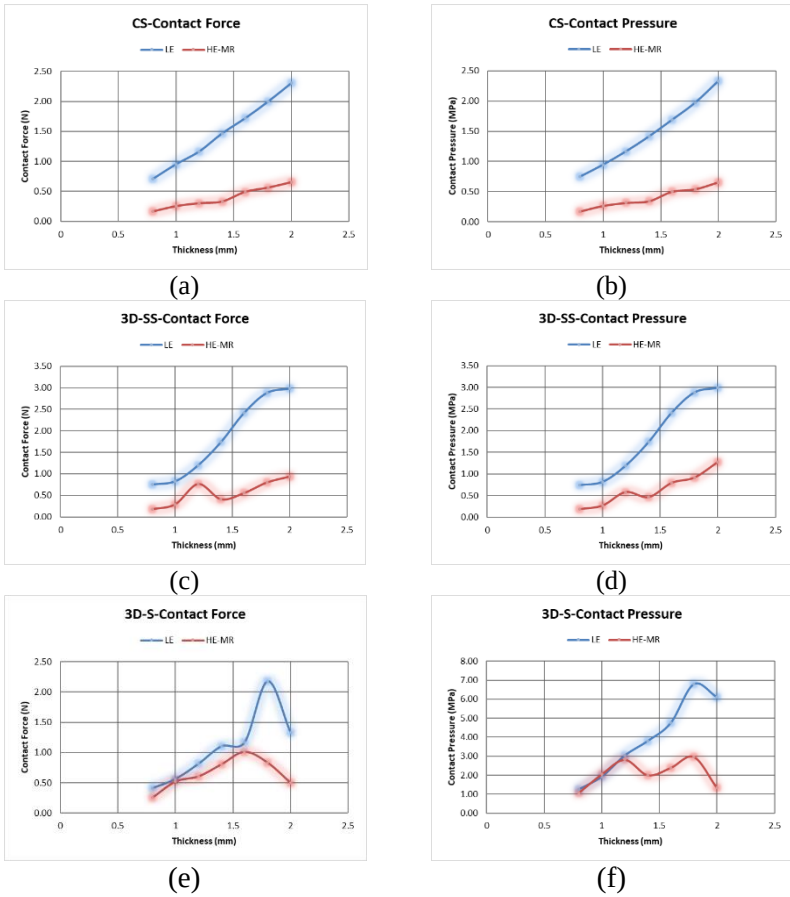


*Figure 5.13. Sensitive analysis using LE and HE-MR (a): Contact force sensibility in CS geometrical model with respect to the thickness, (b): Contact pressure sensibility in CS geometrical model with respect to the thickness (c): Contact force sensibility in 3D-SS geometrical model with respect to the thickness (d): Contact pressure sensibility in 3D-SS geometrical model with respect to the thickness (e): Contact force sensibility in 3D-S geometrical model with respect to the thickness (f): Contact pressure sensibility in 3D-S geometrical model with respect to the thickness.*

# *6. Discussion of Results*

In surgical scenarios using FEA, simplified 3D geometry may help to understand the phenomena that are present in real geometries or to provide a simplified solution suitable for virtual environments. Previous works on FEA of soft tissue [27] recommends to study a simplified geometry, as uniform and symmetrical as possible in order to avoid errors or wrong analysis caused by geometrical irregularities and also to develop procedures that are not influenced by specific cases. Nevertheless, in the specific case of colon simulations, it should be kept in mind that geometrical characteristics (e.g. small thickness) and irregularities (folds of different shapes) may induce large deformations that may interact with the non linearity of the material. The possibility of studying this kind of characteristics is obviously contrasted by the increase in difficulties and calculation time. This represents one of the current limits and thus, a target for improvement of the research in this field.

By comparing the results between the different geometrical models of this Chapter, an indirect evidence of the effects induced by geometric non-linearity can be seen. The absence of curvature in the PS simulation highlights a higher maximum stress and strain for the HE models (HE-MR and HE-Y) in comparison to LE model. The FEA simulations made for PS case via OptiStruct, let us able to affirm that according to the material parameters adopted for the HE models, a remarkable difference is present between the maximum values of HE strains and the LE one. HE-Y presents a higher maximum strain in comparison to HE-MR as a consequence of a less stiff behaviour than the HE-MR one. Generally speaking, without taking care of the specific problems related to soft tissue in case of strain higher than 100%, HE-Y can fit the real trends of an HE material better than HE-MR [117]. So, its adoption instead of the HE-MR can be necessary when these ranges of strain to occur. Due to the fact that the observed range of strains, in our analysis, is more or less under 100%, we can assume HE-MR as more reliable.

In addition, in the PS case, simulations show an overall deflection that is less than 5% of the characteristic length of the geometry; in fact, the maximum deflection is about 0.4 mm with a characteristic length of 100 mm that means a ratio of 0.4%.

Generally speaking, intestine strain distribution during motion is obviously related to its geometry [124]. Although 3D-SS pertains a more

complex shape in comparison to the PS and CS as its shape is different from the actual shape of a colon. The geometrical lack of accuracy in 3D-SS model, is due to the fact that complex shapes of the folds are partially reconstructed and approximated. By considering some evidence of the effects on the stress-strain values of the organ's actual 3D-SS have been provided here (Section 5.2), we want to highlight that these values may also be affected by accuracy of its reconstruction as it happens in 3D-S. Ultimately, it can be said that a geometrical lack of accuracy can influence the local displacement evaluation of the surface that interfaces with the surgical tool due to the different local behaviours connected to different local shapes. The reasons for this loss of geometrical accuracy are related to different aspects that pertains to DICOM. They concern with: the accuracy of the acquisitions (technological principle and set up of the acquiring process), the type of segmentation that has been adopted to isolate different tissue area (e.g. threshold application mode and set-up) and its geometrical post-processing to achieve surface tessellation or 3D modeling via NURBS (approximation of point interpolation, slice merging and smoothing). According to [94], [125], a precise and automatic segmentation of colon from images is yet a challenge and crucial problem for many clinical applications in colonography including computer-aided detection of colon polyps, 3D virtual flythrough of the colon and prone/supine registration. In general, when a tumor is present in colorectal zone, segmentation operations may be complex due to difficulties in discretizing different tissues. Because of this, manual segmentation operations with the assistance of a radiologist are often employed in these cases. The importance of the segmentation phase and the need of its automation are confirmed by recent studies that focus on rectal cancer [84], which suggest that 3D anatomical imaging segmentation obtained from DICOM of MRI, could contribute in the definition of the circumferential resection margins and in the pre-operative assessment of the tumor regression grade following chemo-radiation treatments.

In the reported case of 3D-SS model, a manual segmentation was performed by means of Slicer3D [113], version 4.5 (according to DICOM procedures). Manual operations may increase accuracy in small area but are complex to be checked and replicated on a large number of slices, [88], [89], [126]. Figure 3.15 shows an enhanced model obtained by Computer Tomography (CT) scan and automatic segmentation [93], [95],

[127], [128]. Its simulation is set-up to investigate the role of folds in stress-strain distribution in comparison to 3D-SS results (Section 5.2).

According to the results shown in Section 5.1, the approximation of an actual portion of colon with an equivalent cylinder (CS case) is consistent with 3D-SS model in terms of stress-strain gradient (Figure 5.4) but not in terms of maximum stress values and has been confirmed by using both LE and HE-MR material models. Due to the adopted material constants that are used to describe the LE and the HE-MR models, the LE model always overestimates the maximum stress with respect to the HE-MR (Figure 5.4(a) and Figure 5.10(a)). Nevertheless Figure 5.6 shows an analysis of geometrical influences with use of the LE and HE-MR models and on the basis of the results obtained, it is appreciable that the change of geometrical models have a greater influence when the linear elastic model approximation is used (Figure 5.6(a)). Whereas when the HE-MR model is used, the influence of geometrical model decreases (Figure 5.6(c)). By concerning change in element's length, both geometrical models show variations. This can be seen as an effect of the local changes in the diametrical sections but in general from 2mm of element size, the solution seems to be stabilize.

Concerning the results as effect of variation on the thickness as shown in Section 5.2. The increasing trend in terms of stress and strain (Figure 5.10) is a consequence of the increase of the initial thickness. In addition, the increasing trend may be also partially connected to the fact that the FEA condition has an imposed motion on the clamp that is stopped at a specific gap-value (1.5mm) related to clamp tightness. This means a maximum limit for the distance between clamps but with an increase of the initial thickness, it leads to higher stress in the tissue that is more compressed.

In terms of stress-strain gradient (Figure 5.9), the approximation of an actual portion of colon with an equivalent cylinder (CS case) is consistent with 3D-SS and 3D-S model but not in terms of maximum stress values. In fact, Figure 5.10 shows an overestimation of the maximum stress when the LE model is used with respect to the case when the HE-MR is applied. Nevertheless, switching from the CS to the 3D-S model, this effect is amplified and can be seen as a proof of the effect induced by the large deformation related to the irregularities present in a real geometry. Regarding to the influence of geometrical models when the thickness change, as it is appreciable in Figure 5.11, which depicts that the change

of geometrical models have a greater influence when the linear elastic model approximation is used (Figure 5.11(a)). While when the HE-MR model is used, the values of stress and strain are quite similar even in its trend (Figure 5.11(c)). This behaviour implies that the influence of geometrical model decreases.

Regarding to the results obtained from force and pressure contact, as was mentioned before, FEA tools may increase the understanding of this phenomena. All surgeries present a certain type of interaction between soft tissues and surgical instrument. Therefore, at this point FEA may play an important role in order to understand the reaction between tissues and surgical instrument.

With a more precise evaluation in terms of force, pressure contact, kinematic chain and haptic systems, it can be possible to deliver a more realistic and immersive simulation to the surgical practitioners.

As consequence of adopted material constants to describe the LE and the HE-MR models, the LE model present higher values in terms of force and pressure contact with respect to the HE-MR (Figure 5.12 and Figure 5.13). By the change of element's length, both geometrical model shows changes but in general from 2mm of element size, the solution seems to stabilize in terms of force contact while the pressure contact presents an irregular trend, whereas this irregular trend is amplified when the LE mechanical behaviour is considered.

With respect to the results as effect of variation on the thickness, as shown in Section 5.2, the Figure 5.13 shows an increasing regular trend in terms of force and pressure contact when the LE mechanical behaviour is considered. It can be seen as consequence of the increase in the initial thickness. Similar to the stress analysis, the increasing trend may be also partially connected to the fact that the FEA condition has an imposed motion on the clamp that is stopped at a specific gap-value. This means that the maximum limit for the distance between the clamps occurs with an increase of the initial thickness. It leads to higher reaction force towards the clamp. In general, when the element's length or thickness change (Figure 5.11 and Figure 5.13), LE always overestimates the maximum force and pressure contact.

In particular, the pressure contact shows an increase in irregular behaviour as the geometric model considers the local changes in the diametrical sections or particular colon folds (3D-S).

# Conclusions and future work

FEA simulations of the grasping operation in large intestine surgery have been provided here according to four different level of complexity for the geometrical model (plane surface, cylindrical surface, 3D-SS and 3D-S), that are joint with different mechanical behaviors for the soft tissues (LE, HE-MR, HE-Y). All these cases have been solved through commercial softwares of the Hyperworks suite as explained in Section 4.4, by using load and boundary conditions that are appropriate to fix the tissues into surgical clamp.

The target of this work is to evaluate the effects of non-linearities in a grasping process through FEA; This represents a preliminary contribution to the development of real-time simulations between surgical instrument and colon tissues.

About the nonlinear effects induced by different material models, the adoption of a hyperelastic material has been declared as necessary in order to obtain a good level of reliability in an increasing deformation field, also due to the large displacements involved in the process. This has been evaluated through simulations made on CS, 3D-SS and 3D-S models of the colon. In fact, it emerges that with an imposed load that is comparable with the real closing process, the linear elastic (LE) formulation provided an overestimation of stress average value with respect to the one found with the hyperelastic (HE-MR) formulation. In addition, the simulations made with the planar surface (PS) model, LE model resulted the most rigid under the same load conditions which is followed by HE-MR and HE-Y that implies for the analysis of complex geometries (free-form shapes) such as colorectal tissue, the LE model may fail to predict the fields of tensions and deformations and thus, overestimate stresses and strains on the tissue. These results matches with the experimental proofs that demonstrate the visco-elasticity of soft tissues (that usually means hyperelasticity if unloading is not provided). This behaviour induces local large displacements before start of generating stress and strain.

From the obtained results in terms of strain, we can assume as reported in literature that in range of minor than 100%, HE-MR model can be considered as more reliable than HE-Y.

In order to guarantee the convergence and accuracy of the solution by concerning the mesh dependency, we obtained a stable solution from 2 mm of element's length for all geometric models.

For what concerns with the comparison between different geometrical models, the results obtained presents considerable difference in terms of stress when linear elastic is considered as soft tissue mechanical behaviour as in Figure 5.6(a). From the geometrical point of view, the 3D-S is the most reliable model because it considers the colon folds but at the same time it presents the greatest overestimation of stress and strain values for LE formulation (Figure 5.11(a)). This can be induced by large displacements and more rigid behaviour in comparison with HE-MR and it is connected to geometrical irregularities of the model. It has to be highlighted that when LE is considered, the maximum values of stress and strain that results are directly connected to the geometrical model even when the thickness or element's length is changed.

On the other hand, the comparison between different geometrical models using HE-MR mechanical behaviour, it seems to have no relevant influence. The trend in terms of stress and strain is quite similar when the thickness or element's length change even in comparison of maximum values of stress-strain.

Obviously, compromise solutions between accuracy and speed when possible, it has to be searched in order to limit computational costs. The results obtained can help to the development of models which can lead to fast and reliable simulations. Mainly it is to regard that the approximations in geometrical models are possible as long as HE-MR mechanical behaviour is considered. It is clear that how it can allow to obtain more fast simulation when time is a mandatory factor, as for example in preoperative planning, it also can help to real time simulations that can be used as a basis for virtual reality.

These results may be correlated to the force feedback on the tool handle. In the upcoming years, together with the sensitivity analysis, will be used for setting-up a real-time model and simulation of the closing step.

Another interesting future development in this issue could be an experimental test campaign in order to confirm this assumption. In terms of stress, the comparison between LE, HE-MR and HE-Y, made in the PS case, highlights that the hyperelastic models leads to analogous values

which are also similar to the LE ones with a difference of lower than 4%. This could be useful in simulations focused on surgical tools as for example, in anastomosis applications instead of soft tissues deformation. In fact, in this kind of issues, the possibility of using LE model without considering nonlinearities may led to faster simulations and give results with less loss of reliability. Nevertheless, in terms of strain, it has to be kept in mind that there are significant differences between material models in PS case generated by different stiffness. Clearly, the LE model has a higher value of stiffness thus, producing lower values of deformation in the analysed soft tissues. Otherwise, PS simulations have been loaded with an equivalent force. On the contrary, 3d-SS, 3D-S and CS have been loaded by imposed displacement. This produces difference in the strain behaviour by changing the material models.

# References


[1] C. Carpue, Joseph Constantine and Turner, *An account of two successful operations for restoring a lost nose from the integuments of the forehead*, 1st ed. Birmingham: Classics of Medicine Library, 1981.

[2] G. Salerno, "MACCHINE ANATOMICHE," 1764. [Online]. Available: http://www.museosansevero.it/macchine-anatomiche/.

[3] A. B. Davis, *Louis Thomas Jerôme Auzoux and the papier mâché anatomical model*. Firenze: in La Ceroplastica nella Scienza e nell'Arte: atti del I Congresso Internazionale Firenze, 1975.

[4] K. S. Gurusamy, R. Aggarwal, L. Palanivelu, and B. R. Davidson, "Virtual reality training for surgical trainees in laparoscopic surgery," in *Cochrane Database of Systematic Reviews*, K. S. Gurusamy, Ed. Chichester, UK: John Wiley & Sons, Ltd, 2009.

[5] T. P. Grantcharov, V. B. Kristiansen, J. Bendix, L. Bardram, J. Rosenberg, and P. Funch-Jensen, "Randomized clinical trial of virtual reality simulation for laparoscopic skills training," *Br. J. Surg.*, vol. 91, no. 2, pp. 146–150, 2004.

[6] V. Nováček *et al.*, "Finite element modelling of stapled colorectal end-to-end anastomosis: Advantages of variable height stapler design," *J. Biomech.*, vol. 45, no. 15, pp. 2693–2697, 2012.

[7] P. Ström, L. Hedman, L. Särnå, A. Kjellin, T. Wredmark, and L. Felländer-Tsai, "Early exposure to haptic feedback enhances performance in surgical simulator training: A prospective randomized crossover study in surgical residents," *Surg. Endosc. Other Interv. Tech.*, vol. 20, no. 9, pp. 1383–1388, 2006.

[8] S. Misra, "Realistic tool–tissue interaction models for surgical simulation and planning," *Doctor*, p. 275, 2009.

[9] R. Guachi, F. Bini, M. Bici, F. Campana, and F. Marinozzi, "Finite Element Model Set-up of Colorectal Tissue for Analyzing Surgical Scenarios," 2018, pp. 599–609.

[10] L. Guachi, R. Guachi, F. Bini, and M. Franco, "Automatic Colorectal Segmentation with Convolutional Neural Network," in *CAD'18*, 2018.

[11] R. Guachi, M. Bici, L. Guachi, F. Campana, F. Bini, and F.

Marinozzi, “Geometrical Modelling Effects on FEA of Colorectal Surgery,” in *CAD’18*, 2018.

[12] G. Martel, “Evaluating Surgical Outcomes: A Systematic Comparison of Evidence from Randomized Trials and Observational Studies in Laparoscopic Colorectal Cancer Surgery,” University of Ottawa, 2012.

[13] M. M. Tiwari, J. F. Reynoso, R. High, A. W. Tsang, and D. Oleynikov, “Safety, efficacy, and cost-effectiveness of common laparoscopic procedures,” *Surg. Endosc. Other Interv. Tech.*, vol. 25, no. 4, pp. 1127–1135, 2011.

[14] J. E. Varela, S. E. Wilson, and N. T. Nguyen, “Laparoscopic surgery significantly reduces surgical-site infections compared with open surgery,” *Surg. Endosc. Other Interv. Tech.*, vol. 24, no. 2, pp. 270–276, 2010.

[15] D. Cheng *et al.*, “Video-assisted thoracic surgery in lung cancer resection: A meta-analysis and systematic review of controlled trials,” *Innov. Technol. Tech. Cardiothorac. Vasc. Surg.*, vol. 2, no. 6, pp. 261–292, 2007.

[16] C. Y. Kang *et al.*, “Outcomes of laparoscopic colorectal surgery: Data from the Nationwide Inpatient Sample 2009,” *Am. J. Surg.*, vol. 204, no. 6, pp. 952–957, 2012.

[17] H. L. Tian, J. H. Tian, K. H. Yang, K. Yi, and L. Li, “The effects of laparoscopic vs. open gastric bypass for morbid obesity: A systematic review and meta-analysis of randomized controlled trials,” *Obes. Rev.*, vol. 12, no. 4, pp. 254–260, 2011.

[18] S. Trastulli *et al.*, “Systematic review and meta-analysis of randomized clinical trials comparing single-incision versus conventional laparoscopic cholecystectomy,” *Br. J. Surg.*, vol. 100, no. 2, pp. 191–208, 2013.

[19] B. Wei *et al.*, “Laparoscopic versus open appendectomy for acute appendicitis: A metaanalysis,” *Surg. Endosc. Other Interv. Tech.*, vol. 25, no. 4, pp. 1199–1208, 2011.

[20] D. S. Supermaniam, “Selva’s Fertility, Obstetrics & Gynaecology Clinic.” [Online]. Available: https://melakafertility.com/about-us/.

[21] R. Schmoll, *Co-Simulation und Solverkopplung*, vol. 3/2015.

2015.

[22] U. G. Kühnapfel, C. Kuhn, M. Hübner, H. G. Krumm, H. Maass, and B. Neisius, “The Karlsruhe Endoscopic Surgery Trainer as an example for virtual reality in medical education,” *Minim. Invasive Ther. Allied Technol.*, vol. 6, no. 2, pp. 122–125, 1997.

[23] R. L. Zienkiewicz, Olgierd Cecil and Taylor, Robert Leroy and Zienkiewicz, Olgierd Cecil and Taylor, *The finite element method*. London: McGraw-hill, 1977.

[24] G. P. Moustris, S. C. Hiridis, K. M. Deliparaschos, and K. M. Konstantinidis, “Evolution of autnomous and semi-autnomous robotic surgical systems: a review of the literature,” *Int. J. Med. Robot.*, vol. 7, no. April, pp. 375–392, 2011.

[25] Z. W. Chen, P. Joli, Z. Q. Feng, M. Rahim, N. Pirró, and M. E. Bellemare, “Female patient-specific finite element modeling of pelvic organ prolapse (POP),” *J. Biomech.*, vol. 48, no. 2, pp. 238–245, 2015.

[26] E. Jeanditgautier, O. Mayeur, M. Brieu, G. Lamblin, C. Rubod, and M. Cosson, “Mobility and stress analysis of different surgical simulations during a sacral colpopexy, using a finite element model of the pelvic system,” *Int. Urogynecol. J.*, vol. 27, no. 6, pp. 951–957, 2016.

[27] O. Mayeur, J. F. Witz, P. Lecomte, M. Brieu, M. Cosson, and K. Miller, “Influence of Geometry and Mechanical Properties on the Accuracy of Patient-Specific Simulation of Women Pelvic Floor,” *Ann. Biomed. Eng.*, vol. 44, no. 1, pp. 202–212, 2016.

[28] L. E. Malvern, *Introduction to the Mechanics of a Continuous Medium*. Englewood Ciffs: Prentice-Hall, 1969.

[29] M. P. Ottensmeyer, A. E. Kerdok, R. D. Howe, and S. L. Dawson, “The Effects of Testing Environment on the Viscoelastic Properties of Soft Tissues,” *Perfusion*, vol. 24, pp. 219–238, 2007.

[30] E. Kester, U. Rabe, L. Presmanes, W. Arnold, and U. P. Sabatier, “Measurement of Mechanical Properties of,” *Acta Metall.*, vol. 12, no. 99, pp. 779–782, 1999.

[31] D. Liao, J. Zhao, and H. Gregersen, “3d Mechanical properties of the partially obstructed guinea pig small intestine,” *J. Biomech.*, vol. 43, no. 11, pp. 2079–2086, 2010.

[32] C. Rubod *et al.*, “Biomechanical properties of human pelvic organs,” *Urology*, vol. 79, no. 4, p. 968.e17-968.e22, 2012.

[33] M. B. Christensen, K. Oberg, and J. C. Wolchok, “Tensile properties of the rectal and sigmoid colon: a comparative analysis of human and porcine tissue,” *Springerplus*, vol. 4, no. 1, 2015.

[34] S. F. F. Gibson *et al.*, “Biomechanical properties of human pelvic organs,” *J. Biomech.*, vol. 24, no. 11, pp. 1–31, 2010.

[35] Melvin Mooney, “A theory of large elastic deformation,” *J. Appl. Phys.*, vol. 11, no. 9, pp. 582–592, 1940.

[36] P. Chantereau, M. Brieu, M. Kammal, J. Farthmann, B. Gabriel, and M. Cosson, “Mechanical properties of pelvic soft tissue of young women and impact of aging,” *Int. Urogynecol. J.*, vol. 25, no. 11, pp. 1547–1553, 2014.

[37] S. F. F. Gibson and B. Mirtich, “A Survey of Deformable Modeling in Computer Graphics,” *Merl - a Mitsubishi Electr. Res. Lab.*, pp. 1–31, 1997.

[38] T. Chung, *General continuum mechanics*. Cambridge University Press, 2007.

[39] H. P. Charalambous, P. C. Roussis, and A. E. Giannakopoulos, “The Effect of Strain Hardening on the Dynamic Response of Human Artery Segments,” *Open Biomed. Eng. J.*, vol. 11, no. 1, pp. 85–110, 2017.

[40] N. de Cesare, C. Trevisan, E. Maghin, M. Piccoli, and P. G. Pavan, “A finite element analysis of diaphragmatic hernia repair on an animal model,” *J. Mech. Behav. Biomed. Mater.*, vol. 86, no. June, pp. 33–42, 2018.

[41] G. A. Holzapfel, T. C. Gasser, and R. W. Ogden, “A new constitutive framework for arterial wall mechanics and a comparative study of material models,” *J. Elast.*, vol. 61, no. 1–3, pp. 1–48, 2000.

[42] R. Jayendiran, B. Nour, and A. Ruimi, “Computational fluid–structure interaction analysis of blood flow on patient-specific reconstructed aortic anatomy and aneurysm treatment with Dacron graft,” *J. Fluids Struct.*, vol. 81, pp. 693–711, 2018.

[43] M. N. Hamza and H. M. Alwan, “Hyperelastic Constitutive Modeling of Rubber and Rubber- Like Materials under Finite

Strain," vol. 28, no. 13, 2010.

[44] R. Rivlin, "Large elastic deformations of isotropic materials IV. Further developments of the general theory," *Br. Rubber Prod. Res. Assoc.*, vol. 241, no. 835, pp. 379–397, 1948.

[45] M. Shahzad, A. Kamran, M. Z. Siddiqui, and M. Farhan, "Mechanical Characterization and FE Modelling of a Hyperelastic Material," *Mater. Res.*, vol. 18, no. 5, pp. 918–924, 2015.

[46] A. N. Gent, *Engineering with rubber*. Munich: Carl Hanser Verlag, 2001.

[47] E. M. Arruda and M. C. Boyce, "Evolution of plastic anisotropy in amorphous polymers during finite straining," *Int. J. Plast.*, vol. 9, no. 6, pp. 697–720, Jan. 1993.

[48] R. Lakes and R. S. Lakes, *Viscoelastic materials*. Cambridge University Press, 2009.

[49] J. L. Calvo-Gallego, J. Domínguez, T. Gómez Cía, G. Gómez Ciriza, and J. Martínez-Reina, "Comparison of different constitutive models to characterize the viscoelastic properties of human abdominal adipose tissue. A pilot study," *J. Mech. Behav. Biomed. Mater.*, vol. 80, no. September 2017, pp. 293–302, 2018.

[50] R. D. Cook, *Concepts and applications of finite element analysis*, 3rd ed. New York: John Wiley, 2007.

[51] J. Reddy, "Energy and variational methods," *Appl. Mech.*, pp. 367–393, 1984.

[52] Altair, "HyperWorks." [Online]. Available: https://connect.altair.com/CP/kb-browse.html?filterResults=1&type=User Manuals.

[53] H. Shi, "Finite element modeling of soft tissue deformation .," 2007.

[54] M. Cosson, C. Rubod, A. Vallet, J. F. Witz, P. Dubois, and M. Brieu, "Simulation of normal pelvic mobilities in building an MRI-validated biomechanical model," *Int. Urogynecol. J. Pelvic Floor Dysfunct.*, vol. 24, no. 1, pp. 105–112, 2013.

[55] G. Venugopala Rao, C. Rubod, M. Brieu, N. Bhatnagar, and M. Cosson, "Experiments and finite element modelling for the study of prolapse in the pelvic floor system," *Comput. Methods*

*Biomech. Biomed. Engin.*, vol. 13, no. 3, pp. 349–357, 2010.

[56] SIMULIA, "ABACUS." [Online]. Available: https://www.3ds.com/products-services/simulia/products/abaqus/.

[57] ANSYS INC., "ANSYS." [Online]. Available: https://www.ansys.com/.

[58] COMSOL INC., "COMSOL." [Online]. Available: https://www.comsol.com/.

[59] MSC Software Corporation, "MSC Nastran." [Online]. Available: http://www.mscsoftware.com/product/msc-nastran.

[60] MSC Software Corporation, "MSC/Marc." [Online]. Available: http://www.mscsoftware.com/product/marc.

[61] R. W. Ogden, *Non-linear elastic deformations*. Courier Corporation, 1997.

[62] W. Lacarbonara, *Nonlinear Structural Mechanics*. Springer Science, 2013.

[63] K.-J. Bathe, *Finite element procedures*. Klaus-Jurgen Bathe, 2006.

[64] K. Xu, R. E. Goldman, J. Ding, P. K. Allen, D. L. Fowler, and N. Simaan, "System design of an insertable robotic effector platform for Single Port Access (SPA) surgery," *2009 IEEE/RSJ Int. Conf. Intell. Robot. Syst. IROS 2009*, pp. 5546–5552, 2009.

[65] E. Gladilin, S. Zachow, P. Deuflhard, and H.-C. Hege, "A biomechanical model for soft tissue simulation in craniofacial surgery," in *Proceedings International Workshop on Medical Imaging and Augmented Reality*, pp. 137–141.

[66] M. Bro-Nielsen, "Finite element modeling in medical VR," *J. IEEE*, vol. 86, no. 4, pp. 490–503, 1998.

[67] S. Cotin, H. Delingette, and N. Ayache, "Real-time elastic deformations of soft tissues for surgery simulation," *IEEE Trans. Vis. Comput. Graph.*, vol. 5, no. 1, pp. 62–73, 1999.

[68] A. H. Gosline, S. E. Salcudean, and J. Yan, "Haptic simulation of linear elastic media with fluid pockets," in *12th International Symposium on Haptic Interfaces for Virtual Environment and*

*Teleoperator Systems, 2004. HAPTICS '04. Proceedings.*, 2004, pp. 266–271.

[69] X. Wu, M. S. Downes, T. Goktekin, and F. Tendick, "Adaptive Nonlinear Finite Elements for Deformable Body Simulation Using Dynamic Progressive Meshes," *Comput. Graph. Forum*, vol. 20, no. 3, pp. 349–358, Sep. 2001.

[70] H. Talbot *et al.*, "Interactive Training System for Interventional Electrocardiology Procedures To cite this version : HAL Id : hal-01078209 Interactive Training System for Interventional Electrocardiology Procedures," 2015.

[71] C. C. Mitchell and D. G. Schaeffer, "A two-current model for the dynamics of cardiac membrane," *Bull. Math. Biol.*, vol. 65, no. 5, pp. 767–793, 2003.

[72] N. Haouchine, J. Dequidt, I. Peterlik, E. Kerrien, M.-O. Berger, and S. Cotin, "Image-guided simulation of heterogeneous tissue deformation for augmented reality during hepatic surgery," in *2013 IEEE International Symposium on Mixed and Augmented Reality (ISMAR)*, 2013, pp. 199–208.

[73] M. Harders *et al.*, "Virtual Reality Based Simulation of Hysteroscopic Interventions," *Presence Teleoperators Virtual Environ.*, vol. 17, no. 5, pp. 441–462, 2008.

[74] "Reachin Technologies AB." [Online]. Available: www.reachin.se.

[75] 3D SYSTEMS, "Simbionix USA Corp." [Online]. Available: https://simbionix.com/.

[76] Immersion Corporation, "Immersion Medical." [Online]. Available: https://www.immersion.com/.

[77] Surgical Science Ltd, "Surgical Science." [Online]. Available: https://surgicalscience.com/.

[78] Haptica Inc, "Haptica." [Online]. Available: http://www.haptica.com/.

[79] Mimic Technologies Inc, "Mimic Technologies." [Online]. Available: http:%0A//www.mimic.ws/.

[80] Mentice AB, "Mentice AB." [Online]. Available: https://www.mentice.com/.

[81] Medical Educational Technologies Inc, “Medical Educational Technologies.” [Online]. Available: http://www.meti.com/.

[82] VRmagic, “VRmagic Medical Simulators.” [Online]. Available: https://www.vrmagic.com/.

[83] Elspeth M. McDougall., “Validation of Surgical Simulators,” *J. Endourol.*, vol. 21, no. 3, 2007.

[84] L. Lorenzon, F. Bini, G. Balducci, M. Ferri, P. F. Salvi, and F. Marinozzi, “Laparoscopic versus robotic-assisted colectomy and rectal resection: a systematic review and meta-analysis,” *Int. J. Colorectal Dis.*, vol. 31, no. 2, pp. 161–173, 2016.

[85] R. S. Baker, J. Foote, P. Kemmeter, R. Brady, T. Vroegop, and M. Serveld, “The science of stapling and leaks,” *Obes. Surg.*, vol. 14, no. 10, pp. 1290–1298, 2004.

[86] A. Boschetto, F. Campana, and D. Pilone, “Comparison through image analysis between al foams produced using two different methods,” *J. Mater. Eng. Perform.*, vol. 23, no. 2, pp. 572–580, 2014.

[87] A. Campbell, P. Murray, E. Yakushina, S. Marshall, and W. Ion, “New methods for automatic quantification of microstructural features using digital image processing,” *Mater. Des.*, vol. 141, pp. 395–406, 2018.

[88] B. R. Franco Marinozzi, Fabiano Bini, Andrea Marinozzi, Zuppante Francesca, De Paolis Annalisa, Pecci Raffaela, “Technique for bone volume measurement from human femur head samples by classification of micro-CT image histograms,” *Ann Ist Super Sanità*, vol. 49, no. 3, pp. 300–305, 2013.

[89] M. Franco and B. R. Marinozzi Andrea, Bini Fabiano, Zuppante Francesca, Pecci Raffaella, “Variability of morphometric parameters of human trabecular tissue from coxo-arthritis and osteoporotic samples,” *Ann Ist Super Sanità*, vol. 48, no. 1, pp. 19–25, 2012.

[90] K. Gayathri Devi and R. Radhakrishnan, “Automatic segmentation of colon in 3D CT images and removal of opacified fluid using cascade feed forward neural network,” *Comput. Math. Methods Med.*, vol. 2015, no. 2, 2015.

[91] W. He, L. Zhang, H. Yang, and Z. Jiang, “Local Region Based

Active Contours for Colon Tissue Segmentation," pp. 993–998, 2015.

[92] M. Bici, F. Campana, S. Petriaggi, and L. Tito, "Study of a Point Cloud Segmentation with Part Type Recognition for Tolerance Inspection of Plastic Components via Reverse Engineering," *Comput. Aided. Des. Appl.*, vol. 11, no. 6, pp. 640–648, 2014.

[93] G. Cocorullo, P. Corsonello, F. Frustaci, L. de los A. Guachi-Guachi, and S. Perri, "Multimodal background subtraction for high-performance embedded systems," *J. Real-Time Image Process.*, pp. 1–17, 2016.

[94] X. Yang, X. Ye, and G. Slabaugh, "Multilabel region classification and semantic linking for colon segmentation in CT colonography," *IEEE Trans. Biomed. Eng.*, vol. 62, no. 3, pp. 948–959, 2015.

[95] S. Kim, "Method of Background Subtraction for Medical Image Segmentation."

[96] Sareena, A. Mittal, and M. Kaur, "Computer-aided-diagnosis in colorectal cancer: A survey of state of the art techniques," *2016 Int. Conf. Inven. Comput. Technol.*, pp. 1–6, 2016.

[97] M. Caon, J. Sedlář, M. Bajger, and G. Lee, "Computer-assisted segmentation of CT images by statistical region merging for the production of voxel models of anatomy for CT dosimetry," *Australas. Phys. Eng. Sci. Med.*, vol. 37, no. 2, pp. 393–403, 2014.

[98] D. Chen, H. Abdelmunim, A. A. Farag, R. Falk, and G. Dryden, "Segmentation of Colon Tissue in CT Colonography Using Adaptive Level Sets Method," pp. 108–115, 2008.

[99] H. Yoshida and J. Näppi, "Three-dimensional computer-aided diagnosis scheme for detection of colonic polyps," *IEEE Trans. Med. Imaging*, vol. 20, no. 12, pp. 1261–1274, 2001.

[100] Z. Tu, X. (Sean) Zhou, D. Comaniciu, and L. Bogoni, "A Learning Based Approach for 3D Segmentation and Colon Detagging," 2006, pp. 436–448.

[101] A. M. Ali and A. A. Farag, "Graph cut based segmentation of multimodal images," in *ISSPIT 2007 - 2007 IEEE International Symposium on Signal Processing and Information Technology*, 2007, pp. 1036–1041.

[102] S.-C. B. Lo, S.-L. a Lou, J.-S. Lin, M. T. Freedman, M. V Chien, and S. K. Mun, "Artificial convolution neural network techniques and applications for lung nodule detection," *IEEE Trans. Med. Imaging*, vol. 14, no. 4, pp. 711–718, 1995.

[103] T. C. Haj-Hassan Hawraa, Chaddad Ahmad, Harkouss Youssef, Desrosiers Christian, Toews Matthew, "Classifications of Multispectral Colorectal Cancer Tissues Using Convolution Neural Network," *J. Pathol. Inform.*, vol. 8, no. 38, pp. 1–12, 2017.

[104] N. Codella, J. Cai, M. Abedini, R. Garnavi, A. Halpern, and J. R. Smith, "Deep Learning, Sparse Coding, and SVM for Melanoma Recognition in Dermoscopy Images," 2015, pp. 118–126.

[105] P. Kainz, M. Pfeiffer, and M. Urschler, "Semantic Segmentation of Colon Glands with Deep Convolutional Neural Networks and Total Variation Segmentation," pp. 1–15, 2015.

[106] W. Li, S. Manivannan, S. Akbar, J. Zhang, E. Trucco, and S. J. Mckenna, "GLAND SEGMENTATION IN COLON HISTOLOGY IMAGES USING HAND-CRAFTED FEATURES AND CONVOLUTIONAL NEURAL NETWORKS Center for Advanced Imaging Innovation and Research , NYU School of Medicine , New York , USA," pp. 1405–1408, 2016.

[107] Y. Lecun *et al.*, "Learning Algorithms for Classification: a Comparison on Handwritten Digit Recognition."

[108] Funded by Frederick Nat. Lab for Cancer Research, "The Cancer Imaging Archive." [Online]. Available: https://wiki.cancerimagingarchive.net/display/Public/CT+COLONOGRAPHY#ddac1809036649d98.

[109] M. Braham and M. Van Droogenbroeck, "Deep background subtraction with scene-specific convolutional neural networks," *Int. Conf. Syst. Signals, Image Process.*, vol. 2016–June, 2016.

[110] A. Bronstein, "Deep Neural Networks : A Universal Classification Strategy ? ( Deep ) neural network," vol. 64, no. 13, pp. 3444–3457, 2016.

[111] A. Mohamed, C. Davatzikos, and R. Taylor, "A Combined Statistical and Biomechanical Model for Estimation of Intra-operative Prostate Deformation," 2002, pp. 452–460.

[112] E. Dehghan and S. E. Salcudean, “Comparison of linear and non-linear models in 2D needle insertion simulation,” *Proc. Work. Comput. Biomech. Med.*, pp. 117–124, 2006.

[113] A. Fedorov *et al.*, “3D Slicer as an image computing platform for the Quantitative Imaging Network,” *Magn. Reson. Imaging*, vol. 30, no. 9, pp. 1323–1341, 2012.

[114] R. J. Campbell and P. J. Flynn, “A survey of free-form object representation and recognition techniques,” *Comput. Vis. Image Underst.*, vol. 81, no. 2, pp. 166–210, 2001.

[115] Fung, *Biomechanics: mechanical properties of living tissues*. Springer Science, 2013.

[116] H. Yamada, *Strength of biological materials*. Williams & Wilkins, 1970.

[117] M. Sasso, G. Palmieri, G. Chiappini, and D. Amodio, “Characterization of hyperelastic rubber-like materials by biaxial and uniaxial stretching tests based on optical methods,” *Polym. Test.*, vol. 27, no. 8, pp. 995–1004, 2008.

[118] J. Ribeiro, H. Lopes, and P. Martins, “A hybrid method to characterise the mechanical behaviour of biological hyper-elastic tissues,” *Comput. Methods Biomech. Biomed. Eng. Imaging Vis.*, vol. 5, no. 3, pp. 157–164, 2017.

[119] E. Chekan and R. L. Whelan, “Surgical stapling device - tissue interactions: What surgeons need to know to improve patient outcomes,” *Med. Devices Evid. Res.*, vol. 7, pp. 305–318, 2014.

[120] V. I. Egorov, I. V. Schastlivtsev, E. V. Prut, A. O. Baranov, and R. A. Turusov, “Mechanical properties of the human gastrointestinal tract,” *J. Biomech.*, vol. 35, no. 10, pp. 1417–1425, 2002.

[121] H. Elariny, H. González, and B. Wang, “Tissue thickness of human stomach measured on excised gastric specimens from obese patients,” *Surg. Technol. Int.*, vol. 14, p. 119—124, 2005.

[122] A. C. Offodile, D. L. Feingold, A. Nasar, R. L. Whelan, and T. D. Arnell, “High Incidence of Technical Errors Involving the EEA Circular Stapler: A Single Institution Experience,” *J. Am. Coll. Surg.*, vol. 210, no. 3, pp. 331–335, 2010.

[123] K. Okano *et al.*, “Pancreatic thickness as a predictive factor for

postoperative pancreatic fistula after distal pancreatectomy using an endopath stapler," *Surg. Today*, vol. 43, no. 2, pp. 141–147, Feb. 2013.

[124] C. Gao and H. Gregersen, "Biomechanical and morphological properties in rat large intestine.," *J. Biomech.*, vol. 33, no. 9, pp. 1089–1097, 2000.

[125] D. R. and P.Aljabar, *Handbook of Biomedical Imaging*. 2015.

[126] P. Trimboli *et al.*, "Analysis of tissue surrounding thyroid nodules by ultrasound digital images," *Endocrine*, vol. 48, no. 2, pp. 434–438, 2015.

[127] G. Cocorullo, P. Corsonello, F. Frustaci, L. Guachi, and S. Perri, "Embedded surveillance system using background subtraction and Raspberry Pi," *AEIT Int. Annu. Conf. (AEIT). IEEE*, pp. 1–5, 2015.

[128] L. Guachi, G. Cocorullo, P. Corsonello, F. Frustaci, and S. Perri, "A novel background subtraction method based on color invariants," *Secur. Technol. (ICCST), 2014 Int. Carnahan Conf. on. IEEE*, pp. 1–5, 2014.